ISTANBUL TECHNICAL UNIVERSITY ★ GRADUATE SCHOOL OF SCIENCE ENGINEERING AND TECHNOLOGY

METOCEAN PUSHOVER ANALYSIS OF A JACKET-TYPE OFFSHORE PLATFORM WITH DIFFERENT BRACING SYSTEMS

M.Sc. THESIS

Erdem EREZ

Department of Civil Engineering

Structural Engineering Programme

JUNE 2020

ISTANBUL TECHNICAL UNIVERSITY ★ GRADUATE SCHOOL OF SCIENCE ENGINEERING AND TECHNOLOGY

METOCEAN PUSHOVER ANALYSIS OF A JACKET-TYPE OFFSHORE PLATFORM WITH DIFFERENT BRACING SYSTEMS

M.Sc. THESIS

Erdem EREZ
501171012

Department of Civil Engineering

Structural Engineering Programme

Thesis Advisor: Assoc.Prof.Dr. Kadir ÖZAKGÜL

JUNE 2020

ISTANBUL TEKNİK ÜNİVERSİTESİ ★ FEN BİLİMLERİ ENSTİTÜSÜ

FARKLI ÇAPRAZ SİSTEMLİ CEKET TİPİ AÇIK DENİZ PETROL PLATFORMUNUN OKYANUSSAL YÜKLERLE STATİK İTME ANALİZİ

YÜKSEK LİSANS TEZİ

Erdem EREZ
501171012

İnşaat Mühendisliği Anabilim Dalı

Yapı Mühendisliği Programı

Tez Danışmanı: Doç. Dr. Kadir ÖZAKGÜL

HAZİRAN 2020

Erdem EREZ, a M.Sc. student of ITU Graduate School of Science Engineering and Technology student ID 501171012, successfully defended the thesis entitled "METOCEAN PUSHOVER ANALYSIS OF A JACKET-TYPE OFFSHORE PLATFORM WITH DIFFERENT BRACING SYSTEMS", which he prepared after fulfilling the requirements specified in the associated legislations, before the jury whose signatures are below.

Thesis Advisor :	**Assoc. Prof. Dr. Kadir ÖZAKGÜL** İstanbul Technical University	....
Jury Members :	**Prof. Dr. Elişan Filiz Piroğlu** Istanbul Technical University	....
	Asst. Prof. Dr. Meltem Şahin Mimar Sinan Fine Arts University	....

Date of Submission : 15 June 2020
Date of Defense : 08 July 2020

FOREWORD

This thesis carried out within the scope of ITU Civil Engineering Department, Structural Engineering Program is aimed to perform metocean pushover analysis of a jacket-type offshore platform with different bracing systems.

I would like to thank to my supervisor Assoc.Prof. Dr. Kadir ÖZAKGÜL for his support and guidance during my study.

I would like to thank to my dear family for invaluable supports throughout my life.

June 2020

Erdem EREZ
(Civil Engineer)

TABLE OF CONTENTS

Page

FOREWORD .... **vii**
TABLE OF CONTENTS .... **ix**
ABBREVIATIONS .... **xi**
SYMBOLS .... **xiii**
LIST OF TABLES .... **xvii**
LIST OF FIGURES .... **xix**
SUMMARY .... **xxi**
ÖZET .... **xxiii**
1. INTRODUCTION **1**
1.1 General Information 1
1.2 Platform Types 2
1.2.1 Fixed platforms 2
1.2.1.1 Jacket-type platforms 2
1.2.1.2 Compliant towers 3
1.2.1.3 Gravity structures 3
1.2.2 Floating platforms 3
1.3 Literature Review 4
1.4 Objective and Scope 5
2. THEORY AND SPECIFICATIONS **7**
2.1 Environmental Considerations 7
2.1.1 Waves 8
2.1.1.1 Transformation of dynamic wave loadings to the static loadings 8
2.1.2 Tide 11
2.1.3 Current 12
2.1.4 Marine growth 12
2.2 Method of Analysis 12
2.2.1 Concept of non-linearity in jacket-type offshore structures 13
2.2.2 Force deformation relationship 13
2.2.3 Nonlinear pushover analysis procedure 15
2.3 Reserve Strength Ratio (RSR) 16
3. PLATFORM OVERVIEW **17**
3.1 Material Properties 17
3.2 Platform Properties 19
3.3 Nonstructural Members 22
3.4 Determination of Geometric Properties of Members 23
3.4.1 Class of sections 23
3.4.2 Tensile strength 26
3.4.3 Strength of structural steel under shear 26
3.4.4 Compressive strength 27
3.4.5 Flexural strength 28
3.4.5.1 Flexural strength of I-shaped member 28
3.4.5.2 Flexural strength of the circular hollow sections 29

3.4.6 Torsional capacity of the circular hollow sections 30
3.4.7 Round HSS members subjected to combined forces 30
4. METOCEAN CRITERIA AND LOADS 33
4.1 Metocean Criteria 33
4.1.1 Determination of metocean criteria 33
4.2 Loads 37
4.2.1 Dead loads 37
4.2.2 Live loads 37
4.2.3 Wave and current forces 38
4.3 Load Combinations 42
5. PRELIMINARY-LINEAR ANALYSIS 45
5.1 Linear Analysis for Diagonal Bracing System 46
5.1.1 Capacity check for braces 47
5.1.2 Capacity check for columns 48
5.1.3 Capacity check for beams 49
5.2 Linear Analysis for X-Bracing System 51
5.2.1 Capacity check for braces 52
5.2.2 Capacity check for columns 53
5.2.3 Capacity check for beams 55
5.3 Linear Analysis for V-Bracing System 57
5.3.1 Capacity check for braces 58
5.3.2 Capacity check for columns 59
5.3.3 Capacity check for beams 60
5.4 Linear Analysis for Inverted V-Bracing System 62
5.4.1 Capacity check for braces 63
5.4.2 Capacity check for columns 64
5.4.3 Capacity check for beams 66
5.5 Linear Analysis for K-Bracing System 68
5.5.1 Capacity check for braces 69
5.5.2 Capacity check for columns 70
5.5.3 Capacity check for beams 72
5.6 Linear Analysis Results 74
6. METOCEAN PUSHOVER ANALYSIS 75
6.1 Metocean Pushover Analysis Results for Diagonal Bracing System 79
6.2 Metocean Pushover Analysis Results for X-Bracing System 82
6.3 Metocean Pushover Analysis Results for V-Bracing System 85
6.4 Metocean Pushover Analysis Results for Inverted V-Bracing System 87
6.5 Metocean Pushover Analysis Results for K-Bracing System 90
7. CONCLUSION 93
REFERENCES 97
CURRICULUM VITAE 99

ABBREVIATIONS

BS	**:** Base Shear
CHSS	**:** Circular Hollow Structural Section
CSI	**:** Computer and Science Inc.
FEMA	**:** Federal Emergency Management Agency
ISO 19902	**:** International Organization for Standardization, Fixed Steel Offshore Strucutures
MHHW	**:** Mean Higher High Water
RSR	**:** Reserve Strength Ratio
WSD	**:** Working Stress Design

SYMBOLS

$\mathbf{A}$	: Area of a member
$\mathbf{A_g}$	: Gross area of a member
$\mathbf{A_n}$	: Net area of a member
$\mathbf{A_p}$	: Projected area of a member
$\mathbf{A_w}$	: Web area of a member
$\mathbf{BS_{100}}$	: Base shear at 100-year metocean loading
$\mathbf{BS_{collapse}}$	: Base shear at collapse
$\mathbf{C_b}$	: Lateral torsional buckling modification factor
$\mathbf{C_d}$	: Drag coefficient
$\mathbf{C_L}$	: Lift force coefficient
$\mathbf{C_v}$	: Web shear coefficient
$\mathbf{c}$	: Lateral torsional buckling coefficient
$\mathbf{D}$	: Diameter of the cylinder
$\mathbf{D}$	: Dead load
$\mathbf{E}$	: Young’s modulus
$\mathbf{E}$	: Eartquake load
$\mathbf{E_e^0}$	: Extreme environmental loading with wave direction 0^0 in x-y plane
$\mathbf{E_e^{45}}$	: Extreme environmental loading with wave direction 45^0 in x-y plane
$\mathbf{E_e^{90}}$	: Extreme environmental loading with wave direction 90^0 in x-y plane
$\mathbf{E_s}$	: Elastic modulus of steel
$\mathbf{F_{cr}}$	: Critical stress
$\mathbf{F_D}$	: Drag force
$\mathbf{F_e}$	: Elastic buckling stress
$\mathbf{F_I}$	: Inertia force
$\mathbf{F_u}$	: Ultimate stress
$\mathbf{F_{ue}}$	: Expected ultimate stress
$\mathbf{F_W}$	: Hydrodynamic force
$\mathbf{F_x}$	: Force in x-axis
$\mathbf{F_y}$	: Force in y-axis
$\mathbf{F_y}$	: Yield stress

$\mathbf{F_{ye}}$	: Expected yield stress
$\mathbf{F_z}$	: Force in z-axis
G	: Shear modulus
g	: Gravitational acceleration
$\mathbf{h_0}$	: Distance between the flange centroids
I	: Moment of inertia
$\mathbf{I_x}$	: Moment of inertia about x-axis
$\mathbf{I_y}$	: Moment of inertia about y-axis
J	: Torsional constant
K	: Effective length factor
L	: Length
L	: Live load
$\mathbf{L_b}$	: Length of brace
$\mathbf{L_r}$	: Roof live load
$\mathbf{L_v}$	: Distance from maximum to zero shear force
$\boldsymbol{l_b}$	: Length of the beam member
$\boldsymbol{l_{br}}$	: Length of the brace member
$\boldsymbol{l_c}$	: Length of the column member
M	: Moment
$\mathbf{M_A}$	: Moment at the fisrt quarter of a member
$\mathbf{M_B}$	: Moment at the midspan
$\mathbf{M_C}$	: Moment the third quarter of a member
$\mathbf{M_{cx}}$	: Moment capacity for x axis
$\mathbf{M_{cy}}$	: Moment capacity for y axis
$\mathbf{M_{max}}$	: Maximum moment
$\mathbf{M_n}$	: Nominal flexural capacity
$\mathbf{M_p}$	: Plastic moment
$\mathbf{M_{rx}}$	: Required moment for x axis
$\mathbf{M_{ry}}$	: Required moment for y axis
$\mathbf{M_y}$	: Yield moment
P	: Axial force
$\mathbf{P_c}$	: Axial compressive force
$\mathbf{P_n}$	: Nominal axial strength
$\mathbf{P_r}$	: Required axial strength
$\mathbf{P_t}$	: Axial tensile force

$\mathbf{P_y}$	: Axial yield force
$\mathbf{P_{ye}}$	: Axial expected yield force
$\mathbf{Q}$	: Generalized force
$\mathbf{Q_y}$	: Generalized yield force
$\mathbf{R}$	: Rain Load
$\mathbf{R_n}$	: Nominal strength
$\mathbf{R_u}$	: Required strength based on LRFD load combination
$\mathbf{r}$	: Radius of gyration
$\mathbf{r_{ts}}$	: Radius of gyration for lateral torsional buckling
$\mathbf{r_y}$	: Radius of gyration about y-axis
$\mathbf{S}$	: Elastic section modulus
$\mathbf{S}$	: Snow load
$\mathbf{S_x}$	: Elastic section modulus taken about x-axis
$\mathbf{T_c}$	: Torsional capacity
$\mathbf{T_n}$	: Nominal torsional strength
$\mathbf{t}$	: Thickness of a member
$\mathbf{U}$	: Vector of velocity
$\mathbf{U_m}$	: Maximum alongwave water particle velocity
$\mathbf{V}$	: Volume for per length
$\mathbf{V_c}$	: Shear capacity
$\mathbf{V_n}$	: Nominal shear strength
$\mathbf{V_r}$	: Required shear strength
$\mathbf{W}$	: Wind load
$\mathbf{w}$	: Weight density of water
$\mathbf{Z}$	: Plastic section modulus
$\mathbf{Z_x}$	: Plastic section modulus about the x-axis
$\boldsymbol{\delta U/\delta t}$	: Acceleration of a water particle
$\boldsymbol{\rho}$	: Density of water
$\boldsymbol{\rho_{steel}}$	: Density of steel
$\boldsymbol{\Delta}$	: Displacement
$\boldsymbol{\Delta_y}$	: Yield displacement
$\boldsymbol{\theta}$	: Rotation
$\boldsymbol{\theta_p}$	: Plastic rotation
$\boldsymbol{\theta_y}$	: Yield rotation
$\boldsymbol{\nu}$	: Poisson’s ratio

$\boldsymbol{\gamma_i}$	: Load factor
$\boldsymbol{\lambda}$	: Width to thickness ratio
$\boldsymbol{\Phi_c}$	: Compressive resistance factor
$\boldsymbol{\Phi_t}$	: Tensile resistance factor
$\boldsymbol{\Phi_T}$	: Torsional resistance factor
$\boldsymbol{\Phi_v}$	: Shear resistance factor

LIST OF TABLES

Page

Table 3.1 : Material properties. **17**
Table 3.2 : Parametric strain data. **17**
Table 3.3 : Platform geometric properties. **20**
Table 3.4 : Effective length factors of structural members. **28**
Table 4.1 : Determination of metocean criteria [13]. **33**
Table 4.2 : Current profile data. **36**
Table 4.3 : Summary of metocean data. **36**
Table 4.4 : Partial action factors in ISO 19902 [14]. **44**
Table 5.1 : Base reactions for diagonal bracing system. **46**
Table 5.2 : Base reactions for x-bracing system. **51**
Table 5.3 : Base reactions for v-bracing system. **57**
Table 5.4 : Base reactions for inverted v-bracing system. **62**
Table 5.5 : Base reactions for k-bracing system. **68**
Table 5.6 : Base shears at storm conditions for different bracing systems. **74**
Table 6.1 : Force deformation relationship for members. **75**
Table 7.1 : Base shears and RSR values of all bracing systems. **95**
Table 7.2 : Base shears and RSR values of all bracing systems. **96**

LIST OF FIGURES

Page

Figure 1.1 : Figure of jacket-type platform [3]. **2**
Figure 1.2 : Figure of gravity platform [3]. **3**
Figure 1.3 : Figure of tension leg platform [3]. **4**
Figure 2.1 : Wave profile [15]. **8**
Figure 2.2 : Steps of the transformation of dynamic wave loadings to the static loadings [13]. **9**
Figure 2.3 : Applicability of wave theories [15]. **10**
Figure 2.4 : Illustration of drag and inertia forces acting on a rigid cylinder [3]. **11**
Figure 2.5 : Definition of water levels [15]. **11**
Figure 2.6 : Force and deformation relationship [16]. **14**
Figure 3.1 : Stress-strain curve. **18**
Figure 3.2 : Elevation view of bare model. **19**
Figure 3.3 : Bracing configuration. **21**
Figure 3.4 : Bracing configuration with appurtenances. **22**
Figure 3.5 : Limit of slenderness ratios of different shape of steel members for compression members [18]. **24**
Figure 3.6 : Limit of slenderness ratios of different shape of steel members for flexural members [18]. **25**
Figure 4.1 : Omnidirectional wave height vs. mean water depth for Gulf of Mexico. **34**
Figure 4.2 : Storm tide vs. mean water depth for Gulf of Mexico. **35**
Figure 4.3 : Elevation of underside of deck vs. mean water depth for Gulf of Mexico. **35**
Figure 4.4 : Current profile. **36**
Figure 4.5 : Deck dead loads (kN). **37**
Figure 4.6 : Deck live loads (kN). **38**
Figure 4.7 : Wave load pattern parameters in SAP200 [12]. **39**
Figure 4.8 : Wave characteristics. **39**
Figure 4.9 : Current profile data. **40**
Figure 4.10 : Marine growth data. **40**
Figure 4.11 : Wave velocity wit current (m/s). **41**
Figure 4.12 : Example of wave plus current forces acting on members. **42**
Figure 5.1 : Selected cross sections for diagonal bracing system. **46**
Figure 5.2 : Capacity ratio for structural members for diagonal bracing system. **51**
Figure 5.3 : Selected cross sections for x-bracing system. **52**
Figure 5.4 : Capacity ratio for structural members for x-bracing system. **56**
Figure 5.5 : Selected cross sections for v-bracing system. **57**
Figure 5.6 : Capacity ratio of structural members for v-bracing system. **62**
Figure 5.7 : Selected cross sectionf for inverted v-bracing system. **63**
Figure 5.8 : Capacity ratio of structural members for inverted v-bracing system. **68**
Figure 5.9 : Selected cross sections for k-bracing system. **69**
Figure 5.10 : Capacity ratio of structural members for k-bracing system. **73**

Figure 6.1 : Force deformation relationship for circular hollow structural sections. **76**
Figure 6.2 : Axial force vs. axial deformation for circular hollow structural sections. **76**
Figure 6.3 : Generating nonlinear load case for 0^0 wave direction. **77**
Figure 6.4 : Generating nonlinear load case for 45^0 wave direction. **77**
Figure 6.5 : Generating nonlinear load case for 90^0 wave direction. **78**
Figure 6.6 : Base shear vs. top displacement curve for diagonal bracing system E_e^0. .... **79**
Figure 6.7 : Base shear vs. top displacement curve for diagonal bracing system E_e^{45}. **80**
Figure 6.8 : Base shear vs. top displacement curve for diagonal bracing system E_e^{90}. **80**
Figure 6.9 : Base shear vs. top displacement curve for diagonal bracing system. **81**
Figure 6.10 : Base shear vs. top displacement curve for x-bracing system E_e^0. .... **82**
Figure 6.11 : Base shear vs. top displacement curve for x-bracing system E_e^{45}. **83**
Figure 6.12 : Base shear vs. top displacement curve for x-bracing system E_e^{90}. **83**
Figure 6.13 : Base shear vs. top displacement curve for x-bracing system. **84**
Figure 6.14 : Base shear vs. top displacement curve for v-bracing system E_e^0. .... **85**
Figure 6.15 : Base shear vs. top displacement curve for v-bracing system E_e^{45}. **85**
Figure 6.16 : Base shear vs. top displacement curve for v-bracing system E_e^{90}. **86**
Figure 6.17 : Base shear vs. top displacement curve for v-bracing system. **87**
Figure 6.18 : Base shear vs. top displacement curve for inverted v-bracing system E_e^0. .... **87**
Figure 6.19 : Base shear vs. top displacement curve for inverted v-bracing system E_e^{45}. **88**
Figure 6.20 : Base shear vs. top displacement curve for inverted v-bracing system E_e^{90}. **89**
Figure 6.21 : Base shear vs. top displacement curve for inverted v-bracing system. **89**
Figure 6.22 : Base shear vs. top displacement curve for k-bracing system E_e^0. .... **90**
Figure 6.23 : Base shear vs. top displacement curve for k-bracing system E_e^{45}. **91**
Figure 6.24 : Base shear vs. top displacement curve for k-bracing system E_e^{90}. **91**
Figure 6.25 : Base shear vs. top displacement curve for k-bracing system. **92**
Figure 7.1 : Base shear vs. top displacement curve for all bracing systems. **94**

METOCEAN PUSHOVER ANALYSIS OF A JACKET-TYPE OFFSHORE PLATFORM WITH DIFFERENT BRACING SYSTEMS

SUMMARY

Today, as the human population increases, the need for energy increases accordingly. However, energy sources are limited. A result of this, people have started to get energy from different places. Oil and gas platforms are now installed in offshores around the world in order to exploit gas and oil from the under seafloor. These offshore platforms have hundreds of meter length and large structural members on the sea. Since offshore platforms are located on the water, many engineering problems occurs at the design process. In the design of offshore structures unlike onshore structures, extreme storm conditions are generally major considerations.

Offshore structures can be categorized in three main types. These are fixed offshore platforms, floating platforms and gravity structures. In this study, a jacket-type fixed offshore platform which has form of steel frames includes tubular legs, braces and beams is examined subjected to extreme storm conditions.

In this study, nonlinear metocean pushover analysis is performed with using a jacket-type offshore platform with different bracing configurations (diagonal, x-bracing, v bracing, inverted v-bracing and k-bracing) by using finite element software SAP2000. Therefore, five different structural models are used and the selection of the same type and size of columns, beams and diagonals are considered in order to take the equivalent qualities in the comparison of different bracing systems. The main aim of this study is to investigate and to compare the performances of different bracing systems for a jacket-type offshore platform subjected to 100-year extreme metocean conditions with different direction. The behavior of the platform with different bracing systems is examined under metocean pushover analysis. For all storm cases and all systems, ultimate platform resistances and reserve strength ratios are determined.

Due to insufficient national specifications and guidelines, international guidelines are used in this study. These are American Petroleum Institute (API) Recommended Practice and International Standards Organization (ISO) 19902. This study is mainly conducted in accordance with these two guidelines. Furthermore, DNV Recommended Practice helps the calculation of metocean loads acting on structures.

Metocean loadings (wave plus current) which may be dominated in the design of fixed offshore platforms are generally intensive, irregular, dynamic and cyclic loads and they may cause the platform to behave nonlinear. Although pushover analysis is extensively used for only the estimation of seismic performance of the structure, in the analysis of jacket-type offshore platform nonlinear pushover analysis is also applicable for the estimation of the performance of the structure on extreme storm conditions. In other words, nonlinear metocean pushover analysis is also well suited for analyzing offshore platforms after transforming dynamic loadings which can be identified by equivalent static loadings such as wave plus current forces.

In all structural models, the platform has four legs, 90 meters total height and the parts of 75 meters of the platform is on the water and also all framing have square forms. The deck of the platform is not modelled so the total dead load of 5000 tones is applied as vertical load on the four legs. In 3D model of the platform, non-structural members such as conductors, risers, and appurtenances should be developed because of the purpose of calculation of accurate wave/current forces. Therefore, local wave plus current forces should be calculated for both structural members and these non-structural members. Then, the global wave/current forces should be calculated with the summation of all local forces.

Additionally, the global stiffness of the platform does not change with the existence of non-structural members. They only contribute equivalent wave/current forces. In all 3D models of the platform, appurtenances are represented by 7 non-structural pipes with the diameter of 0.40 meter.

Metocean parameters mean both meteorological and oceanographic parameters. Metocean parameters should include 100-year storm data and should include several subjects. These are wave height, water depth, storm tide, deck elevation, wave direction, wave period, current profile and current direction. In all models, water depth, wave height, wave period, current speed, wave directions, current direction, storm tide and elevation of underside of the deck are 75 m, 20 m, 13 s, 1.08 ~ 0.85 m/s, 0^0 - 45^0 - 90^0, 0^0, 1 m, and 15 m respectively.

Before nonlinear metocean pushover analysis, linear analysis is performed to obtain geometric properties of the members and all structural members have sufficient strength according to LRFD method. The procedures are carried out according to AISC 360-10 LRFD method. In the result of linear analysis, CHSS1400x50, CHSS1200x30, and CHSS1000x30 are selected for columns, beams and braces, respectively. In nonlinear metocean pushover analysis, these sections are used to identify and compare the systems.

In order to represent platform nonlinearity, only axial force-axial deformation relationships are used for circular hollow sections according to ASCE41-17. After performing nonlinear metocean pushover analysis, reserve strength ratios of a jacket type offshore platform with 5 different bracing systems are determined for 3 wave directions and results are identified.

FARKLI ÇAPRAZ SİSTEMLİ CEKET TİPİ AÇIK DENİZ PETROL PLATFORMUNUN OKYANUSSAL YÜKLERLE STATİK İTME ANALİZİ

ÖZET

Günümüzde insan nüfusu arttıkça enerjiye olan ihtiyaç da artmaktadır. Ancak, her kaynak gibi enerji kaynakları da sınırlıdır. Bunun sonucunda insanlar farklı bölgelerden enerji elde etmeye başlamışlardır. Karadaki petrol ve gaz kaynaklarının sınırlılığı sebebiyle petrol ve gaz platformları, deniz tabanından gaz ve petrol çıkartabilmek için artık dünyanın dört bir yanındaki denizlerde ve okyanuslarda kurulmaktadır.

Bu açık deniz platformları yüzlerce metre uzunluğunda ve su içerisinde büyük yapısal elemanlara sahiptir. Açık deniz platformları su üzerinde olduğundan, tasarım aşamasında birçok mühendislik problemlerini birlikte getirir. Bir başka deyişle, kıyı yapılarının aksine açık deniz yapılarının tasarımında, ekstrem fırtına koşulları genellikle ana hususlardır.

Açık deniz platformları yapısal farklılıklarına göre üç ana türe ayrılabilir. Bunlar sabit deniz platformları, yüzer platformlar ve yerçekimi yapılarıdır. Bu çalışmada, çelik boru profillerin oluşturduğu çerçeveler ve çaprazlar içeren ceket tipi sabit açık deniz platformu, aşırı fırtına koşullarına tabi olarak incelenmiştir.

Bu çalışmada, sonlu elemanlar kullanılarak farklı çapraz sistemler (diyagonal, x-çapraz, v-çapraz, ters v-çapraz ve k-çapraz) ile ceket tipi bir açık deniz platformunun 3-D modeli üzerinde doğrusal olmayan metocean (metorolojik ve okyanussal) itme analizi SAP2000 programı ile yapılmıştır. Bu nedenle, beş farklı yapısal model kullanılmış olup farklı çapraz sistemlerinin karşılaştırılmasında, eşdeğer nitelikleri dikkate almak için aynı tip ve boyutta kolon, kiriş ve çapraz seçilmiştir. Bu çalışmanın temel amacı, tekrarlanma periyodu 100 yıl olan ekstrem metocean koşullara tabi tutulan ceket tipi bir açık deniz platformu için farklı çapraz sistemlerin performansını araştırmak ve karşılaştırmaktır. Çalışmada, tüm fırtına koşulları ve tüm çapraz sistemler için, nihai platform dayanımları, tepe yer değiştirmeleri ve rezerv mukavemet oranları belirlenmiştir.

Ulusal yönetmelik ve standartların yetersizliği nedeniyle, bu çalışmada uluslararası yönetmelikler kullanılmıştır. Bunlar Amerikan Petrol Enstitüsü (API) ve Uluslararası Standartlar Örgütü (ISO) 19902'dir. Bu çalışma esas olarak bu iki yönerge uyarınca yürütülmüştür. Ayrıca, Norveç DNV-C205 yönetmeliği, çevresel koşulların tahmini ve yapılara etki eden çevresel yüklerin hesaplanması için rehberlik sağlamıştır. Ek olarak, ulusal ve uluslararası çelik yapıların tasarımı, hesap ve yapım esaslarını içeren yönetmelikler, eleman dayanımlarının belirlenmesinde kullanılmıştır.

Sabit deniz platformlarının tasarımında önemli rol oynayabilen dalga ve akıntı yükleri genellikle yoğun, düzensiz, dinamik ve döngüsel yüklerdir ve platformun doğrusal olmayan davranışlar sergilemesine neden olabilirler. Doğrusal olmayan itme analizi, genellikle yapının sadece sismik performansının tahmini için yaygın olarak kullanılmasına rağmen, ceket tipi sabit açık deniz platformunun analizinde de, yapının

ekstrem fırtına koşullarındaki performansının tahmin edilmesi için de uygulanabilir. Başka bir deyişle, doğrusal olmayan metocean itme analizi, dalga ve akıntı kuvvetleri gibi eşdeğer statik yüklerle makul bir şekilde temsil edilebilen dinamik yüklere dönüştürdükten sonra bu yapıların davranışlarını analiz etmek için de uygundur.

Bu çalışmada 5 farklı 3 boyutlu model kullanılmıştır. Bu 5 modelde de, platformun toplam yüksekliği 90 metredir ve dört adet düşey taşıyıcıya sahiptir. Platformun 75 metrelik bölümü su içerisinde kalmaktadır. Ayrıca tüm çerçeveler kare formlara sahiptir. Platformun güvertesi doğrusal olmayan davranış sergilemesi beklenmediği için modellenmemiştir, bu nedenle 5000 tonun toplam güverte yükü olarak dört düşey taşıyıcı üzerine konsantre dikey yük olarak uygulanmıştır. Platformun tüm 3 boyutlu modellerinde, doğru şekilde dalga ve akıntı kuvvetlerinin hesaplanması amacıyla operasyon ekipmanları, yükselticiler ve ek parçalar gibi yapısal olmayan elemanlar da yer almalıdır. Bu nedenle, hem yapısal elemanlar hem de bu yapısal olmayan elemanlar için yerel dalga ve akıntı kuvvetleri hesaplanmalıdır. Daha sonra, global dalga ve ankıntı kuvvetleri tüm yerel kuvvetlerin vektör toplamı olarak hesaplanmalıdır. Fakat, yapısal olmayan elemanlar platformun genel rijitliğine katkıda bulunmazlar. Sadece eşdeğer dalga ve akıntı kuvvetlerine katkıda bulunurlar. Platformun tüm 3 boyutlu modellerinde, bu yapısal olmayan elemanlar, platform yüksekliği boyunca devam eden 0.40 metre çapında 7 adet boru ile temsil edilir.

Metocean parametreleri hem meteorolojik hem de okyanussal parametreler anlamına gelir. Metocean parametreleri 100 yıllık fırtına verilerini içermelidir. Bunlar dalga yüksekliği, su derinliği, fırtına gelgitleri, güverte yüksekliği, dalga yönü, dalga periyodu, akıntı profili ve akıntı yönüdür. Tüm modellerde, su derinliği, dalga yüksekliği, dalga periyodu, akıntı hızı, dalga yönleri, akıntı yönü, fırtına gelgit yüksekliği ve güverte alt kısım yüksekliği sırasıyla 75 m, 20 m, 13 s, 1.08 ~ 0.85 m/s, 0^0 - 45^0 - 90^0, 0^0, 1 m, ve 15 m alınmıştır.

Doğrusal olmayan metocean itme analizinden önce, elemanların geometrik özelliklerini belirlemek için doğrusal analiz yapılmıştır ve tüm yapısal elemanlar LRFD yöntemine göre yeterli mukavemete sahiptir. Çalışmada hesap adımları AISC 360-10 LRFD yöntemine göre yapılmıştır. Doğrusal analiz sonucunda, kolonlar, kirişler ve çaprazlar için sırasıyla CHSS1400x50, CHSS1200x30 ve CHSS1000x30 kesitlerindeki boru profiller uygun görülmüştür. Doğrusal olmayan metocean itme analizinde 5 farklı çapraz sistemini karşılaştırmak için tüm 3 boyutlu modellerde bu profiller kullanılmıştır.

Yapıya tüm düşey yükler etki ettirildikten sonra, dalga ve akıntı gibi yatay yükler her bir elemana (yapısal ve yapısal olmayan), elemanların konumuna, geometrik yapısına ve su altındaki pozisyonları gibi çeşitli faktörlere bağlı olarak farklı büyüklük ve dağılımlarda uygulanır. Daha sonra lineer olmayan bu yükler adım adım arttırılır. Her bir adımda yapının düğüm noktalarındaki yerdeğiştirmesi, eleman kuvvetleri, eleman rijitliği ve yapının global rijitliği güncellenir. Herhangi bir veya birkaç elemanda oluşan plastikleşme, yapının toptan göçmesini ima etmez ve yatay yükler arttırılarak uygulanmaya devam ettirilir. Yapı göçme durumuna geldiğinde ise, tepe yerdeğiştirmesi ve taban kesme kuvveti eğrileri elde edilebilir. Rezerv mukavemet oranı ise, göçme anında yapının tabanında oluşan kesme kuvvetinin, yapıya tekrarlanma periyodu 100 yıl olan fırtına yüklerinin oranı ile bulunabilir. Rezerv mukavemet oranları yapıya etki eden farklı yönlerdeki dalga yükleri için ayrı ayrı hesaplanmalıdır. Yapının nihai rezerv mukavemet oranı ise her bir yön için elde edilen rezerv mukavemet oranlarının en küçüğünü temsil eder.

Platform doğrusal olmayan davranışını temsil etmek için, ASCE41-17 yönetmeliğinde yer alan eksenel kuvvet-eksenel deformasyon ilişkileri kullanılmış olup, yığılı plastic mafsal hipotezi esas alınmıştır. Doğrusal olmayan metocean itme analizi yapıldıktan sonra, çalışmanın sonuç kısmında 3 dalga yönü için 5 farklı çapraz sisteme sahip ceket tipi sabit açık deniz platformunun rezerv mukavemet oranları belirlenmiş ve sonuçlar karşılaştırılarak irdelenmiştir.

1. INTRODUCTION

1.1 General Information

With the increase in the human population, the need of energy is increasing and as a result of this, people have started to get energy from different places. Nowadays, offshore structures are installed in bays, gulfs and oceans around the world in order to exploit gas and oil from the reservoirs. These structures which have hundreds of meter length may be made of concrete, steel or made of both steel and concrete.

Offshore structures generally consist of 4 main parts which are deck, jacket, piling and wells. Deck is the upper part of a platform that includes living quarters, process equipment, helideck, and working areas. The part consisting of structural members like columns, beam, and diagonals is called as jacket. The main responsibility of a jacket part is to transfer both vertical and lateral forces to the piles. Piling is used only in fixed type of offshore platforms. Piling is very important structural component of a platform in order to fix and stable a platform against sinking and overturning. Wells are appurtenances that drill and transport oil and gas.

Thanks to advance in offshore structure technology, the number of offshore structures tend to increase and today there are more than 7000 offshore structures with different types [1]. There are several kinds of offshore platforms depending on mainly the method of constructions and the depth of the water. Also, determination of types of offshore platform may be governed by government regulations, owner specifications, industry guidelines, functional requirements, site conditions, exposure categories, design life and safety considerations.

There are big differences between designing offshore and onshore structures. Environmental conditions are extremely important for analyzing and designing offshore platforms compared to onshore structures. Offshore structures that installed in water bring some engineering problems. Especially metocean (meteorological and oceanographic) loadings are always major concern for engineers. The complexity of dynamic behavior of metocean loadings makes the determination of the responses of offshore structures difficult. Fortunately, metocean pushover analysis is capable of to show the behavior of the platform subjected to hydrodynamic forces. Therefore, nonlinear pushover analysis is necessary to show that an offshore structure has adequate resistance against extreme metocean conditions.

1.2 Platform Types

1.2.1 Fixed platforms

1.2.1.1 Jacket-type platforms

Jacket-type offshore platforms are the platforms that extend above the sea level and they are fixed by pilings at the ocean floor. In order to fix the jacket part of the platform onto the seabed, the piles of the platforms can be penetrated into the soil (Figure 1.1).

The jacket-type platforms are generally installed in areas which have less than 400 m water depths.

Approximately ninety-five percent of the offshore structures in the world are jacket-type offshore platforms [2].

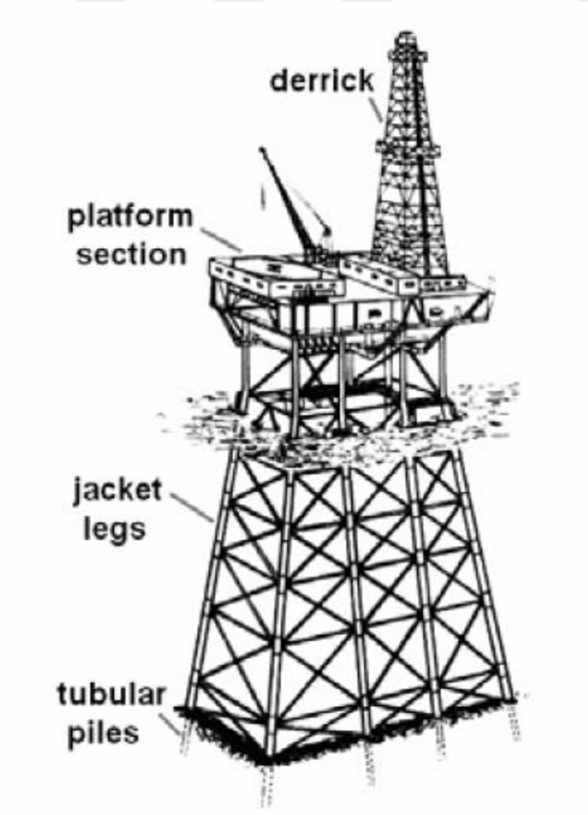

Figure 1.1 : Figure of jacket-type platform [3].

1.2.1.2 Compliant towers

The compliant tower offshore platforms are another type of fixed offshore structures. In these type platforms, the structural members consist of narrow and flexible frames. The compliant towers are suitable for areas which have less than 600 m water depths.

1.2.1.3 Gravity structures

Gravity structures are concrete structures that settle on the seabed instead of pilling to resist lateral loads with the help of the weight of the structures (Figure 1.2). Gravity structures are well-used in the locations which have at least 300 m water depths. The most important advantage of this type of platform is that it requires less repairs and maintenances.

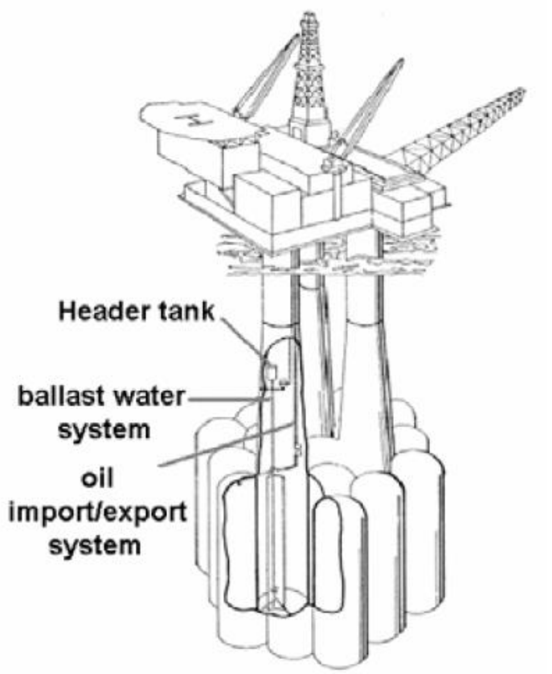

Figure 1.2 : Figure of gravity platform [3].

1.2.2 Floating platforms

These type of structures are not fixed. They are equipped with production and drilling equipment (Figure 1.3). Floating platforms may be used in the locations that have 600 m water depth to 2500 m water depth [4]. Tension leg platforms, spars, semisubmersibles and SPARS are the examples of floating platforms.

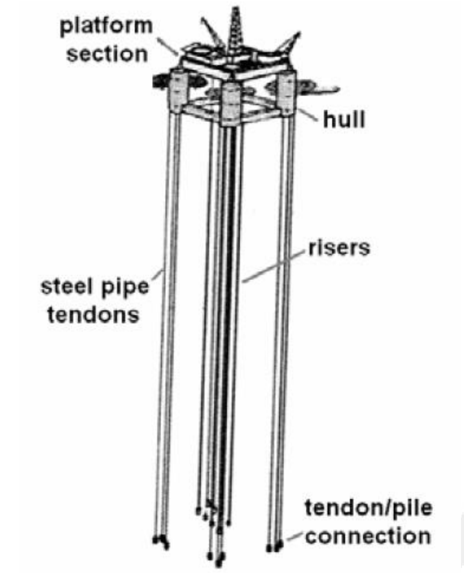

Figure 1.3 : Figure of tension leg platform [3].

1.3 Literature Review

In this section, previous studies about analysis of offshore platforms are reviewed. Some studies that may be relevant with the topic of this thesis and published in international journals are detailed below.

Sadeghi and Dilek (2019) published a study in Journal of Academic Research International. They basically introduced offshore platform types, related codes, and concept of analysis and design of offshore platform [1].

Bea (1996) published a study in Journal of Waterway, Port, Coastal, and Ocean Engineering. He studied inelastic behavior of offshore structures in extreme metocean conditions. According to Bea (1996), "Dynamic-transient loading effects from extreme storm waves can have important influences on the nonlinear ultimate limit state performance of fixed offshore platforms" (p.68). He also idealized the dynamic-transient wave loadings and performed static pushover analysis [5].

Raheem (2013) published a paper in Journal of Coupled Systems Mechanics and studied about linear response of a fixed jacket-type offshore platform subjected to nonlinear and time dependent wave plus current loading. He compared the top displacements of a jacket-type offshore platform with different load combinations that include current and wave loads separately and together. He found that the direction of the current has a fewer impact on the lateral displacement, while the wave direction plays a great effect on both the direction of displacement and the value of displacements [6].

The another study, published by Ishwarya, Arockiasamy and Senthil (2016) in Journal of Shipping and Ocean Engineering, is about inelastic behavior of fixed offshore structures. They examined platform response under seismic loading with different bracing systems and soil conditions. They also used both platform model with fixed end boundary condition and platform model with piles in order to determine effects of soil condition [7].

Mahar and Adnan (2018) published a study in American Journal of Innovative Research and Applied Sciences. They studied about linear response of a fixed jacket-type offshore platform with x-bracing system. They figured out the base shears and overturning moments of the platform with respect to linear analysis for different wave directions [8].

Tabandeh, Biria and Karimi (2018) found out reserve strength ratios of a platform with x-bracing system for different wave directions. They determined that whether the platform has sufficient strength or not according to international codes for each storm direction [9].

Das and Janardhan (2017) studied about the relationship between platform top displacement and water depth with using linear approaches. They also compared overturning moments and water depth of a jacket-type offshore platform with using different metocean data [10].

Nguyen and Sinsabvarodon (2015) published a research that involved nonlinear behaviour of a jacket-type platform for seismic forces and different bracing configurations. They studied with x-bracing, v-bracing and diagonal systems. They found out that the platform with x-bracing has highest performance against seismic loading [11].

1.4 Objective and Scope

In the literature, there are lots of studies which are related to the nonlinear response of jacket-type offshore platform. However, none of them compared to the reserve strength ratios of a platform with different bracing system subjected to metocean loads.

In this study, nonlinear metocean pushover analysis is studied with using three dimensional model of a jacket-type offshore platform with different bracing systems by using finite element software SAP2000 [12]. The main aim of this study is to investigate the performances of different bracing systems for a jacket-type offshore platform subjected to 100-year extreme metocean conditions with different direction. The behavior of the platform with different bracing systems is examined under metocean pushover analysis. For all storm cases and all systems, ultimate platform resistances and reserve strength ratios are determined. Furthermore, the base shear at collapse and for 100-year storm conditions and top displacements are obtained for each models.

In the scope of the study, the selection of the same type and size of columns, beams and diagonals are taken into account in order to consider the equivalent qualities in the comparison of different bracing systems. A total of 5 different structural models have been studied. These are diagonal bracing, X-bracing, inverted V-bracing, V-bracing and K-bracing systems.

In this study, before performing nonlinear metocean pushover analysis, sizes of structural members are determined by linear analysis with using appropriate loads and load combinations which are recommended in API [13], ISO 19902 [14] and DNV Recommended Practices [15]. The same sizes of the structural members determined as a result of the linear analysis are also used in nonlinear metocean pushover analysis for all bracing systems.

In all models, non-structural members such as appurtenances are also taken into account. They do not contribute to the overall stiffness of the structure. However, appurtenances should be modeled for the purpose of calculation of accurate environmental loadings.

Deck of the platform is not modelled because it is expected that all structural members of the deck part behaves linear-elastic so for the sake of simplicity, deck of the platform is considered as only gravity loads. Therefore, wind forces acting on the platform are neglected because of the absence of deck part of the platform. The buoyancy forces and transverse (lift) wave forces are also considered for each analysis.

In addition, for each bracing system metocean pushover analysis is performed for 3 different wave directions that are 0^0, 45^0, and 90^0 in x-y plane counter-clockwise direction.

2. THEORY AND SPECIFICATIONS

In Turkey, recently, there is no national specification or guideline for designing offshore platforms. Fortunately, there are two common international guidelines for designing the jacket-type offshore platforms. These are API Recommended Practice 2A WSD (American Petroleum Institute) [13], and ISO 19902 (International Standards Organization) [14] so this study is mainly conducted in accordance with these two guidelines. Furthermore, DNV [15] code helps for prediction of environmental loadings from metocean parameters.
Also, national and international steel design codes are used in this study.

2.1 Environmental Considerations

The safety of a platform based on the loads and the strength of the platform. The appropriate metocean parameters are needed for the representative environmental loads. According to both API and ISO guidelines, it is recommended that the recurrence interval of extreme environmental conditions for metocean design parameters should be 100 years. Therefore, in this study 100-year return period metocean parameters are considered. The main terms which are related to metocean criteria are clarified in API Recommended Practice 2A [13] and DNV Recommended Practice [15] as below.

2.1.1 Waves

Waves are an essential component of metocean loadings on the fixed offshore structures. Waves have generally nonuniform shapes that vary in height, amplitude, length and period like in Figure 2.1. Also, they may hit to an offshore structure from a single or more directions.

Furthermore, in the nature, the wave loadings are dynamic. However, they can be transformed to the static form with using wave theories.

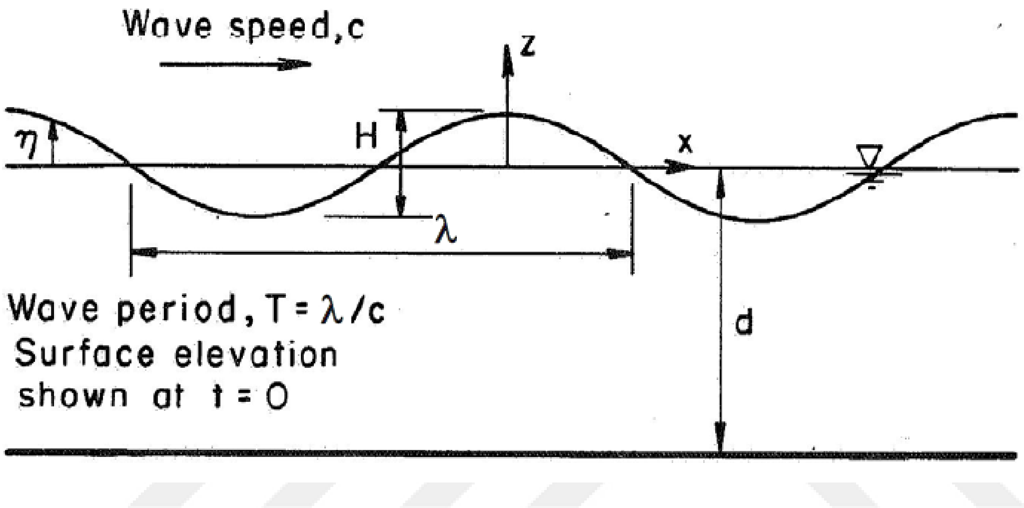

Figure 2.1 : Wave profile [15].

2.1.1.1 Transformation of dynamic wave loadings to the static loadings

Fıgure 2.2 shows the steps of the transformation of dynamic wave loading to the static wave loading with considering current actions. The process starts with a determination of 100-year metocean data [13].

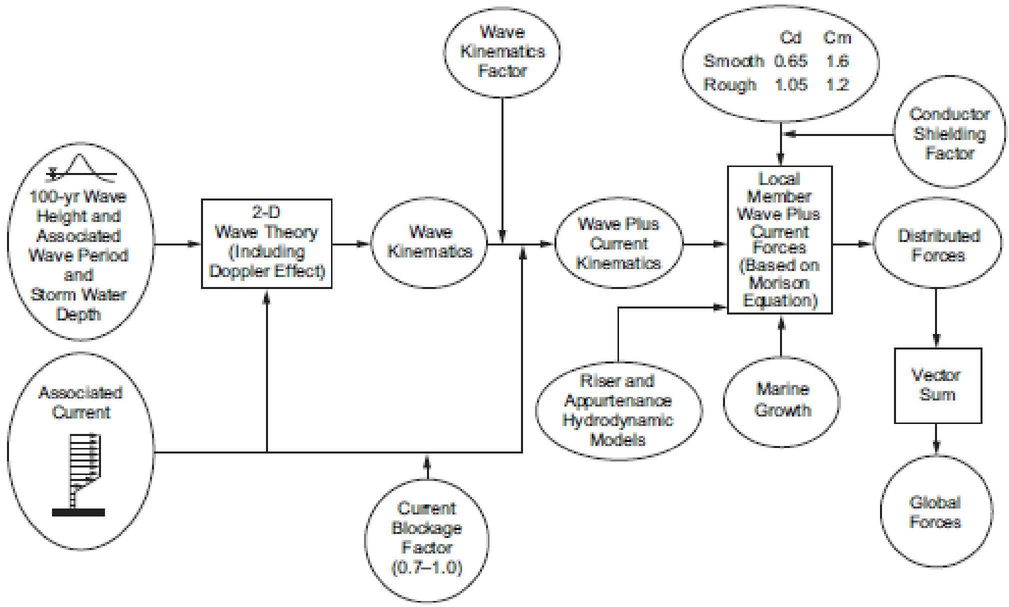

Figure 2.2 : Steps of the transformation of dynamic wave loadings to the static loadings [13].

According to API Recommended Practice 2A [13], the steps of the transformation of the static wave loadings are below.

- Firstly, the metocean parameters (wave period, wave height, water depth, etc.) should be determined.
- The wave kinematics should be determined with using proper wave theory for the metocean parameters.
- The velocity and accelerations can be decreased by multiplying wave kinematics factor.
- The current profile can be determined by using metocean parameters and the magnitude of current velocity can be reduced by using the current blockage factor.
- Member local forces can be obtained considering with marine growth. Member outer dimensions can be increased due to existence of marine growth.
- Depends on the shape of platforms, size of members, orientation of the members and existence of marine growth inertia and drag forces can be calculated.
- If the appurtanences exist, they can be considered in the model of the platform so the total metocean loading can be calculated more accurately.
- Finally, the total metocean loadings can be calculated.

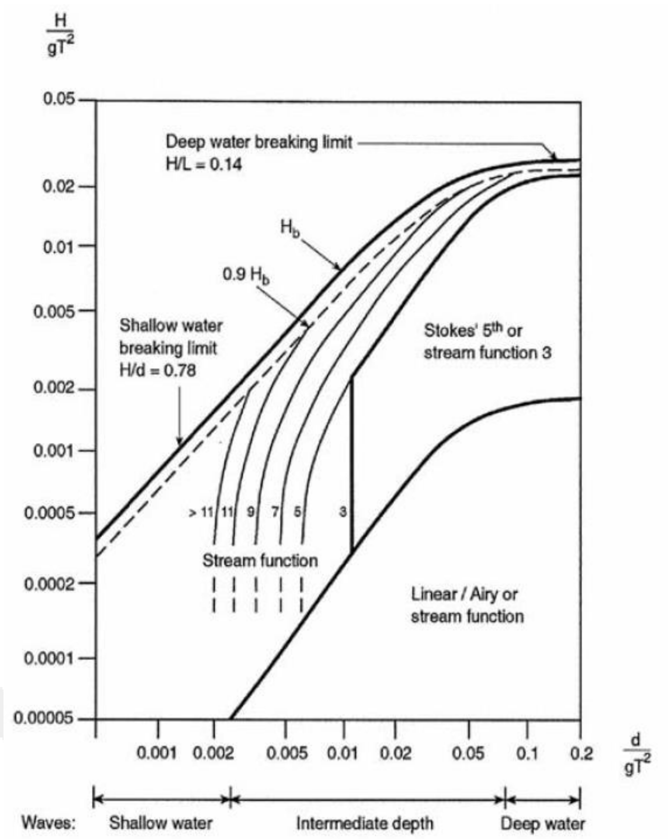

Figure 2.3 : Applicability of wave theories [15].

The kinematics of wave can be obtained from using proper wave theory. There are several wave theories available depending on mean water depth, wave period, wave height and breaking wave height. The applicability of the wave theories depending on shallowness and steepness of the waves are given in Figure 2.3. If stream function wave theory or Stokes fifth order wave theory is selected for obtaining the two-dimensional wave kinematics, the horizontal velocities and accelerations are multiplied with a wave kinematic factor. Wave kinematics factors are in the range of 0.85 to 1.00 depending on storm types (tropical or extra-tropical storm). In this study, Airy wave theory is selected and wave kinematics factor is taken as 1.00 because of assuming the occurrence of extra-tropical storm conditions.

The wave forces (drag plus inertia forces) can be obtained by using Morison's equation and equation 2.1.

$$F_W = F_D + F_I = C_d \frac{w}{2g} A_p U|U| + C_m \frac{w}{g} V \frac{\delta U}{\delta t} \tag{2.1}$$

The values of drag coefficient C_d and inertia coefficient C_m may be taken from equation 2.2 and 2.3. Also, Figure 2.4 shows drag and inertia forces acting on a rigid cylinder.

$$smooth \quad C_d = 0.65, C_m = 1.6 \tag{2.2}$$

$$rough \quad C_d = 1.05, C_m = 1.2 \tag{2.3}$$

Furthermore, the lift forces can develop due to waves [3]. The transverse (lift) wave force per unit length, f_L can be formulated as in equation 2.4.

$$f_L = \frac{1}{2}\rho C_L D U_m |U_m| \tag{2.4}$$

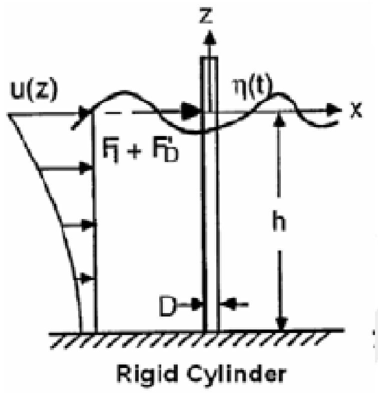

Figure 2.4 : Illustration of drag and inertia forces acting on a rigid cylinder [3].

2.1.2 Tide

Tide is another important issue in the design of platforms because the water depth must be determined properly. The water depth can change due to tides with depending on time.

Storm tide is called as the sum of positive storm surge, astronomical tide, and negative storm surge [15]. Figure 2.5 shows water levels and their definitions.

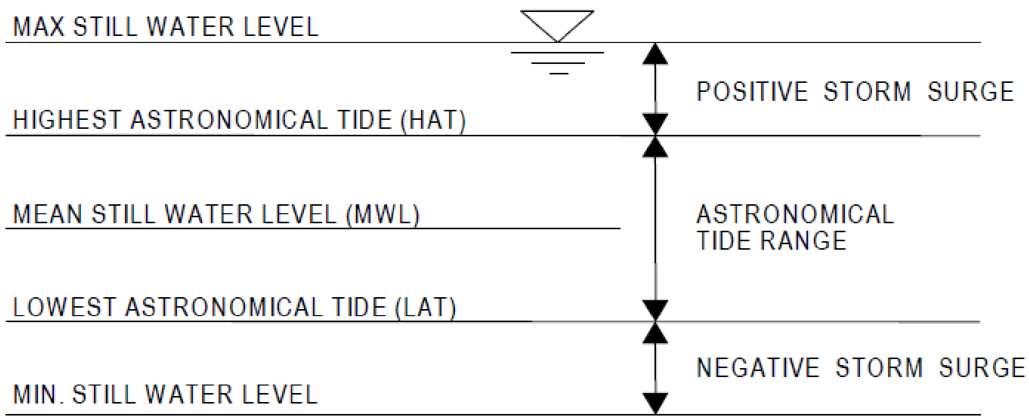

Figure 2.5 : Definition of water levels [15].

2.1.3 Current

Current is another significant consideration in the design of fixed offshore platforms because they affect platforms in both operational and structural concerns. For operational concerns, current forces may cause the determination of the location and orientation of the platform equipment such as boat landings and barge bumpers.

In order to evaluate current forces acting on the platform, site specific current profile is needed.

The current blockage factor is introduced when water particles pass by the platform instead of through the structure so the current speed within the structure is reduced. API document recommends that the range of current blockage factor is 0.70 to 1.00 depending on member configurations and number of legs. However, in this study, current blockage factor is neglected because in all cases diagonals have different configurations and their current blockage factors are different from each other. Therefore, current blockage factor is taken as 1.00 for each case.

2.1.4 Marine growth

Sea creatures may stick and stand on the surface of the members that below the water surface so the growth of marine increases the diameter and roughness of the members. If marine growth exists, the thickness of all structural and non-structural members such as appurtenances must be increased to take marine growth effects [13]. However, the increase in thickness should only be considered in the projected area of the members and it should not be cause the increase in the rigidity of the structure.

2.2 Method of Analysis

Jacket-type of platforms typically have tubular vertical, horizontal and diagonal members. These members carry both vertical and lateral loads acting on the platform and transfer these loads to the piles. These loads are gravity loads (dead and live) and environmental loads (earthquake, wind, wave, current, ice etc.). Although in many onshore structures earthquake loads are dominant loads to design the structures, in the design of fixed offshore structures metocean loads (wind, wave and current forces) can play major role. These metocean loads are generally intensive, irregular, dynamic and cyclic loads and they may cause the non-linear behavior of the platforms. Although nonlinear pushover analysis has been extensively used for only the estimation of seismic performance of the structure, in the analysis of jacket-type offshore platform nonlinear pushover analysis is also applicable for the estimation of the performance of the structure on extreme storm conditions. In other words, nonlinear metocean pushover analysis is also well suited for analyzing offshore platforms after transforming dynamic loadings to the static loadings like wave plus current forces.

2.2.1 Concept of non-linearity in jacket-type offshore structures

Each structural member in jacket-type offshore structures is expected to behave differently in the application of gravity and environmental loadings. They can be classified according to their expected behaviors.

- **Elastic members:** The many of the structural members in offshore structures are expected to have stresses less than their yield stresses in order to fulfill the operational and service requirements. These members would not be expected to approach their yield capacity during the non-linear pushover analysis. Members in upper part of the structure such as deck beams and girders are example of elastic members in jacket-type offshore platforms.
- **Brace members(inelastic):** The brace members generally have high slenderness and they are subjected to significant axial loads so they are expected to approach their yield capacity or buckling during the non-linear analysis [13].
- **Beam and column members(inelastic):** These members generally have low slenderness and they are subjected to high bending moments so it is expected that the plastic hinges in the ends of these members exist. Jacket legs (both vertical & horizontal members) and piles are examples for moment resisting members.
- **Foundations:** In order to detail pile-soil interaction analysis, the soil resistance including both lateral and axial soil resistances can be represented as nonlinear springs.

2.2.2 Force deformation relationship

Material nonlinearity is known as the inelastic behavior of a member. Inelastic behavior is generally represented by a force-deformation relationship and backbone curve. In non-linear analysis, force-deformation relationships should be properly defined in order to represent the nonlinearity of the structure for all structural members. The force displacement relationship is generally represented as assigning concentric plastic hinges where the end locations of frame members that are expected to occur the yielding. Plastification can be basically represented by nonlinear moment-curvature for beams, axial force-bending moment interaction for columns and axial force-axial deformation curve for brace members.

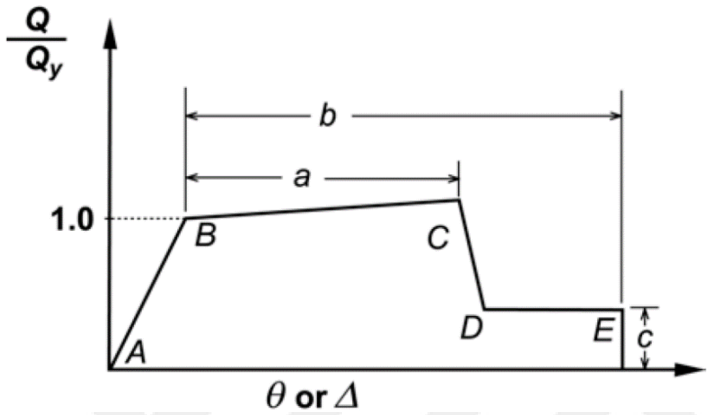

Figure 2.6 : Force and deformation relationship [16].

The force and deformation relationship curve is shown in Figure 2.6.

- Point A is the starting point and shows the origin.
- The region between point A and point B represents linear-elastic deformations.
- Yielding starts at point B and no plastic deformation occurs up to point B.
- Region a (between point B and C) shows strain-hardening with slope of 3% of the elastic slope. [16].
- The ultimate capacity for pushover analysis is reached at point C.
- A residual strength occurs after point C.
- Point E represents total failure of the structures.

The yield moment, yield rotation, yield axial force and yield deformation defined by FEMA-356 [9] are calculated as follows for beams, columns and braces.

Beams: $\theta_y = \frac{ZF_{ye}l_b}{6EI_b}$ $\quad M_y = ZF_{ye}$ (2.6)

Columns: $\theta_y = \frac{ZF_{ye}l_b}{6EI_b}(1-\frac{P}{P_{ye}})$ $\quad M_y = 1.18ZF_{ye}\left(1-\frac{P}{P_{ye}}\right) \leq ZF_{ye}$ (2.7)

Braces: $P_y = F_{ye}A$ $\quad \Delta_y = \frac{P_y l_{br}}{EA}$ (2.8)

There are two main approaches in explaining force-deformation relationships. These approaches may characterize the material nonlinearity. These are;

- **Monotonic Curve:** When a specified load is regularly applied to a member or a structure, a monotonic curve is introduced. Static pushover analysis is a nonlinear method analysis method that a specified load is progressively applied to a member so pushover analysis generates a monotonic curve. Monotonic force-deformation relationships may include stress-strain curves for axial loads, moment-curvature curves for flexure. Therefore, P-M2-M3 hinge is a best representation of nonlinearity for static pushover analysis.
- **Hysteretic Curve:** Hysteretic curve is another relationship type that expresses the material nonlinearity. When a cyclic loading is applied to a member or a structure, hysteretic loops are introduced. Hysteretic curve is generally used for determination of dynamic response of a member or a structure under application of a time-history record. The fiber hinge is suitable for modeling hysteretic dynamics.

Therefore, in this study, static pushover analysis is performed so monotonic curve approach is much more reasonable than hysteretic curve approach.

2.2.3 Nonlinear pushover analysis procedure

The model of the offshore platform is created in SAP2000 [12] software and all gravity (dead and live) loads are applied to the structure. Then, a lateral load pattern that includes wave, current, and wind forces is generated and applied to the members with different magnitudes and directions due to different geometry, orientations and water elevations. After that, nonlinear pushover load case is created and this load case is the application of metocean loading applied to the structure which is incremented in steps in any specific direction until whole collapse. The joint displacements and member forces are updated for each step. The stiffness matrix of the structure is obtained for each step. The yielding in any member is not the limit of the load-carrying capacity of the structure. When the stress in a structural member approaches the yield stress, plasticity stage starts. Plasticity reduces the stiffness of the platform and the loads are redistributed to the other members. This procedure is continued until the control displacement or whole collapse.

After performing pushover analysis local overstresses are acceptable. However, whole collapse is unacceptable. When the base shear-displacement curve is obtained, the reserve strength ratio of the platform may be easily found.

2.3 Reserve Strength Ratio (RSR)

Reserve strength ratio of a platform means the ratio of base shear at collapse to base shear at metocean loading for 100-year return period data. Overall reserve strength ratio of a platform is the lowest one for all directions considered. According to API Recommended Practice 2A [13], reserve strength ratio of new platforms should be at least 1.60. Reserve strength ratio can be calculated as in equation 2.5.

$$RSR = \frac{BS_{collapse}}{BS_{100}} \tag{2.5}$$

3. PLATFORM OVERVIEW

3.1 Material Properties

The expected yield coefficient and expected tensile coefficients are taken as 1.1 in equation 3.1 and equation 3.2, as with FEMA 356 Table 5-3 [16]. Table 3.1 shows the material properites of the platform and Table 3.2 show the parametric strain data. Also, Figure 3.1 shows the stress-strain curve.

$$F_{ye} = 1.1\, F_y = 1.1 * 275 * 10^3 = 302.5 * 10^3\ kN/m^2 \tag{3.1}$$

$$F_{ue} = 1.1\, F_u = 1.1 * 430 * 10^3 = 473 * 10^3\ kN/m^2 \tag{3.2}$$

Table 3.1 : Material properties.

Material	Steel – S275JR
Young's Modulus, E	2×10^8 kN/m^2
Shear Modulus, G	76.9×10^6 kN/m^2
Poisson's Ratio, ν	0.3
Steel Density, ρ_{steel}	78.5 kN/m^3
Yield Stress, F_y	275×10^3 kN/m^2
Expected Yield Stress, F_{ye}	302.5×10^3 kN/m^2
Ultimate Stress, F_u	430×10^3 kN/m^2
Expected U Stress, F_{ue}	473×10^3 kN/m^2

Table 3.2 : Parametric strain data.

Strain at Onset of Strain Hardening	0.015
Strain at Maximum Stress	0.11
Strain at Rupture	0.17
Final Slope	-0.1

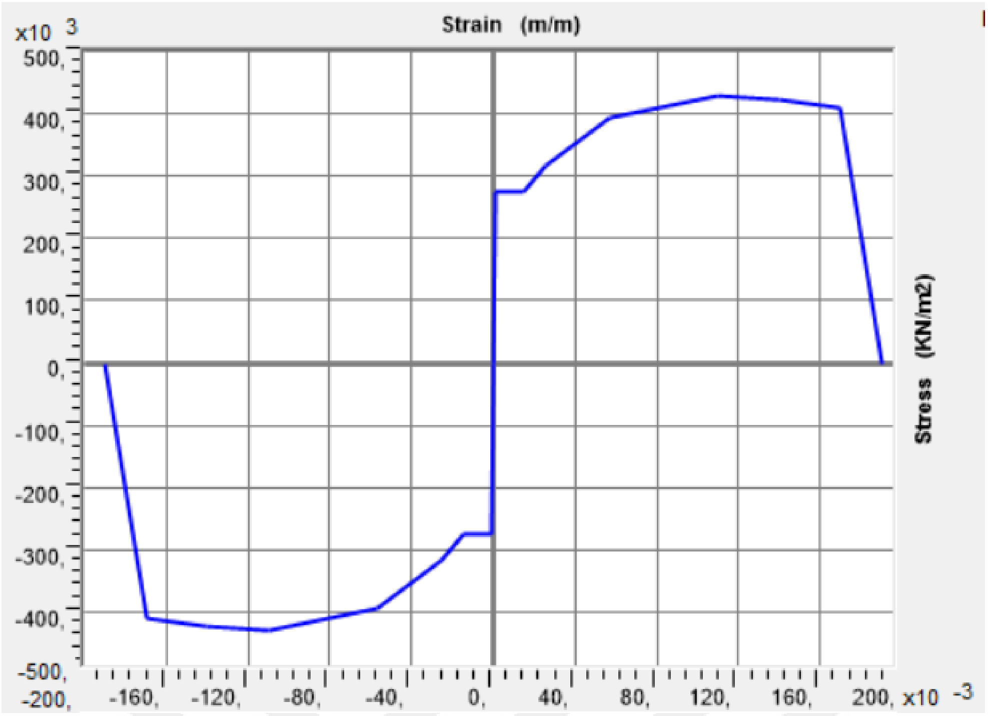

Figure 3.1 : Stress-strain curve.

3.2 Platform Properties

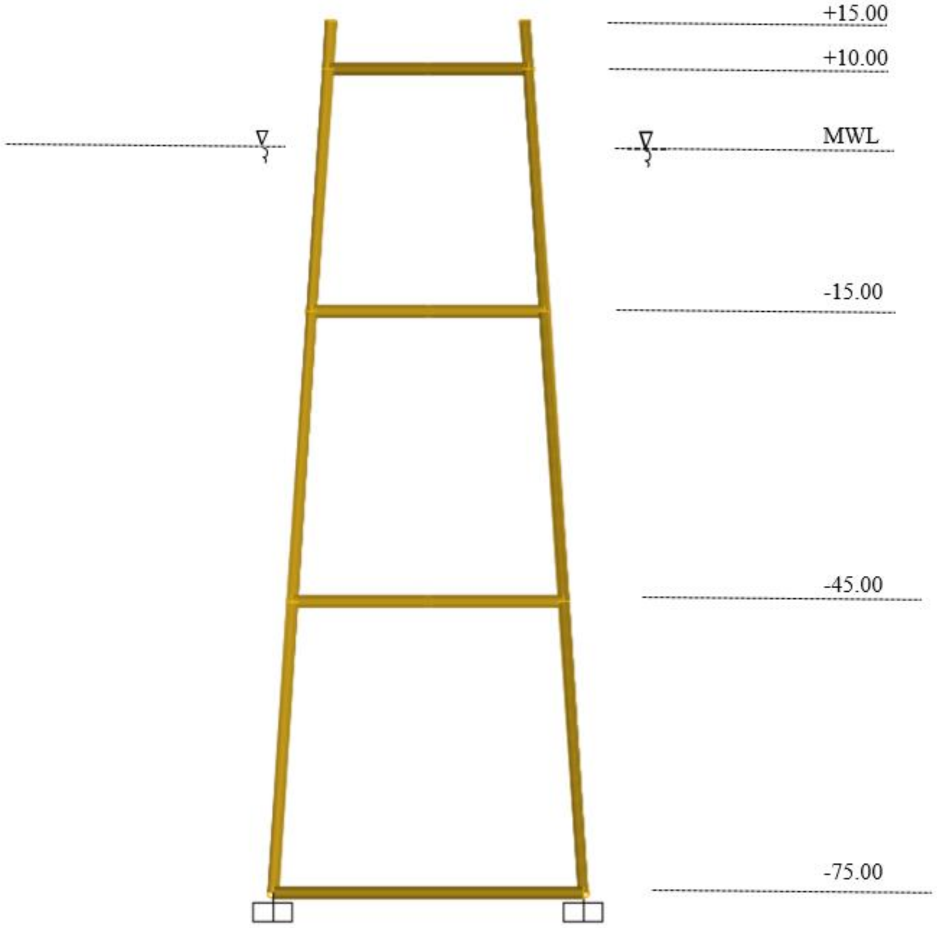

Figure 3.2 : Elevation view of bare model.

Figure 3.2 shows the elevations of the bare platform and these elevations and dimensions are considered for all configurations in this study. Total height of the platform is 90 meters and the platform has square form for x-y plane. The deck of the platform is not modelled so the dead load of 5000 tones is applied to the columns. Table 3.3. shows the summary of the geometric properties of the platform.

Table 3.3 : Platform geometric properties.

Number of Vertical Legs	4
Platform Total Height (m)	90.00
Top Elevation (m)	+15.00
Top Framing Elevation (m)	+10.00
Top Framing Dimensions in Plan (m)	20.67 x 20.67
Second Framing Elevation (m)	-15.00
Second Framing Dimensions in Plan (m)	24.00 x 24.00
Third Framing Elevation (m)	-45.00
Third Framing Dimensions in Plan (m)	28.00 x 28.00
Bottom Framing Elevation (Mud-line) (m)	-75.00
Bottom Framing Dimensions in Plan (m)	32.00 x 32.00
Mass of the Deck (t)	5000

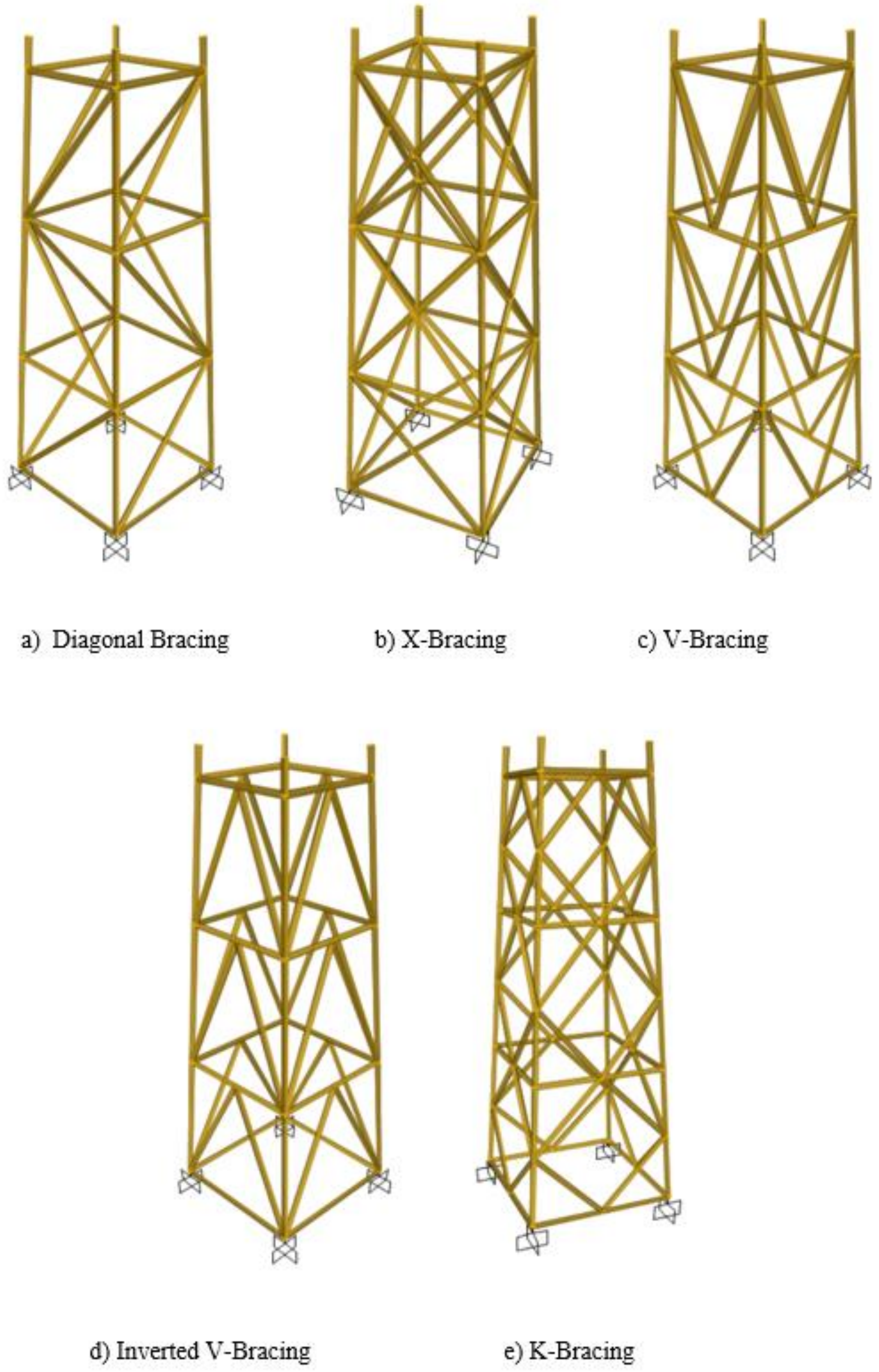

Figure 3.3 : Bracing configuration.

Figure 3.3 shows five different bracing configurations that include diagonal bracing, x-bracing, v-bracing, inverted v-bracing and k-bracing.

3.3 Nonstructural Members

In 3D model of the platform, non-structural members such as conductors, risers, and appurtenances should be developed because of the purpose of calculation of accurate wave/current forces. Therefore, local wave plus current forces should be determined for both structural members and these non-structural members. Then, the global wave/current forces should be calculated as the summation of all the local forces.

Nonstructural members like appurtanences do not increase the overall stiffness of the platform. They only contribute equivalent wave/current forces.

In all 3D models of the platform, appurtenances are represented by 7 non-structural pipes with the diameter of 0.40 meter (Figure 3.4).

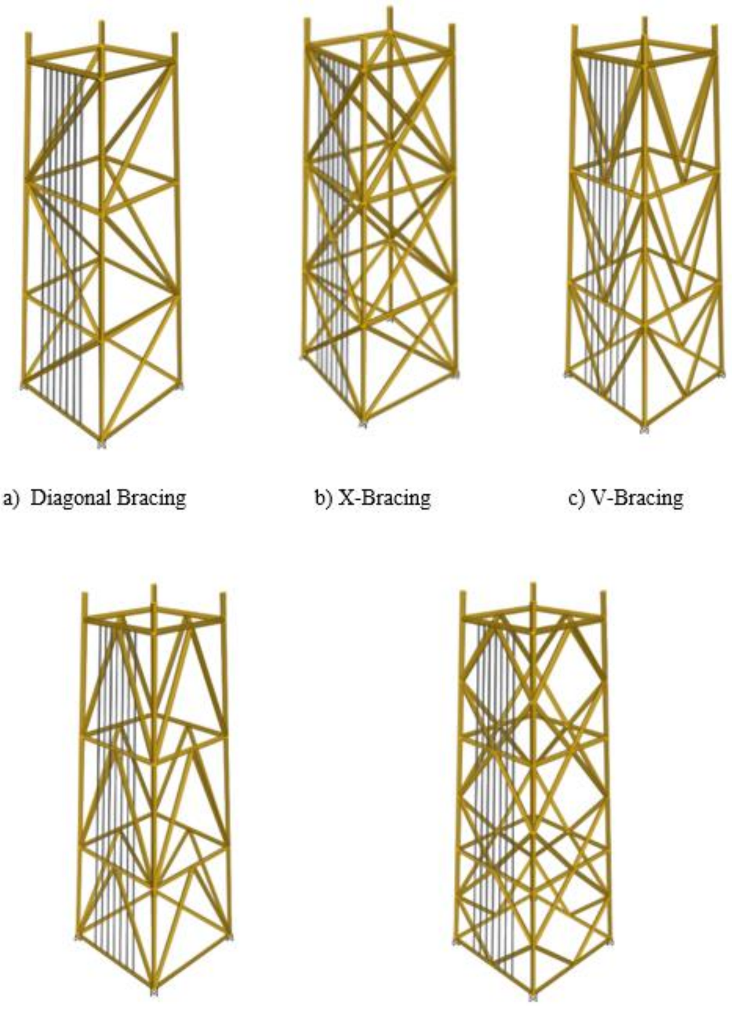

a) Diagonal Bracing b) X-Bracing c) V-Bracing

d) Inverted V-Bracing e) K-Bracing

Figure 3.4 : Bracing configuration with appurtenances.

3.4 Determination of Geometric Properties of Members

AISC 360-10 [17] specification prepared by the American Steel Structures Institute is among the most widely used regulations in the steel structure design. With the help of this specification, the design method is among the topics that should be decided first when designing the steel structure. There are basically two main methods, these are allowable stress design (ASD) and load and resistance factor design (LRFD)

Before performing metocean pushover analysis, linear preliminary analysis can be done in order to obtain geometric properties of the structural members. In this study, the preliminary design of the steel offshore platform is performed with LRFD method. General equation for LRFD method is;

$$\Phi R_n \geq \ R_u = \sum \gamma i Q i \tag{3.3}$$

According to equation 3.3, strength of a member should be at least equal to or greater than the increased loads.

In order to obtain cross sections of the columns and beams, firstly, the properties of the selected sections should be examined and then capacity controls should be performed. The steps to be followed with AISC 360-10 [17] are summarized below.

3.4.1 Class of sections

All steel members can be classified according to their width to thickness ratios and loading conditions (compression and flexure). If a steel member is subjected to axial compression, member can be classified as non-slender member or slender member (Figure 3.5 and Figure 3.6). If a member is subjected to flexure, member can be classified as non-compact, compact or slender member [18].

	Case	Description of Element	Width-to-Thickness Ratio	Limiting Width-to-Thickness Ratio λ_r (nonslender/slender)	Examples
Unstiffened Elements	1	Flanges of rolled I-shaped sections, plates projecting from rolled I-shaped sections, outstanding legs of pairs of angles connected with continuous contact, flanges of channels, and flanges of tees	b/t	$0.56\sqrt{\frac{E}{F_y}}$	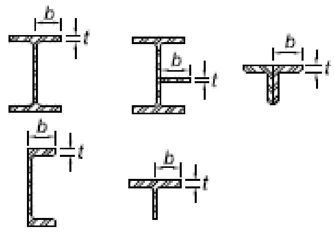
	2	Flanges of built-up I-shaped sections and plates or angle legs projecting from built-up I-shaped sections	b/t	$0.64\sqrt{\frac{k_c E}{F_y}}$ [a]	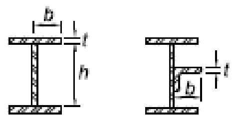
	3	Legs of single angles, legs of double angles with separators, and all other unstiffened elements	b/t	$0.45\sqrt{\frac{E}{F_y}}$	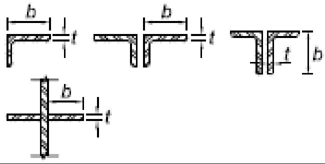
	4	Stems of tees	d/t	$0.75\sqrt{\frac{E}{F_y}}$	
Stiffened Elements	5	Webs of doubly symmetric rolled and built-up I-shaped sections and channels	h/t_w	$1.49\sqrt{\frac{E}{F_y}}$	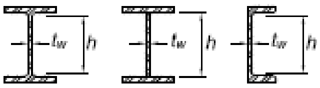
	6	Walls of rectangular HSS	b/t	$1.40\sqrt{\frac{E}{F_y}}$	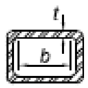
	7	Flange cover plates and diaphragm plates between lines of fasteners or welds	b/t	$1.40\sqrt{\frac{E}{F_y}}$	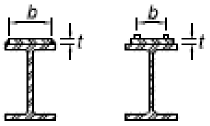
	8	All other stiffened elements	b/t	$1.49\sqrt{\frac{E}{F_y}}$	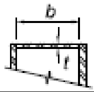
	9	Round HSS	D/t	$0.11\frac{E}{F_y}$	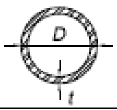

[a] $k_c = 4/\sqrt{h/t_w}$, but shall not be taken less than 0.35 nor greater than 0.76 for calculation purposes.

Figure 3.5 : Limit of slenderness ratios of different shape of steel members for compression members [18].

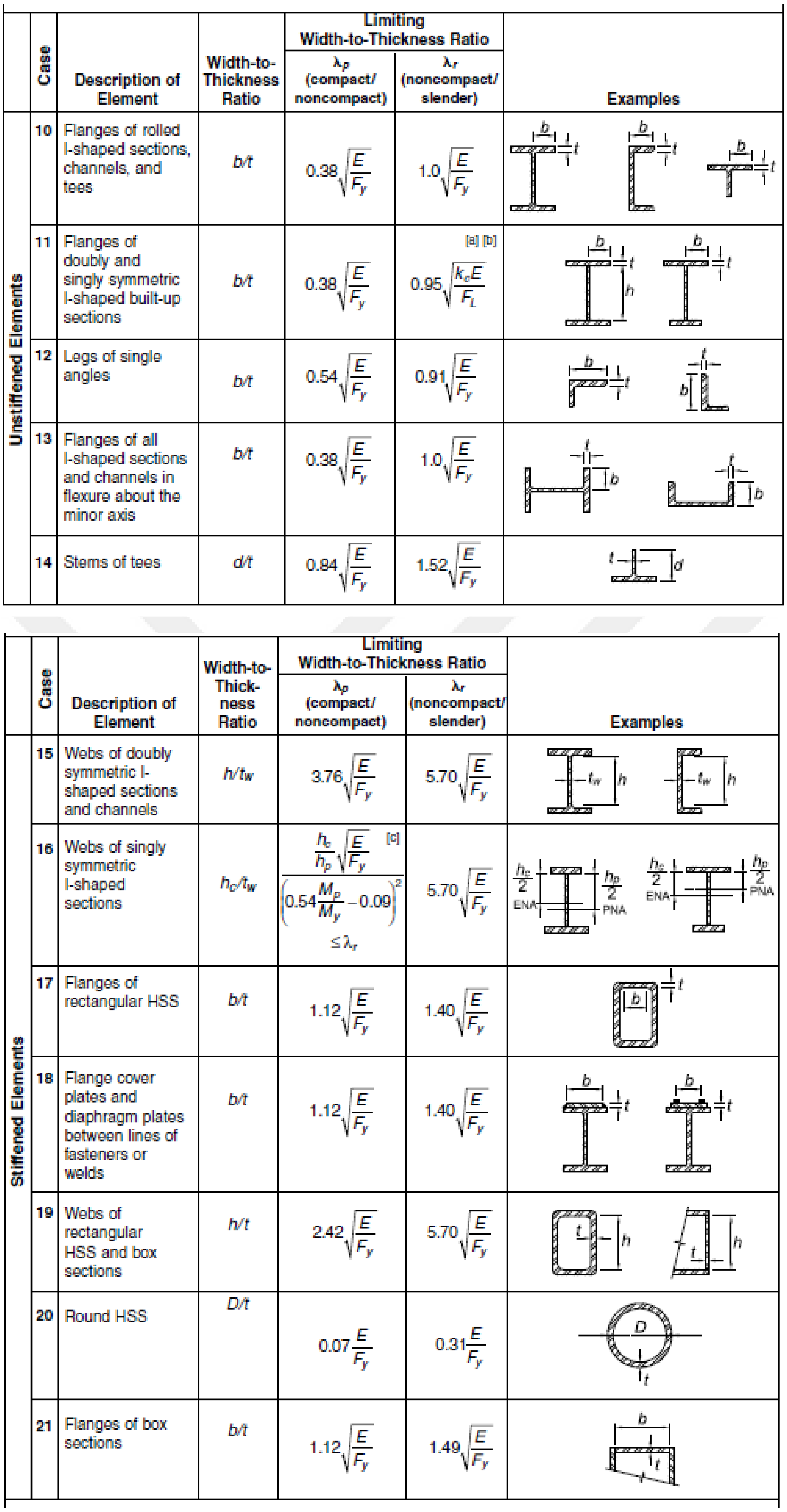

	Case	Description of Element	Width-to-Thickness Ratio	Limiting Width-to-Thickness Ratio λ_p (compact/noncompact)	Limiting Width-to-Thickness Ratio λ_r (noncompact/slender)	Examples
Unstiffened Elements	10	Flanges of rolled I-shaped sections, channels, and tees	b/t	$0.38\sqrt{\frac{E}{F_y}}$	$1.0\sqrt{\frac{E}{F_y}}$	
	11	Flanges of doubly and singly symmetric I-shaped built-up sections	b/t	$0.38\sqrt{\frac{E}{F_y}}$	[a] [b] $0.95\sqrt{\frac{k_c E}{F_L}}$	
	12	Legs of single angles	b/t	$0.54\sqrt{\frac{E}{F_y}}$	$0.91\sqrt{\frac{E}{F_y}}$	
	13	Flanges of all I-shaped sections and channels in flexure about the minor axis	b/t	$0.38\sqrt{\frac{E}{F_y}}$	$1.0\sqrt{\frac{E}{F_y}}$	
	14	Stems of tees	d/t	$0.84\sqrt{\frac{E}{F_y}}$	$1.52\sqrt{\frac{E}{F_y}}$	

	Case	Description of Element	Width-to-Thickness Ratio	Limiting Width-to-Thickness Ratio λ_p (compact/noncompact)	Limiting Width-to-Thickness Ratio λ_r (noncompact/slender)	Examples
Stiffened Elements	15	Webs of doubly symmetric I-shaped sections and channels	h/t_w	$3.76\sqrt{\frac{E}{F_y}}$	$5.70\sqrt{\frac{E}{F_y}}$	
	16	Webs of singly symmetric I-shaped sections	h_c/t_w	$\dfrac{\frac{h_c}{h_p}\sqrt{\frac{E}{F_y}}}{\left(0.54\frac{M_p}{M_y}-0.09\right)^2} \le \lambda_r$ [c]	$5.70\sqrt{\frac{E}{F_y}}$	
	17	Flanges of rectangular HSS	b/t	$1.12\sqrt{\frac{E}{F_y}}$	$1.40\sqrt{\frac{E}{F_y}}$	
	18	Flange cover plates and diaphragm plates between lines of fasteners or welds	b/t	$1.12\sqrt{\frac{E}{F_y}}$	$1.40\sqrt{\frac{E}{F_y}}$	
	19	Webs of rectangular HSS and box sections	h/t	$2.42\sqrt{\frac{E}{F_y}}$	$5.70\sqrt{\frac{E}{F_y}}$	
	20	Round HSS	D/t	$0.07\frac{E}{F_y}$	$0.31\frac{E}{F_y}$	
	21	Flanges of box sections	b/t	$1.12\sqrt{\frac{E}{F_y}}$	$1.49\sqrt{\frac{E}{F_y}}$	

Figure 3.6 : Limit of slenderness ratios of different shape of steel members for flexural members [18].

- **Slender Sections:** In this section, elastic buckling occurs without plastification subjected to compression. If $\lambda > \lambda_r$, then section is slender. According to Figure 3.5 and 3.6 slenderness of a member can be determined.
- **Compact Sections:** Plastification occurs without local buckling. If $\lambda \leq \lambda_p$, then section is compact.
- **Non-compact Sections:** Plastification partially occurs under compression and inelastic buckling occurs before fully plastic stage. If $\lambda_p < \lambda \leq \lambda_r$, then section is compact.

3.4.2 Tensile strength

In an element subjected to axial tensile force, the following condition must be satisfied.

$$\Phi_t P_n \leq P_a \tag{3.4}$$

Nominal tensile strength in the gross section,

$$P_n = F_y A_g \tag{3.5}$$

According to LRFD method nominal tensile strength,

$$\Phi_t P_n = 0.90 P_n \tag{3.6}$$

Fracture in the net section,

$$P_n = F_u A_n \tag{3.7}$$

According to LRFD method fracture in the section,

$$\Phi_t P_n = 0.75 P_n \tag{3.8}$$

3.4.3 Strength of structural steel under shear

If an element is under the shear force, the following formulations must be considered.

$$\Phi_v V_n \leq V_a \tag{3.9}$$

$$V_n = 0.6 F_y A_w C_v \tag{3.10}$$

The shear capacity of a steel member that has a circular hollow cross section can be calculated according to equation 3.11, 3.12 and 3.13.

$$V_n = F_{cr} A_g / 2 \tag{3.11}$$

where F_{cr} should be taken as the higher value of the equation 3.12 and 3.13.

$$F_{cr} = \frac{1.60E}{\sqrt{\frac{L_v}{D}}\left(\frac{D}{t}\right)^{\frac{5}{4}}} \tag{3.12}$$

and

$$F_{cr} = \frac{0.78E}{\left(\frac{D}{t}\right)^{\frac{3}{2}}} \tag{3.13}$$

but F_{cr} should not be higher than $0.6F_y$ [18].

3.4.4 Compressive strength

In an element subjected to axial compressive force, the following condition must be satisfied.

$$\Phi_c P_n \leq P_c \tag{3.14}$$

Axial compressive strength in the gross section

$$P_n = F_{cr} A_g \tag{3.15}$$

where F_{cr} shall be

$$\text{if } KL/r \leq 4.71\sqrt{\frac{E}{F_y}} \qquad F_{cr} = (0.658)^{\frac{F_y}{F_e}} \tag{3.16}$$

$$\text{if } KL/r > 4.71\sqrt{\frac{E}{F_y}} \qquad F_{cr} = 0.877\, F_e \tag{3.17}$$

and where F_e shall be

$$F_e = \frac{\pi^2 E}{\left(\frac{KL}{r}\right)^2} \tag{3.18}$$

Table 3.4 : Effective length factors of structural members.

Situation	Effective Length Factor, K
Superstructure Legs (braced)	1.0
Main Braces	0.8
K-Braces	0.8
X-Braces	0.9
Horizontals	0.7

Table 3.4 is taken from API Recommended Practice 2A [13] and this table shows effective length factor of structural members for jacket-type offshore structures. According to this table, effective length factors are taken as 1.0, 0.9, 0.8, and 0.7 for jacket legs(columns), X braces, braces and horizontals(beams) respectively in this study.

3.4.5 Flexural strength

3.4.5.1 Flexural strength of I-shaped member

The flexural capacity of a I-shaped steel member can be calculated according to following equations considering with lateral torsional buckling. [18].

Yielding,

$$M_n = M_p = F_y Z_x \tag{3.19}$$

Lateral torsional buckling can be considered,

If $L_b \leq L_p$, lateral torsional buckling is not the case.

If $L_p < L_b \leq L_r$, the moment capacity of a I-shaped steel member can be obtained from equation 3.20.

$$M_n = C_b[M_p - \left(M_p - 0.7F_y S_x\right)\left(\frac{L_b - L_p}{L_r - L_p}\right)] \leq M_p \tag{3.20}$$

If $L_b > L_r$, the moment capacity of a I-shaped steel member can be obtained from equation 3.21.

$$M_n = F_{cr} S_x \leq M_p \tag{3.21}$$

where L_b, the length between braced points against lateral displacement of the member or braced points against twisting.
where F_{cr},

$$F_{cr} = \frac{C_b \pi^2}{(\frac{L_b}{r_{ts}})^2} \sqrt{1 + 0.078 \frac{Jc}{S_x h_0} (\frac{L_b}{r_{ts}})^2} \tag{3.22}$$

where L_p, can be determined from equation 3.23.

$$L_p = 1.76 r_y \sqrt{\frac{E}{F_y}} \tag{3.23}$$

where L_r, can be obtained with the help of equation 3.24, 3.25 and 3.26.

$$L_r = 1.95 r_{ts} \frac{E}{0.7F_y} \sqrt{\frac{Jc}{S_x h_0} + \sqrt{\left(\frac{Jc}{S_x h_0}\right)^2 + 6.76 \left(\frac{0.7F_y}{E}\right)^2}} \tag{3.24}$$

$$r_{ts}{}^2 = \frac{\sqrt{I_y C_w}}{S_x} \tag{3.25}$$

$$C_b = \frac{12.5 M_{max}}{2.5 M_{max} + 3M_A + 4M_B + 3M_C} \tag{3.26}$$

3.4.5.2 Flexural strength of the circular hollow sections

If slendernesss ratio(the ratio of outer diameter to thickness) of a steel tube is lesser than $\frac{0.45\mathrm{E}}{F_y}$, then the flexural capacity of this member can be calculated as following equations with considering the classification of the member.
Yielding,

$$M_n = M_p = F_y Z \tag{3.27}$$

If the class of the circular hollow section member is compact section, local buckling is not observed.
If the class of the circular hollow section member is non-compact section, the flexural capacity of the member can be determined by using equation 3.28.

$$M_n = \left[\frac{0.021E}{\left(\frac{D}{t}\right)} + F_y\right] S \tag{3.28}$$

If the class of the circular hollow section member is slender section, the flexural capacity of the member can be determined by using equation 3.29 and equation 3.30.

$$M_n = F_{cr}S \tag{3.29}$$

where F_{cr},

$$F_{cr} = \frac{0.33E}{\left(\frac{D}{t}\right)} \tag{3.30}$$

3.4.6 Torsional capacity of the circular hollow sections

The design torsional capacity, $\Phi_T T_n$, for the members with circular hollow sections can be calculated according to equation 3.31.

$$T_n = F_{cr}C \tag{3.31}$$

According to LRFD method design torsional strength,

$$\Phi_T T_n = 0.90T_n \tag{3.32}$$

where C,

$$C = \frac{\pi(D-t)^2 t}{2} \tag{3.33}$$

The critical stress, F_{cr}, should be taken the larger value of the solutions of the equations 3.34 and 3.35.

$$F_{cr} = \frac{1.23E}{\sqrt{\frac{L}{D}}\left(\frac{D}{t}\right)^{3/2}} \tag{3.34}$$

and

$$F_{cr} = \frac{0.60E}{\left(\frac{D}{t}\right)^{\frac{3}{2}}} \tag{3.35}$$

However, the critical stress, F_{cr}, should not be larger than the 60% of the yield stress of the member.

3.4.7 Round HSS members subjected to combined forces

If the design torsion is lesser than 20% of the torsional capacity of a member, the shear and torsional effects may be neglected [18].

if $\frac{P_r}{P_c} \geq 0.20$ $$\frac{P_r}{P_c} + \frac{8}{9}\left(\frac{M_{rx}}{M_{cx}} + \frac{M_{ry}}{M_{cy}}\right) \leq 1.0 \tag{3.36}$$

if $\frac{P_r}{P_c} < 0.20$ $$\frac{P_r}{2P_c} + \left(\frac{M_{rx}}{M_{cx}} + \frac{M_{ry}}{M_{cy}}\right) \leq 1.0 \tag{3.37}$$

If the design torsion is larger than 20% of the torsional capacity of a member, the shear and torsional effects should be considered [18].

$$\left(\frac{P_r}{P_c}+\frac{M_r}{M_c}\right)+\left(\frac{V_r}{V_c}+\frac{T_r}{T_c}\right)^2 \leq 1.0 \tag{3.38}$$

4. METOCEAN CRITERIA AND LOADS

4.1 Metocean Criteria

Metocean parameters mean both meteorological and oceanographic parameters. Metocean parameters should include 100-year storm data and should includes the below subjects.

- Omni-directional wave height
- Storm tide
- Deck elevation vs. mean water depth
- Wave direction
- Wave period
- Mean water depth
- Current profile and directions

In API Recommended Practice 2A [13] there are detailed metocean parameters for Gulf of Mexico region, US. Therefore, in this study, for the purpose of realistic analysis, metocean parameters are taken from API Recommended Practice 2A [13] and metocean criteria in Gulf of Mexico, US is used. So that API [13] document is very beneficial to get reasonable environmental loads.

4.1.1 Determination of metocean criteria

Table 4.1 : Determination of metocean criteria [13].

Parameter	L-1 High Consequence	L-2 Medium Consequence	L-3 Low Consequence
Wave height, ft	Figure 2.3.4-3	Figure 2.3.4-3	Figure 2.3.4-3
Wave direction	Figure 2.3.4-4	Figure 2.3.4-4	Omnidirectional
Current direction	Figure 2.3.4-5	Figure 2.3.4-5	Omnidirectional
Storm tide, ft	Figure 2.3.4-7	Figure 2.3.4-7	Figure 2.3.4-7
Deck elevation, ft	Figure 2.3.4-8	Figure 2.3.4-8	Figure 2.3.4-8
Current speed, knots	2.1	1.8	1.4
Wave period, sec	13.0	12.4	11.6
Wind speed (1-hr @ 10 m), knots	80	70	58

Table 4.1 shows Gulf of Mexico metocean criteria. It is taken form API Recommended Practice 2A [13]. In this study, high consequence (L-1) of failure category is preferred. Table 4.1 leads the study procedure and the metocean parameters are determined according to this table.

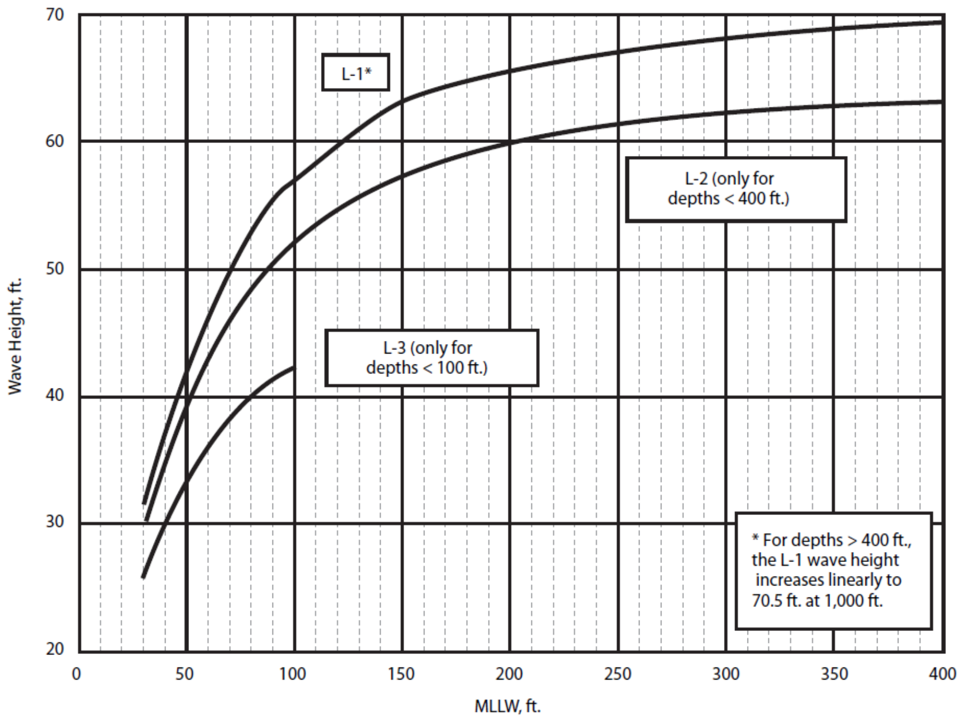

Figure 4.1 : Omnidirectional wave height vs. mean water depth for Gulf of Mexico.

- Mean water depth of the platform = 75 m = 246 ft.
- From Figure 4.1 wave height = 66 ft. = 20 m for L-1 high consequence of failure category.

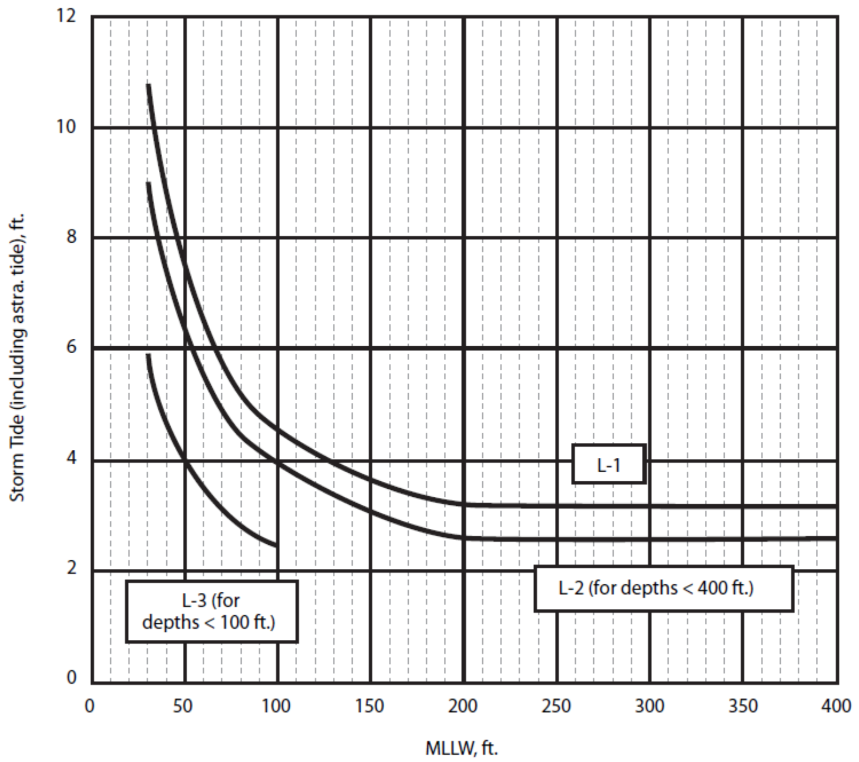

Figure 4.2 : Storm tide vs. mean water depth for Gulf of Mexico.

- Mean water depth of the platform = 75 m = 246 ft.
- From Figure 4.2 storm tide = 3.2 ft. = 1.0 m

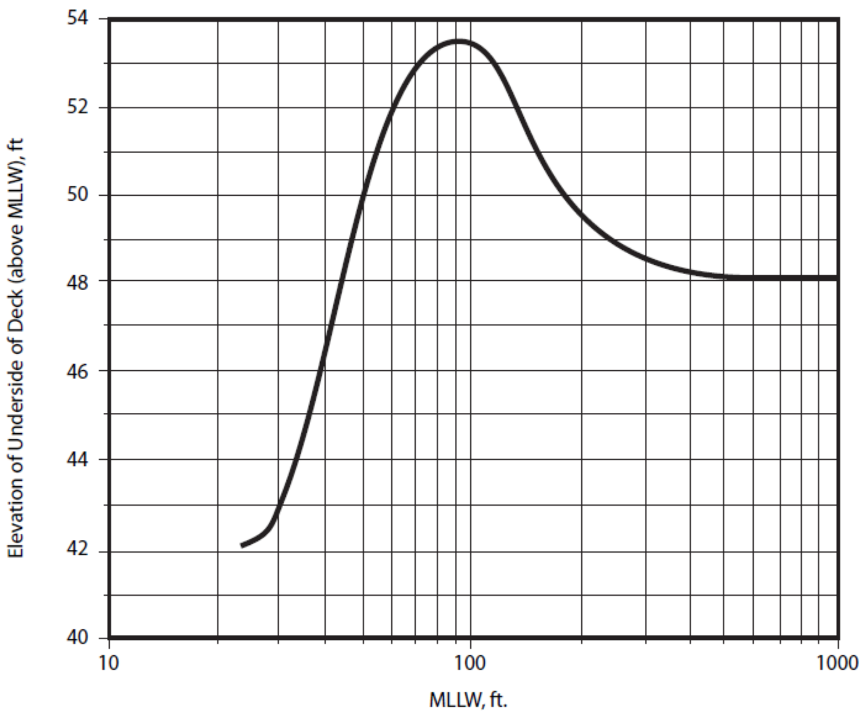

Figure 4.3 : Elevation of underside of deck vs. mean water depth for Gulf of Mexico.

- Mean water depth of the platform = 75 m = 246 ft.
- From Figure 4.3 elevation of underside of deck = 49 ft. = 15 m

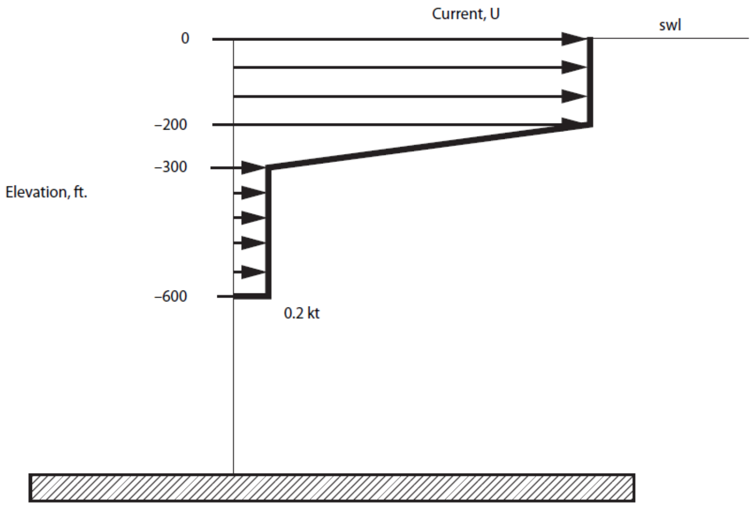

Figure 4.4 : Current profile.

Table 4.2 : Current profile data.

Water Depth (m)	Current Speed (m/s)
0 ~ 61	1.08
61 ~ 75	1.08 ~ 0.85

- For each bracing system 3 different wave directions that are 0^0, 45^0, and 90^0 in x-y plane counter-clockwise direction are used.
- For each bracing system current direction is 0^0 in x-y plane. Table 4.2 and Figure 4.4 shows the current profile, current direction and current velocity.

Furthermore, Table 4.3 shows the summary of metocean data.

Table 4.3 : Summary of metocean data.

Mean Water Depth (m)	75
Wave Height (m)	20
Wave Period (s)	13
Current Speed (m/s)	1.08 ~ 0.85
Wave Direction (in x-y plane)	0^0, 45^0, and 90^0
Current Direction (in x-y plane)	0^0
Storm Tide (m)	1.00
Elevation of Underside of Deck (m)	15

4.2 Loads

4.2.1 Dead loads

Dead loads are the summation of the self-weight of the members, self-weigth of the equipment and non-structural members, and also the deck weight of the platform. The software which is used in this study calculates the self-weight of all members. However, the weight of the deck should be applied to upper joints of the columns because in the three dimensional model of the platform the deck is not modelled.

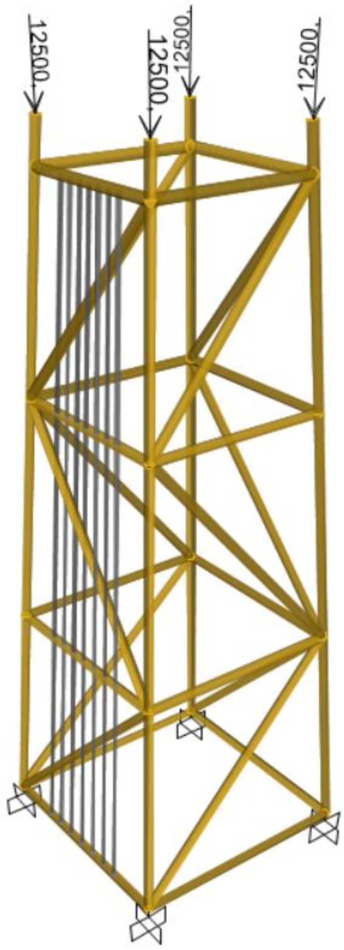

Figure 4.5 : Deck dead loads (kN).

The deck of mass is estimated 5000 tones so 12500 kN point loads are applied to the legs (Figure 4.5).

4.2.2 Live loads

In this study, total deck area is assumed 2000 m^2 and live load 5 kN/m^2 so total live load is 10000 kN and 2500 kN point loads are applied to the legs (Figure 4.6).

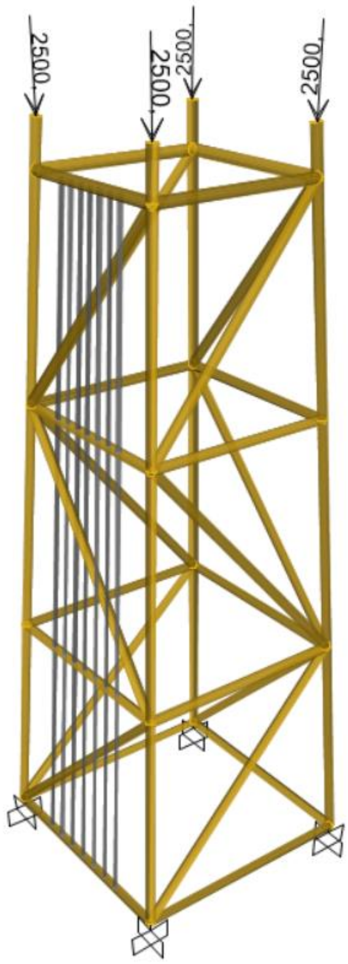

Figure 4.6 : Deck live loads (kN).

4.2.3 Wave and current forces

After determination of metocean parameters (generally 100-year storm data) storm parameters can be formed to distributed and nodal forces on the members and joints with using wave plus current kinematics, related theories and equations such as Morison's Equation in finite element software SAP2000 [12].

Wave plus current forces do not only depend on metocean parameters but also they depend on the geometric properties of members such as shape, outer diameter etc. Therefore, firstly, in order to determine approximate wave plus current loadings, all structural members are selected as round HSS with outer diameter is 1.20 m. After that, wave and current forces are created and applied to the members in SAP2000 [12] (Figure 4.7, Figure 4.8 and Figure 4.9).

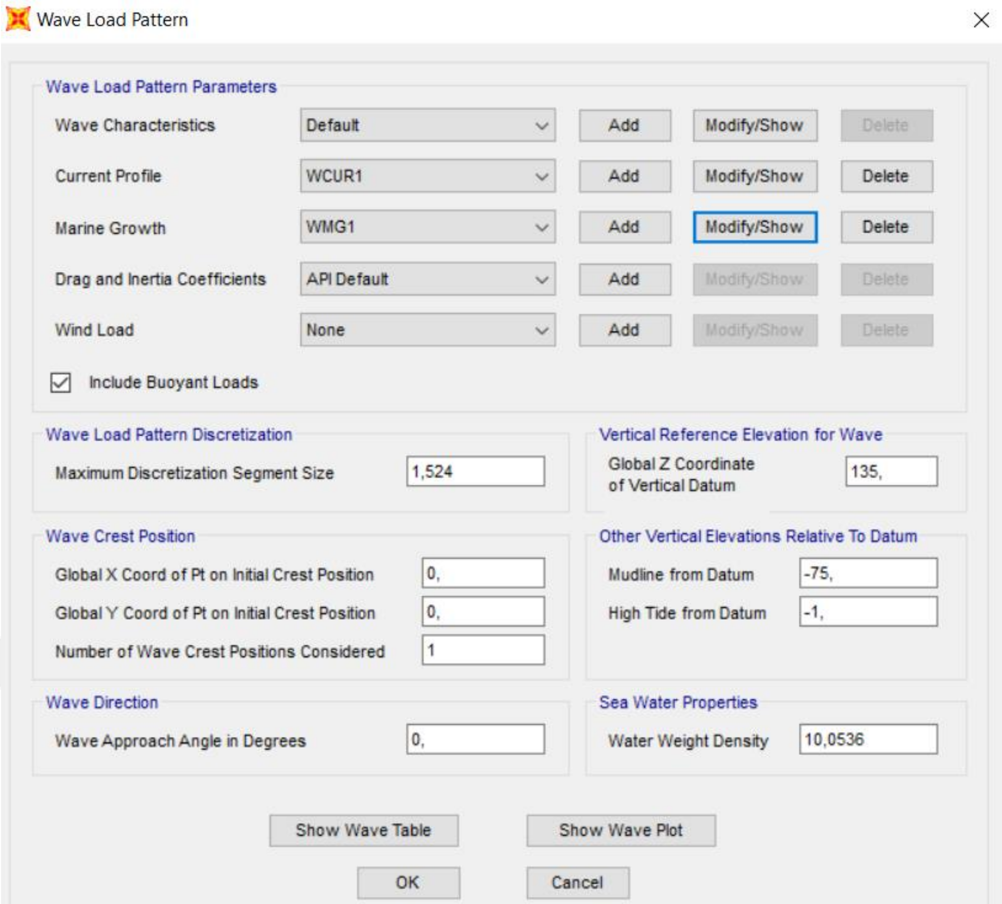

Figure 4.7 : Wave load pattern parameters in SAP200 [12].

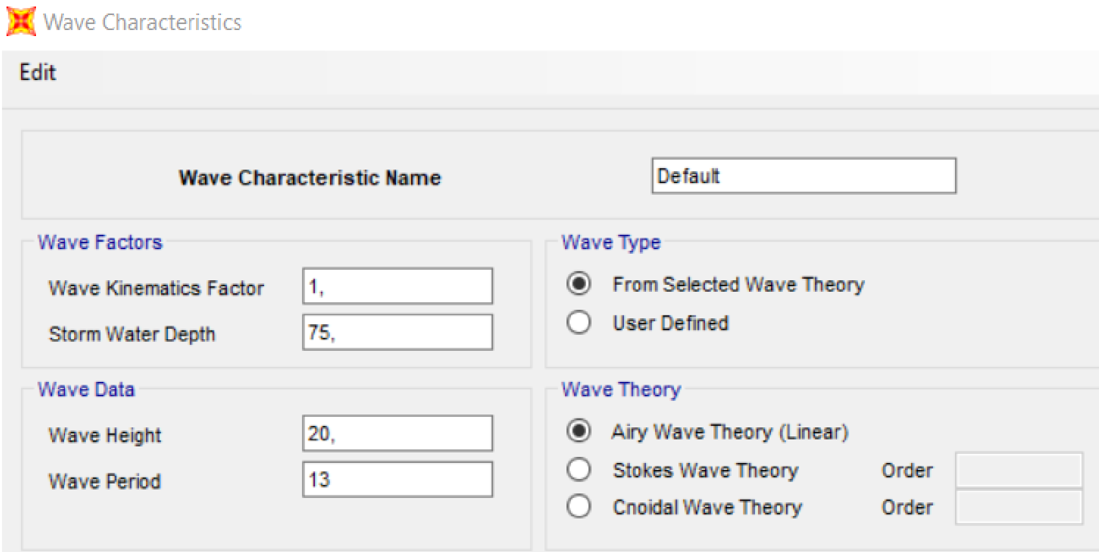

Figure 4.8 : Wave characteristics.

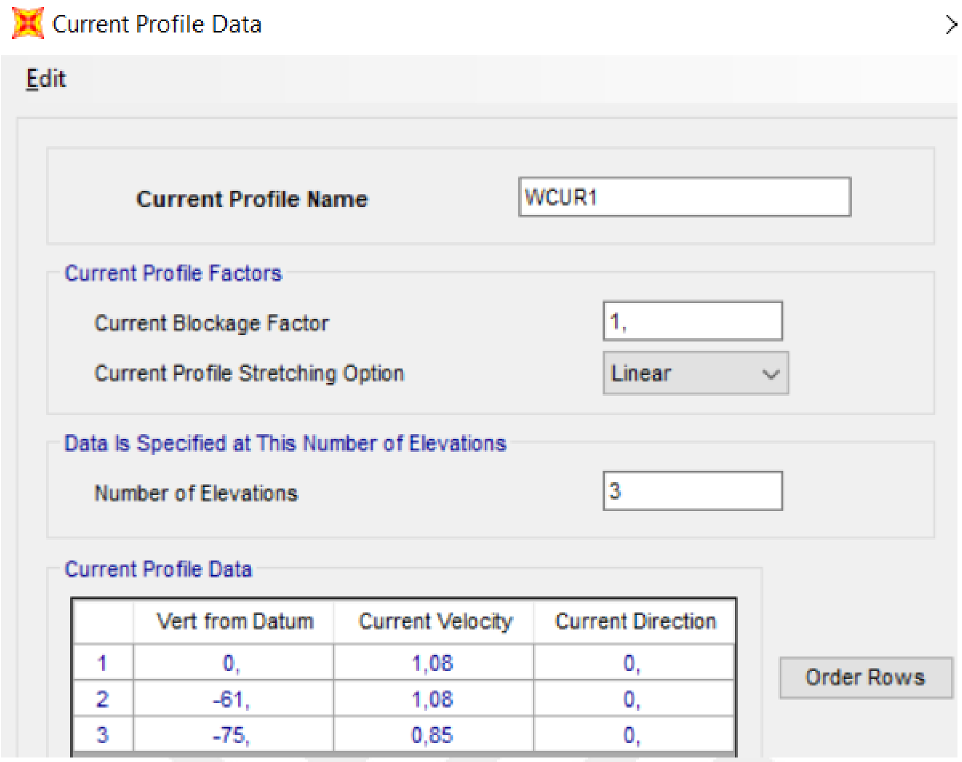

Figure 4.9 : Current profile data.

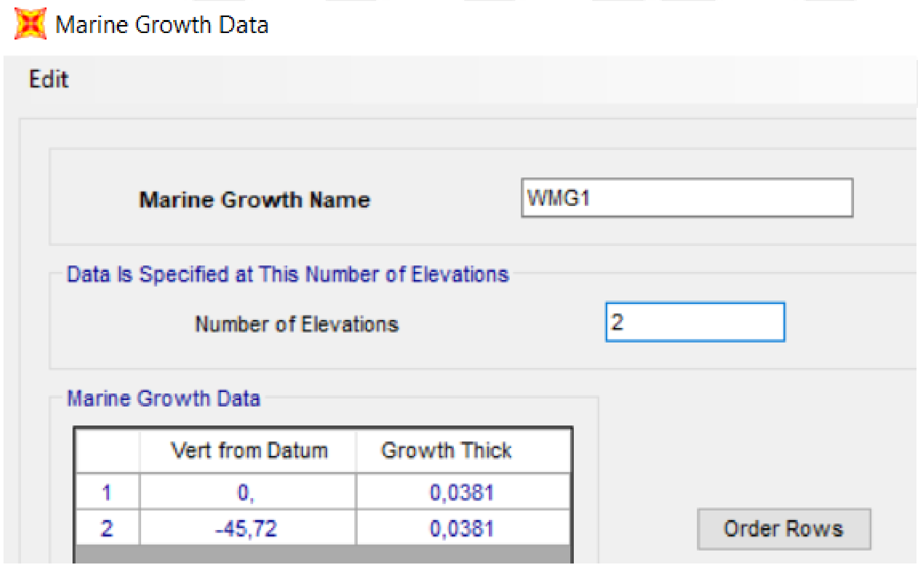

Figure 4.10 : Marine growth data.

API Recommended Practice 2A [13] suggests that outer diameter of members should be increased by 3.81 cm from sea level to -45.72 m for the marine growth consideration [13] (Figure 4.10).

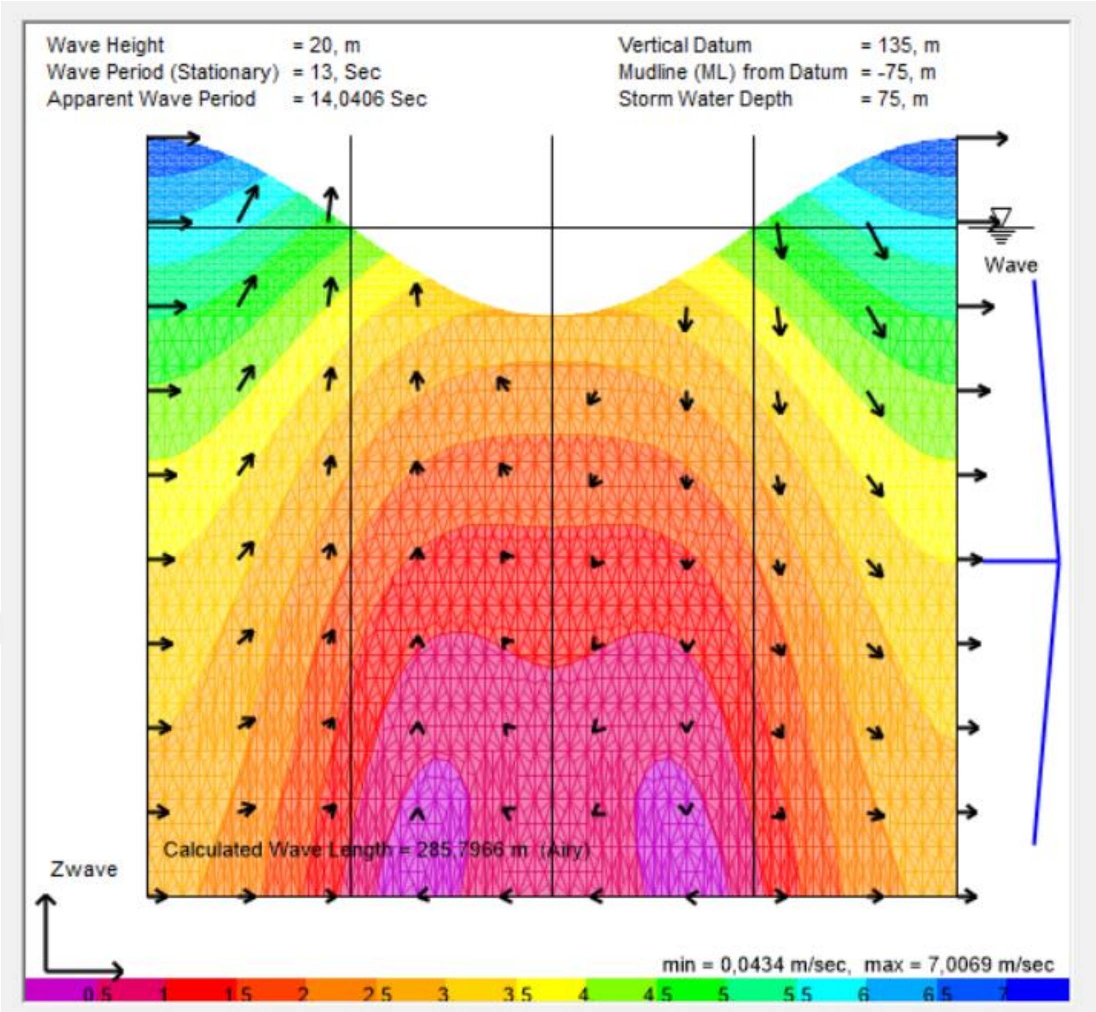

Figure 4.11 : Wave velocity with current (m/s).

Figure 4.11 shows the wave velocity considering with current. After the metocean parameters entered into the program, the final metocean loads are created (Figure 4.12).

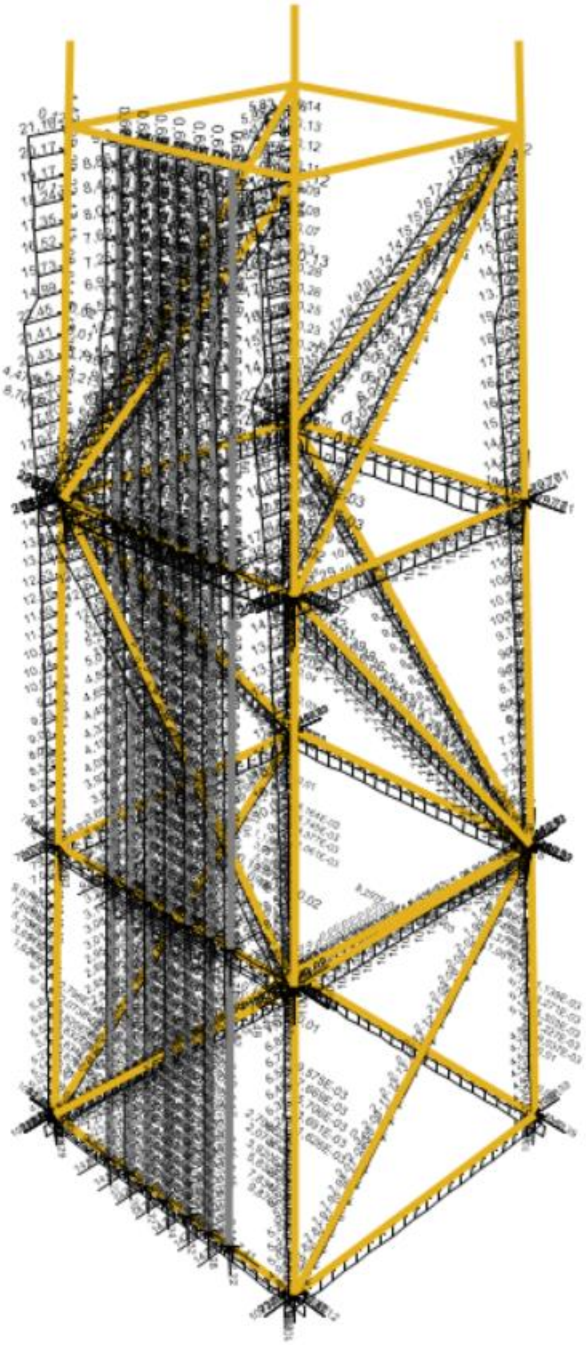

Figure 4.12 : Example of wave plus current forces acting on members.

4.3 Load Combinations

Load combinations for onshore structures are defined by AISC 360-10 [17] standard. These load combinations consist of seven main alternatives according to the LRFD solution method. These are,

- 1.4D
- 1.2D + 1.6L + 0.5(L_r or S or R)

- 1.2D + 1.6(L_r or S or R) + (0.5L_r or 0.8W)
- 1.2D + 1.6W + 0.5L + 0.5(L_r or S or R)
- 1.2D + 1.0E + 0.5L + 0.2S
- 0.9D + 1.6W
- 0.9D + 1.0E

where,

D: Dead load

E: Earthquake load

L: Live load

L_r: Roof live load

R: Rain load

S: Snow load

W: Wind load

However, there is no wave/current loading in any of these load combinations. Fortunately, in API Recommended Practice 2A [13], and ISO 19902 (International Standards Organization) [14] documents, there are detailed load combinations that include extreme environmental conditions.

Also, in ISO 19902 (International Standards Organization) [14] document, loads and loads combinations are expressed in equation 4.1.

$$F_d = \gamma_{f,G1}G_1 + \gamma_{f,G2}G_2 + \gamma_{f,Q1}Q_1 + \gamma_{f,Q2}Q_2 + \gamma_{f,E0}(E_0 + \gamma_{f,D}D_0) + \gamma_{f,Ee}(E_e + \gamma_{f,D}D_e) \quad (4.1)$$

where,

G_1 and G_2 are dead loads.

Q_1 and Q_2 are live loads.

E_0, is the environmental loads due to specified operational conditions.

D_0, is the indirect dynamic forces due to E_0.

E_e, is the environmental loads due to specified metocean conditions.

D_e, is the indirect dynamic forces due to E_e.

Table 4.4 : Partial action factors in ISO 19902 [14].

Design situation	Partial action factors [a]					
	$\gamma_{f,G1}$	$\gamma_{f,G2}$	$\gamma_{f,Q1}$	$\gamma_{f,Q2}$	$\gamma_{f,Eo}$	$\gamma_{f,Ee}$
Permanent and variable actions only	1,3	1,3	1,5	1,5	0,0	0,0
Operating situation with corresponding wind, wave, and/or current conditions[b]	1,3	1,3	1,5	1,5	0,9 $\gamma_{f,E}$	0,0
Extreme conditions when the action effects due to permanent and variable actions are additive[c]	1,1	1,1	1,1	0,0	0,0	$\gamma_{f,E}$
Extreme conditions when the action effects due to permanent and variable actions oppose[d]	0,9	0,9	0,8	0,0	0,0	$\gamma_{f,E}$

[a] A value of 0 for a partial action factor means that the action is not applicable to the design situation.
[b] For this, check that G_2, Q_1 and Q_2 are the maximum values for each mode of operation.
[c] For this, check that G_1, G_2 and Q_1 include those parts of each mode of operation that can reasonably be present during extreme conditions.
[d] For this, check that G_2 and Q_1 exclude any parts associated with the mode of operation considered that cannot be ensured of being present during extreme conditions.

Table 4.4 is taken from ISO 19902 [14] and shows load cases and corresponding load factors. Therefore, in this study load combinations that are used for preliminary-linear analysis are,

1. $1.3D + 1.5L$
2. $1.1D + 1.1L + 1.0E_e^{0}$
3. $1.1D + 1.1L + 1.0E_e^{45}$
4. $1.1D + 1.1L + 1.0E_e^{90}$
5. $0.9D + 0.8L + 1.0E_e^{0}$
6. $0.9D + 0.8L + 1.0E_e^{45}$
7. $0.9D + 0.8L + 1.0E_e^{90}$

where,

D: Dead load

E_e^{0}: Extreme environmental condition (metocean load) with current direction 0^0 and wave direction 0^0 in x-y plane.

E_e^{45}: Extreme environmental condition (metocean load) with current direction 0^0 and wave direction 45^0 in x-y plane.

E_e^{90}: Extreme environmental condition (metocean load) with current direction 0^0 and wave direction 90^0 in x-y plane.

L: Live load

5. PRELIMINARY-LINEAR ANALYSIS

In this section, linear analysis will be performed in order to determine geometric properties of the members and all structural members have sufficient strength according to LRFD method.

Cylindrical members are extensively used in design of jacket-type fixed offshore structures because there are several advantages in application of cylindrical members. These are,

- Cylindrical members minimize hydrodynamic, wind and blast forces due to small surface area exposed to loadings.
- Cylindrical members have a larger torsional rigidity.
- Cylindrical members have a larger strength and resistance against ship impact loading and drop object loadings.
- Cylindrical members have smaller outside surface so they have also the lesser effects of corrosion.
- Cylindrical members have the same resistance against the buckling for all direction.
- Additionally, lateral torsional buckling is not a concern for cylindrical members.

Therefore, in this study, all structural members (columns, beams and braces) are cylindrical shape.

For all storm case and all bracing configurations, below design criteria according to AISC 360-10 [17] LRFD method with ISO 19902 (International Standards Organization) [14] load combinations given in section 4.3. should be satisfied.

- Axial tension – yielding
- Axial compression – global and local buckling
- Bending – yielding and local buckling
- External pressure – yielding and local buckling
- Shear – yielding
- Torsion – yielding

- Combined bending and axial force – yielding and buckling

The procedures are followed according to the formulas defined in previous sections in the calculations of cross sections of the steel members by using AISC 360-10 [17] LRFD method. Capacity checks of the column, beams and braces, which are schematically expressed below, are performed for each storm case and bracing system.

5.1 Linear Analysis for Diagonal Bracing System

Table 5.1 : Base reactions for diagonal bracing system.

Load Case	F_x (kN)	F_y (kN)	F_z (kN)	M_x (kNm)	M_y (kNm)	M_z (kNm)
E_e^0	-11854.95	301.15	-15497.81	-276188.41	-1069385.64	195350.46
E_e^{45}	-8280.14	-4939.98	-15974.78	304731.92	-667643.33	69738.35
E_e^{90}	2300.96	-6411.73	-15975.61	486994.48	-8520.63	-47700.30
D	0	0	62967.16	1007915.06	-1007033.94	0
L	0	0	10000	160000	-160000	0

Table 5.1 shows the base reactions for the platform with diagonal bracing.

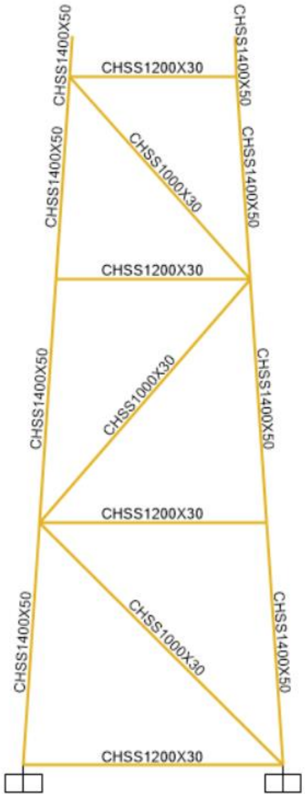

Figure 5.1 : Selected cross sections for diagonal bracing system.

Figure 5.1 shows the selected cross sections for diagonal bracing system. According to Figure 5.1,

Selected cross-section for columns: CHSS1400 x 50

Selected cross-section for beams: CHSS1200 x 30

Selected cross-section for braces: CHSS1000 x 30

5.1.1 Capacity check for braces

Selected cross-section for braces: CHSS1000 x 30

Load Combination: 0.9D + 0.8L + E_e^0 governs.

L_{br} = 39.75 m

A_{br} = 0.0914 m^2

$I_x = I_y$ = 0.0108 m^4

$Z_x = Z_y$ = 0.0282 m^3

r = 0.343 m

P_u = 5227.6 kN (compression)

M_{ux} = 733.3 kNm

M_{uy} = 405.6 kNm

$\Phi_b M_n = \Phi_b M_p = \Phi_b F_y Z = 0.9 * 275 * 10^3 * 0.0282 = 6979.5$ kNm

Slenderness:

$\frac{D}{t} \leq 0.11 \frac{E}{F_y} = 0.11 \frac{200000}{275} = 80$

$\frac{D}{t} = 33.33 \leq 80$ section is non-slender.

Compactness:

$\frac{D}{t} \leq 0.07 \frac{E}{F_y} = 0.07 \frac{200000}{275} = 50.91$

$\frac{D}{t} = 33.33 \leq 50.91$ section is compact.

Global Buckling Check:

$\frac{KL}{r} \leq^{?} 4.71 \sqrt{\frac{E}{F_y}} = 4.71 \sqrt{\frac{200000}{275}} = 127.02$

$\frac{KL}{r} = \frac{0.8*39.75}{0.343} = 92.71 \leq 127.02$

$F_e = \frac{\pi^2 E}{(\frac{KL}{r})^2} = 229.66\ MPa$

$F_{cr} = \left[0.658^{\frac{Fy}{Fe}}\right] * F_y = 0.658^{\frac{275}{229.66}} * 275 = 166.6\ MPa$

$\Phi_c P_n = \Phi_c A_{gbr} F_{cr} = 0.9 * 166.6 * 0.0914 * 1000 = 13705\ kN$

$\Phi_c P_n = 13705\ kN \geq\ P_u = 5227.6\ kN$ no buckling.

Local Buckling:

Since section is compact, local buckling control is not required.

Combined Flexure and Axial Force:

$\frac{P_r}{P_c} \geq 0.20$ $\frac{P_r}{P_c} + \frac{8}{9}(\frac{M_{rx}}{M_{cx}} + \frac{M_{ry}}{M_{cy}}) \leq 1.0$

$$\frac{P_r}{P_c} = \frac{5227.6}{13705} = 0.381$$

$$\frac{P_r}{P_c} + \frac{8}{9}\left(\frac{M_{rx}}{M_{cx}} + \frac{M_{ry}}{M_{cy}}\right) = 0.381 + \frac{8}{9}\left(\frac{733.3}{6979.5} + \frac{405.6}{6979.5}\right) = 0.526 \leq 1.0$$

Section is OK.

5.1.2 Capacity check for columns

Selected cross-section for columns: CHSS1400 x 50

Load Combination: 1.3D + 1.5L governs.

L_c = 25.11 m

A_c = 0.2121 m^2

$I_x = I_y$ = 0.0484 m^4

$Z_x = Z_y$ = 0.0912 m^3

r = 0.4776 m

P_u = 20467 kN (compression)

M_{ux} = 7369 kNm

M_{uy} = 699 kNm

$\Phi_b M_n = \Phi_b M_p = \Phi_b F_y Z = 0.9 * 275 * 10^3 * 0.0912 = 22572$ kNm

Slenderness:

$$\frac{D}{t} \leq 0.11\frac{E}{F_y} = 0.11\frac{200000}{275} = 80$$

$\frac{D}{t} = \frac{1400}{50} = 28 \leq 80$ section is non-slender.

Compactness:

$$\frac{D}{t} \leq 0.07\frac{E}{F_y} = 0.07\frac{200000}{275} = 50.91$$

$\frac{D}{t} = 28 \leq 50.91$ section is compact.

Buckling Check:

$$\frac{KL}{r} \leq^{?} 4.71\sqrt{\frac{E}{F_y}} = 4.71\sqrt{\frac{200000}{275}} = 127.02$$

$\frac{KL}{r} = \frac{1*25.11}{0.4776} = 52.56 \leq 127.02$

$F_e = \frac{\pi^2 E}{(\frac{KL}{r})^2} = \frac{\pi^2*200*10^3}{52.56^2} = 714.5\ MPa$

$F_{cr} = \left[0.658^{\frac{Fy}{Fe}}\right] * F_y = 0.658^{\frac{275}{714.5}} * 275 = 234.08\ MPa$

$\Phi_c P_n = \Phi_c A_{gc} F_{cr} = 0.9 * 0.2121 * 234.08 * 1000 = 44683.53\ kN$

$\Phi_c P_n = 44683.53\ kN \geq\ P_u = 20467\ kN$ no buckling.

Local Buckling:

Since section is compact, local buckling control is not required.

Combined Flexure and Axial Force:

$\frac{P_r}{P_c} \geq 0.20$ $\qquad \frac{P_r}{P_c} + \frac{8}{9}(\frac{M_{rx}}{M_{cx}} + \frac{M_{ry}}{M_{cy}}) \leq 1.0$

$$\frac{P_r}{P_c} = \frac{20467}{44683.53} = 0.458$$

$\frac{P_r}{P_c} + \frac{8}{9}\left(\frac{M_{rx}}{M_{cx}} + \frac{M_{ry}}{M_{cy}}\right) = 0.458 + \frac{8}{9}\left(\frac{7369}{22572} + \frac{699}{22572}\right) = 0.776 \leq 1.0$

Section is OK.

5.1.3 Capacity check for beams

Selected cross-section for beams: CHSS1200 x 30

Load Combination: 0.9D + 0.8L + E_e^0 governs.

L_b = 32.00 m

A_b = 0.1103 m^2

$I_x = I_y$ = 0.0189 m^4

$Z_x = Z_y$ = 0.0411 m^3

r = 0.4138 m

P_u = 5.72 kN (tension)

$V_{u,1}$ = 826.59 kN

$V_{u,2}$ = 259.08 kN

M_{ux} = 5776.18 kNm

M_{uy} = 1706.53 kNm

$\Phi_b M_n = \Phi_b M_p = \Phi_b F_y Z = 0.9 * 275 * 10^3 * 0.0411 = 10172.25$ kNm

Slenderness:

$\frac{D}{t} \leq 0.11\frac{E}{F_y} = 0.11\frac{200000}{275} = 80$

$\frac{D}{t} = \frac{1200}{30} = 40 \leq 80$ section is non-slender.

Compactness:

$\frac{D}{t} \leq 0.07\frac{E}{F_y} = 0.07\frac{200000}{275} = 50.91$

$\frac{D}{t} = 40 \leq 50.91$ section is compact.

Local Buckling:

Since section is compact, local buckling control is not required.

Yielding on Gross Area:

$\Phi_t P_n = \Phi_t A_{gb} F_{cr} = 0.90 * 0.1103 * 275 * 1000 = 27299.25\ kN$

$\Phi_t P_n = 27299.25\ kN \geq \ P_u = 5.72\ kN$ no yielding on gross area.

Shear Check

$\Phi_v V_n = \ F_{cr} A_g/2$

$$F_{cr} = \max\left(\frac{1.60E}{\sqrt{\frac{L_v}{D}}\left(\frac{D}{t}\right)^{\frac{5}{4}}};\frac{0.78E}{\left(\frac{D}{t}\right)^{\frac{3}{2}}}\right) \leq 0.6F_y = 165\ MPa$$

$$\Phi_v V_n = \frac{F_{cr} A_g}{2} = \frac{0.9 * 165 * 0.1103 * 1000}{2} = 8189\ kN$$

$\Phi_v V_n = 8189\ kN > V_{u,1} = 826.59$ kN

Combined Flexure and Axial Force:

$\frac{P_r}{P_c} = \frac{5.72}{27299.25} < 0.20$

$$\frac{P_r}{2P_c} + \left(\frac{M_{rx}}{M_{cx}} + \frac{M_{ry}}{M_{cy}}\right) = 0 + \frac{5776.18}{10172.25} + \frac{1706.53}{10172.25} = 0.736 \leq 1.0$$

Section is OK.

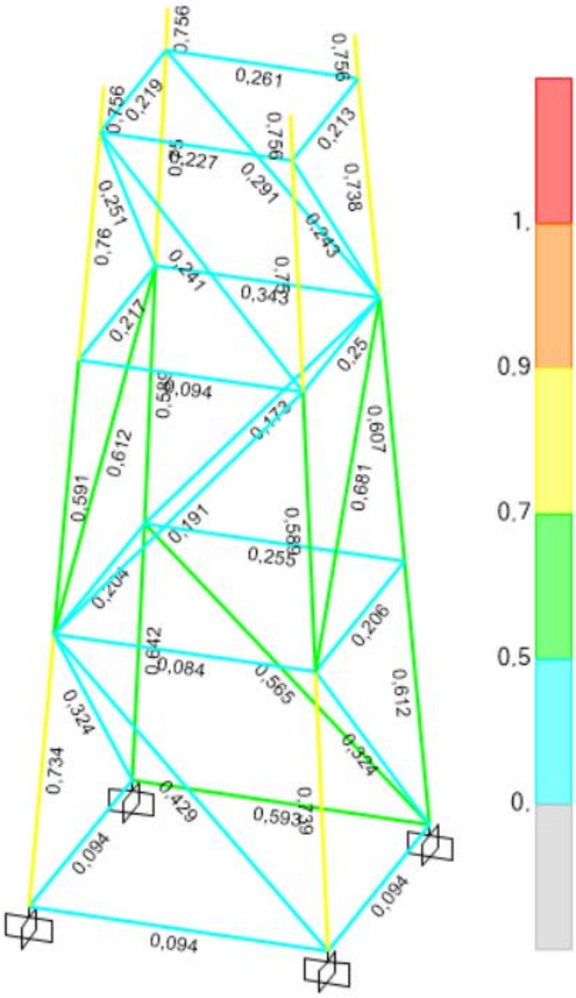

Figure 5.2 : Capacity ratio for structural members for diagonal bracing system.

Figure 5.2 shows the capacity ratios of the members for diagonal bracing system.

5.2 Linear Analysis for X-Bracing System

Table 5.2 : Base reactions for x-bracing system.

Load Case	F_x (kN)	F_y (kN)	F_z (kN)	M_x (kNm)	M_y (kNm)	M_z (kNm)
E_e^0	-13967.51	0	-20211.00	-323376.06	-1230168.06	223480.17
E_e^{45}	-9641.75	-6369.22	-20528.03	388491.71	-745672.68	64495.64
E_e^{90}	-2369.09	-8186.59	-20169.09	618171.95	53292.53	-79149.29
D	0	0	66290.94	1060654.95	-1060654.95	0
L	0	0	10000	160000	-160000	0

Table 5.2 shows the base reactions for the platform with x-bracing.

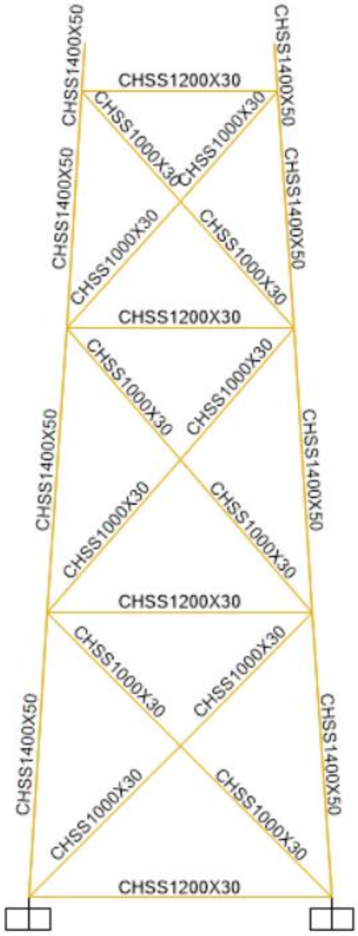

Figure 5.3 : Selected cross sections for x-bracing system.

Figure 5.3 shows the selected cross sections for x-bracing system. According to Figure 5.3,

Selected cross-section for columns: CHSS1400 x 50

Selected cross-section for beams: CHSS1200 x 30

Selected cross-section for braces: CHSS1000 x 30

5.2.1 Capacity check for braces

Selected cross-section for braces: CHSS1000 x 30

Load Combination: 1.1D + 1.1L + E_e^0 governs.

L_{br} = 19.82 m

A_{br} = 0.0914 m^2

$I_x = I_y$ = 0.0108 m^4

$Z_x = Z_y$ = 0.0282 m^3

r = 0.343 m

P_u = 6822.58 kN (compression)

M_{ux} = 345.6 kNm

M_{uy} = 678.8 kNm

$\Phi_b M_n = \Phi_b M_p = \Phi_b F_y Z = 0.9 * 275 * 10^3 * 0.0282 = 6979.5$ kNm

Slenderness:

$\frac{D}{t} \leq 0.11 \frac{E}{F_y} = 0.11 \frac{200000}{275} = 80$

$\frac{D}{t} = 33.33 \leq 80$ section is non-slender.

Compactness:

$\frac{D}{t} \leq 0.07 \frac{E}{F_y} = 0.07 \frac{200000}{275} = 50.91$

$\frac{D}{t} = 33.33 \leq 50.91$ section is compact.

Global Buckling Check:

$\frac{KL}{r} \leq^{?} 4.71 \sqrt{\frac{E}{F_y}} = 4.71 \sqrt{\frac{200000}{275}} = 127.02$

$\frac{KL}{r} = \frac{0.9*19.82}{0.343} = 52 \leq 127.02$

$F_e = \frac{\pi^2 E}{(\frac{KL}{r})^2} = 730 MPa$

$F_{cr} = \left[0.658^{\frac{Fy}{Fe}}\right] * F_y = 0.658^{\frac{275}{730}} * 275 = 234.9\ MPa$

$\Phi_c P_n = \Phi_c A_{gbr} F_{cr} = 0.9 * 234.9 * 0.0914 * 1000 = 19323\ kN$

$\Phi_c P_n = 19323\ kN \geq P_u = 6822.58\ kN$ no buckling.

Local Buckling:

Since section is compact, local buckling control is not required.

Combined Flexure and Axial Force:

$\frac{P_r}{P_c} \geq 0.20$ $\qquad$ $\frac{P_r}{P_c} + \frac{8}{9}(\frac{M_{rx}}{M_{cx}} + \frac{M_{ry}}{M_{cy}}) \leq 1.0$

$$\frac{P_r}{P_c} = \frac{6822.58}{19323} = 0.353$$

$\frac{P_r}{P_c} + \frac{8}{9}\left(\frac{M_{rx}}{M_{cx}} + \frac{M_{ry}}{M_{cy}}\right) = 0.353 + \frac{8}{9}\left(\frac{345.6}{6979.5} + \frac{678.8}{6979.5}\right) = 0.484 \leq 1.0$

Section is OK.

5.2.2 Capacity check for columns

Selected cross-section for columns: CHSS1400 x 50

Load Combination: 1.3D + 1.5L governs.

L_c = 5.02 m

A_c = 0.2121 m^2

$I_x = I_y$ = 0.0484 m^4

$Z_x = Z_y$ = 0.0912 m^3

r = 0.4776 m

P_u = 20019.9 kN (compression)

M_{ux} = 9453.7 kNm

M_{uy} = 0 kNm

$\Phi_b M_n = \Phi_b M_p = \Phi_b F_y Z = 0.9 * 275 * 10^3 * 0.0912 = 22572$ kNm

<u>Slenderness:</u>

$\frac{D}{t} \leq 0.11 \frac{E}{F_y} = 0.11 \frac{200000}{275} = 80$

$\frac{D}{t} = \frac{1400}{50} = 28 \leq 80$ section is non-slender.

<u>Compactness:</u>

$\frac{D}{t} \leq 0.07 \frac{E}{F_y} = 0.07 \frac{200000}{275} = 50.91$

$\frac{D}{t} = 28 \leq 50.91$ section is compact.

<u>Buckling Check:</u>

$\frac{KL}{r} \leq^{?} 4.71\sqrt{\frac{E}{F_y}} = 4.71\sqrt{\frac{200000}{275}} = 127.02$

$\frac{KL}{r} = \frac{1*5.02}{0.4776} = 10.51 \leq 127.02$

$F_e = \frac{\pi^2 E}{(\frac{KL}{r})^2} = \frac{\pi^2 * 200*10^3}{10.51^2} = 17870\ MPa$

$F_{cr} = \left[0.658^{\frac{Fy}{Fe}}\right] * F_y = 0.658^{\frac{275}{17870}} * 275 = 273.2\ MPa$

$\Phi_c P_n = \Phi_c A_{gc} F_{cr} = 0.9 * 0.2121 * 273.2 * 1000 = 52151\ kN$

$\Phi_c P_n = 52151\ kN \geq\ P_u = 20019.9\ kN$ no buckling.

<u>Local Buckling:</u>

Since section is compact, local buckling control is not required.

<u>Combined Flexure and Axial Force:</u>

$\frac{P_r}{P_c} \geq 0.20$ $\frac{P_r}{P_c} + \frac{8}{9}(\frac{M_{rx}}{M_{cx}} + \frac{M_{ry}}{M_{cy}}) \leq 1.0$

$$\frac{P_r}{P_c} = \frac{20019.9}{52151} = 0.384$$

$$\frac{P_r}{P_c} + \frac{8}{9}\left(\frac{M_{rx}}{M_{cx}} + \frac{M_{ry}}{M_{cy}}\right) = 0.384 + \frac{8}{9}\left(\frac{9453}{22572} + \frac{0}{22572}\right) = 0.756 \leq 1.0$$

Section is OK.

5.2.3 Capacity check for beams

Selected cross-section for beams: CHSS1200 x 30

Load Combination: 0.9D + 0.8L + E_e^0 governs.

L_b = 32.00 m

A_b = 0.1103 m^2

$I_x = I_y$ = 0.0189 m^4

$Z_x = Z_y$ = 0.0411 m^3

r = 0.4138 m

P_u = 3.9 kN (tension)

$V_{u,1}$ = 582.1kN

$V_{u,2}$ = 210.6 kN

M_{ux} = 4038 kNm

M_{uy} = 1359 kNm

$\Phi_b M_n = \Phi_b M_p = \Phi_b F_y Z = 0.9 * 275 * 10^3 * 0.0411 = 10172.25$ kNm

<u>Slenderness:</u>

$\frac{D}{t} \leq 0.11\frac{E}{F_y} = 0.11\frac{200000}{275} = 80$

$\frac{D}{t} = \frac{1200}{30} = 40 \leq 80$ section is non-slender.

<u>Compactness:</u>

$\frac{D}{t} \leq 0.07\frac{E}{F_y} = 0.07\frac{200000}{275} = 50.91$

$\frac{D}{t} = 40 \leq 50.91$ section is compact.

<u>Local Buckling:</u>

Since section is compact, local buckling control is not required.

<u>Yielding on Gross Area:</u>

$\Phi_t P_n = \Phi_t A_{gb} F_{cr} = 0.90 * 0.1103 * 275 * 1000 = 27299.25\ kN$

$\Phi_t P_n = 27299.25\ kN \geq\ P_u = 3.9\ kN$ no yielding on gross area.

Shear Check

$$\Phi_v V_n = F_{cr} A_g / 2$$

$$F_{cr} = \max\left(\frac{1.60E}{\sqrt{\frac{L_v}{D}}\left(\frac{D}{t}\right)^{\frac{5}{4}}};\frac{0.78E}{\left(\frac{D}{t}\right)^{\frac{3}{2}}}\right) \leq 0.6F_y = 165\ MPa$$

$$\Phi_v V_n = \frac{F_{cr} A_g}{2} = \frac{0.9 * 165 * 0.1103 * 1000}{2} = 8189\ kN$$

$\Phi_v V_n = 8189\ kN > V_{u,1} = 582.1$ kN

Combined Flexure and Axial Force:

$$\frac{P_r}{P_c} = \frac{3.9}{27299.25} < 0.20$$

$$\frac{P_r}{2P_c} + \left(\frac{M_{rx}}{M_{cx}} + \frac{M_{ry}}{M_{cy}}\right) = 0 + \frac{4038}{10172.25} + \frac{1359}{10172.25} = 0.53 \leq 1.0$$

Section is OK.

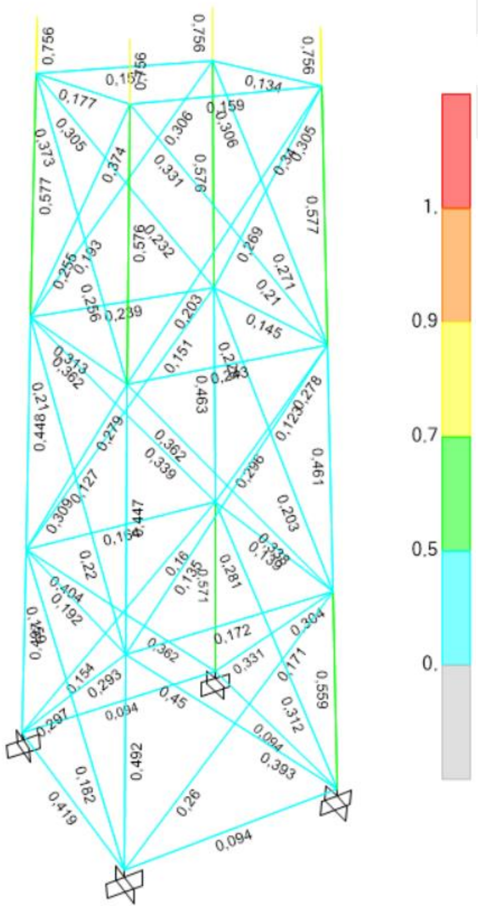

Figure 5.4 : Capacity ratio for structural members for x-bracing system.

Figure 5.4 shows the capacity ratios of the members for x-bracing system.

5.3 Linear Analysis for V-Bracing System

Table 5.3 : Base reactions for v-bracing system.

Load Case	F_x (kN)	F_y (kN)	F_z (kN)	M_x (kNm)	M_y (kNm)	M_z (kNm)
E_e^0	-13804.08	0	-18553.06	-296848.88	-1248254.60	220865.29
E_e^{45}	-9459.80	-6276.58	-18738.47	411218.47	-759945.29	62723.63
E_e^{90}	-2404.55	-7952.83	-18593.93	623103.37	22918.68	-75274.42
D	0	0	64962.12	1039393.99	-1039393.99	0
L	0	0	10000	160000	-160000	0

Table 5.3 shows the base reactions for the platform with v-bracing.

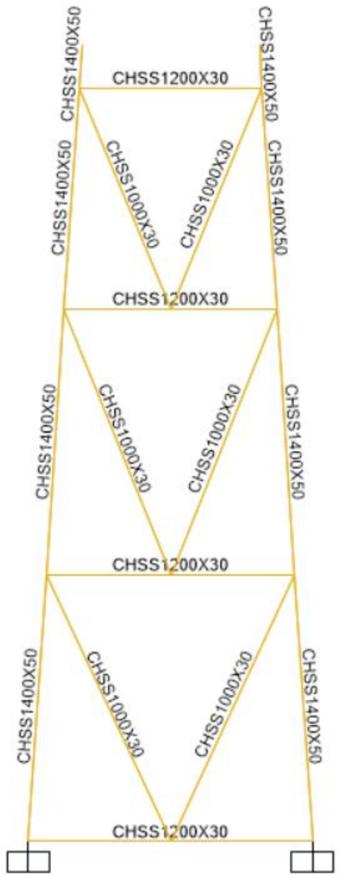

Figure 5.5 : Selected cross sections for v-bracing system.

Figure 5.5 shows the selected cross sections for v-bracing system. According to Figure 5.5,

Selected cross-section for columns: CHSS1400 x 50

Selected cross-section for beams: CHSS1200 x 30

Selected cross-section for braces: CHSS1000 x 30

5.3.1 Capacity check for braces

Selected cross-section for braces: CHSS1000 x 30

Load Combination: 1.1D + 1.1L + E_e^0 governs.

L_{br} = 33.166 m

A_{br} = 0.0914 m^2

$I_x = I_y$ = 0.0108 m^4

$Z_x = Z_y$ = 0.0282 m^3

r = 0.343 m

P_u = 6245 kN (compression)

M_{ux} = 305 kNm

M_{uy} = 458.5 kNm

$\Phi_b M_n = \Phi_b M_p = \Phi_b F_y Z = 0.9 * 275 * 10^3 * 0.0282 = 6979.5$ kNm

Slenderness:

$\frac{D}{t} \leq 0.11 \frac{E}{F_y} = 0.11 \frac{200000}{275} = 80$

$\frac{D}{t} = 33.33 \leq 80$ section is non-slender.

Compactness:

$\frac{D}{t} \leq 0.07 \frac{E}{F_y} = 0.07 \frac{200000}{275} = 50.91$

$\frac{D}{t} = 33.33 \leq 50.91$ section is compact.

Global Buckling Check:

$\frac{KL}{r} \leq^{?} 4.71\sqrt{\frac{E}{F_y}} = 4.71\sqrt{\frac{200000}{275}} = 127.02$

$\frac{KL}{r} = \frac{0.8*33.166}{0.343} = 77.36 \leq 127.02$

$F_e = \frac{\pi^2 E}{(\frac{KL}{r})^2} = 330\ MPa$

$F_{cr} = \left[0.658^{\frac{Fy}{Fe}}\right] * F_y = 0.658^{\frac{275}{330}} * 275 = 194\ MPa$

$\Phi_c P_n = \Phi_c A_{gbr} F_{cr} = 0.9 * 194 * 0.0914 * 1000 = 15958.3\ kN$

$\Phi_c P_n = 15958.3\ kN \geq\ P_u = 6245\ kN$ no buckling.

Local Buckling:

Since section is compact, local buckling control is not required.

Combined Flexure and Axial Force:

$\frac{P_r}{P_c} \geq 0.20$ $\frac{P_r}{P_c} + \frac{8}{9}(\frac{M_{rx}}{M_{cx}} + \frac{M_{ry}}{M_{cy}}) \leq 1.0$

$$\frac{P_r}{P_c} = \frac{6245}{15958.3} = 0.391$$

$$\frac{P_r}{P_c} + \frac{8}{9}\left(\frac{M_{rx}}{M_{cx}} + \frac{M_{ry}}{M_{cy}}\right) = 0.391 + \frac{8}{9}\left(\frac{305}{6979.5} + \frac{458.5}{6979.5}\right) = 0.489 \leq 1.0$$

Section is OK.

5.3.2 Capacity check for columns

Selected cross-section for columns: CHSS1400 x 50

Load Combination: 1.3D + 1.5L governs.

L_c = 5.02 m

A_c = 0.2121 m^2

$I_x = I_y$ = 0.0484 m^4

$Z_x = Z_y$ = 0.0912 m^3

r = 0.4776 m

P_u = 20019.9 kN (compression)

M_{ux} = 9453.7 kNm

M_{uy} = 0 kNm

$$\Phi_b M_n = \Phi_b M_p = \Phi_b F_y Z = 0.9 * 275 * 10^3 * 0.0912 = 22572 \text{ kNm}$$

Slenderness:

$$\frac{D}{t} \leq 0.11\frac{E}{F_y} = 0.11\frac{200000}{275} = 80$$

$\frac{D}{t} = \frac{1400}{50} = 28 \leq 80$ section is non-slender.

Compactness:

$$\frac{D}{t} \leq 0.07\frac{E}{F_y} = 0.07\frac{200000}{275} = 50.91$$

$\frac{D}{t} = 28 \leq 50.91$ section is compact.

Buckling Check:

$$\frac{KL}{r} \leq^? 4.71\sqrt{\frac{E}{F_y}} = 4.71\sqrt{\frac{200000}{275}} = 127.02$$

$$\frac{KL}{r} = \frac{1*5.02}{0.4776} = 10.51 \leq 127.02$$

$$F_e = \frac{\pi^2 E}{(\frac{KL}{r})^2} = \frac{\pi^2 * 200 * 10^3}{10.51^2} = 17870\ MPa$$

$$F_{cr} = \left[0.658^{\frac{Fy}{Fe}}\right] * F_y = 0.658^{\frac{275}{17870}} * 275 = 273.2\ MPa$$

$\Phi_c P_n = \Phi_c A_{gc} F_{cr} = 0.9 * 0.2121 * 273.2 * 1000 = 52151\ kN$

$\Phi_c P_n = 52151\ kN \geq\ P_u = 20019.9\ kN$ no buckling.

Local Buckling:

Since section is compact, local buckling control is not required.

Combined Flexure and Axial Force:

$\frac{P_r}{P_c} \geq 0.20$ $\frac{P_r}{P_c} + \frac{8}{9}(\frac{M_{rx}}{M_{cx}} + \frac{M_{ry}}{M_{cy}}) \leq 1.0$

$$\frac{P_r}{P_c} = \frac{20019.9}{52151} = 0.384$$

$$\frac{P_r}{P_c} + \frac{8}{9}\left(\frac{M_{rx}}{M_{cx}} + \frac{M_{ry}}{M_{cy}}\right) = 0.384 + \frac{8}{9}\left(\frac{9453}{22572} + \frac{0}{22572}\right) = 0.756 \leq 1.0$$

Section is OK.

5.3.3 Capacity check for beams

Selected cross-section for beams: CHSS1200 x 30

Load Combination: 1.1D 1.1L + E_e^{90} governs.

L_b = 32.00 m

A_b = 0.1103 m^2

$I_x = I_y$ = 0.0189 m^4

$Z_x = Z_y$ = 0.0411 m^3

r = 0.4138 m

P_u = 1553 kN (compression)

$V_{u,1}$ = 494 kN

$V_{u,2}$ = 17 kN

M_{ux} = 2181 kNm

M_{uy} = 66.4 kNm

$\Phi_b M_n = \Phi_b M_p = \Phi_b F_y Z = 0.9 * 275 * 10^3 * 0.0411 = 10172.25$ kNm

Slenderness:

$$\frac{D}{t} \leq 0.11 \frac{E}{F_y} = 0.11 \frac{200000}{275} = 80$$

$\frac{D}{t} = \frac{1200}{30} = 40 \leq 80$ section is non-slender.

Compactness:

$$\frac{D}{t} \leq 0.07 \frac{E}{F_y} = 0.07 \frac{200000}{275} = 50.91$$

$\frac{D}{t} = 40 \leq 50.91$ section is compact.

<u>Local Buckling:</u>

Since section is compact, local buckling control is not required.

<u>Buckling Check:</u>

$$\frac{KL}{r} \leq^{?} 4.71\sqrt{\frac{E}{F_y}} = 4.71\sqrt{\frac{200000}{275}} = 127.02$$

$$\frac{KL}{r} = \frac{0.7*32}{0.4138} = 54.13 \leq 127.02$$

$$F_e = \frac{\pi^2 E}{(\frac{KL}{r})^2} = \frac{\pi^2 * 200 * 10^3}{54.13^2} = 674\ MPa$$

$$F_{cr} = \left[0.658^{\frac{Fy}{Fe}}\right] * F_y = 0.658^{\frac{275}{674}} * 275 = 231.8\ MPa$$

$$\Phi_c P_n = \Phi_c A_{gc} F_{cr} = 0.9 * 0.1103 * 231.8 * 1000 = 23010\ kN$$

$\Phi_c P_n = 23010\ kN \geq\ P_u = 1553\ kN$ no buckling.

<u>Shear Check</u>

$$\Phi_v V_n = \ F_{cr} A_g/2$$

$$F_{cr} = \max\left(\frac{1.60E}{\sqrt{\frac{L_v}{D}}\left(\frac{D}{t}\right)^{\frac{5}{4}}}; \frac{0.78E}{\left(\frac{D}{t}\right)^{\frac{3}{2}}}\right) \leq 0.6F_y = 165\ MPa$$

$$\Phi_v V_n = \frac{F_{cr} A_g}{2} = \frac{0.9 * 165 * 0.1103 * 1000}{2} = 8189\ kN$$

$\Phi_v V_n = 8189\ kN > V_{u,1} = 582.1$ kN

<u>Combined Flexure and Axial Force:</u>

$$\frac{P_r}{P_c} = \frac{1553}{23010} = 0.067 < 0.20$$

$$\frac{P_r}{2P_c} + \left(\frac{M_{rx}}{M_{cx}} + \frac{M_{ry}}{M_{cy}}\right) = 0.067 + \frac{2181}{10172.25} + \frac{66.4}{10172.25} = 0.288 \leq 1.0$$

Section is OK.

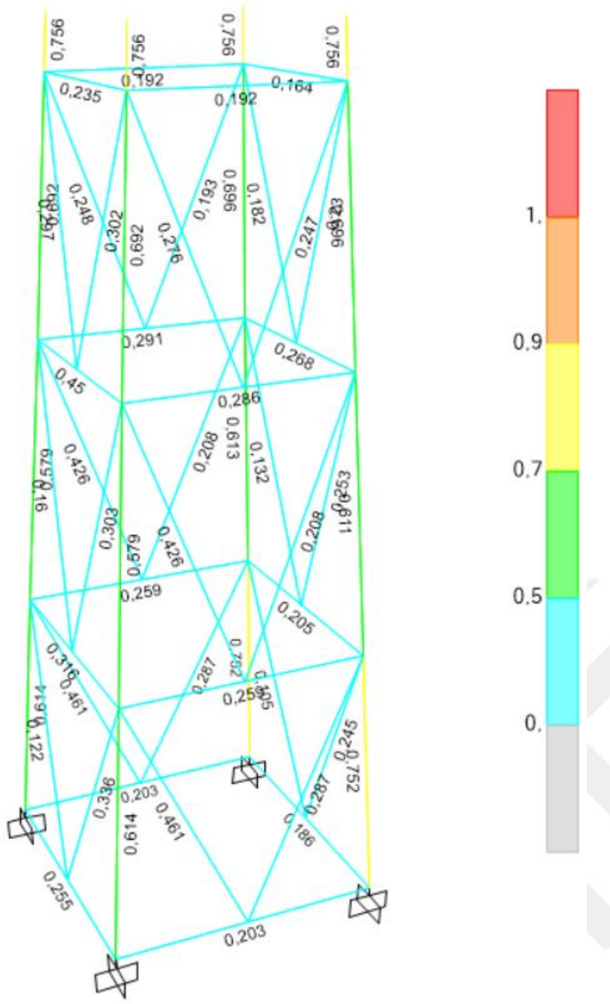

Figure 5.6 : Capacity ratio of structural members for v-bracing system.

Figure 5.6 shows the capacity ratios of the members for v-bracing system.

5.4 Linear Analysis for Inverted V-Bracing System

Table 5.4 : Base reactions for inverted v-bracing system.

Load Case	F_x (kN)	F_y (kN)	F_z (kN)	M_x (kNm)	M_y (kNm)	M_z (kNm)
E_e^0	-14097.56	0	-18898.46	-302375.37	-1261527.24	225560.93
E_e^{45}	-9636.92	-6424.52	-19058.84	416714.16	-764964.80	62924.74
E_e^{90}	-2440.83	-8211.15	-18939.82	640218.81	27403.58	-78726.88
D	0	0	65609.24	1049747.77	-1049747.77	0
L	0	0	10000	160000	-160000	0

Table 5.4 shows the base reactions for the platform with inverted v-bracing.

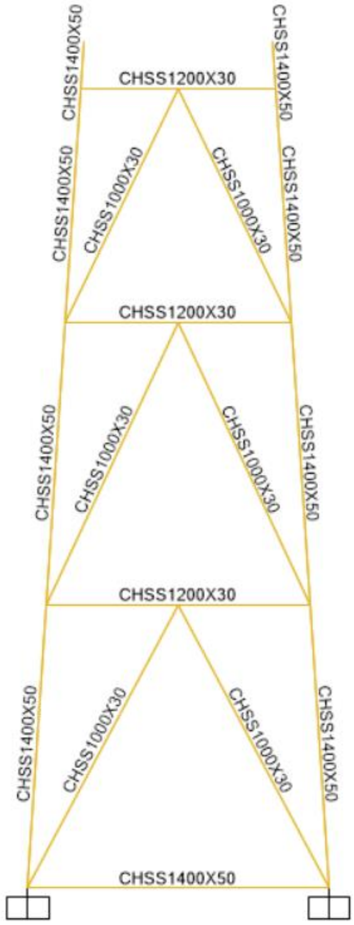

Figure 5.7 : Selected cross section for inverted v-bracing system.

Figure 5.7 shows the selected cross sections for inverted v-bracing system. According to Figure 5.7,

Selected cross-section for columns: CHSS1400 x 50

Selected cross-section for beams: CHSS1200 x 30

Selected cross-section for braces: CHSS1000 x 30

5.4.1 Capacity check for braces

Selected cross-section for braces: CHSS1000 x 30

Load Combination: 0.9D + 0.8L + E_e^0 governs.

L_{br} = 34.059 m

A_{br} = 0.0914 m^2

$I_x = I_y$ = 0.0108 m^4

$Z_x = Z_y$ = 0.0282 m^3

r = 0.343 m

P_u = 6456.3 kN (compression)

M_{ux} = 3502.9 kNm

M_{uy} = 74.8 kNm

$\Phi_b M_n = \Phi_b M_p = \Phi_b F_y Z = 0.9 * 275 * 10^3 * 0.0282 = 6979.5$ kNm

<u>Slenderness:</u>

$\frac{D}{t} \leq 0.11 \frac{E}{F_y} = 0.11 \frac{200000}{275} = 80$

$\frac{D}{t} = 33.33 \leq 80$ section is non-slender.

<u>Compactness:</u>

$\frac{D}{t} \leq 0.07 \frac{E}{F_y} = 0.07 \frac{200000}{275} = 50.91$

$\frac{D}{t} = 33.33 \leq 50.91$ section is compact.

<u>Global Buckling Check:</u>

$\frac{KL}{r} \leq^{?} 4.71\sqrt{\frac{E}{F_y}} = 4.71\sqrt{\frac{200000}{275}} = 127.02$

$\frac{KL}{r} = \frac{0.8*34.059}{0.343} = 79.44 \leq 127.02$

$F_e = \frac{\pi^2 E}{(\frac{KL}{r})^2} = 312.8\ MPa$

$F_{cr} = \left[0.658^{\frac{Fy}{Fe}}\right] * F_y = 0.658^{\frac{275}{312.8}} * 275 = 190.3\ MPa$

$\Phi_c P_n = \Phi_c A_{gbr} F_{cr} = 0.9 * 190.3 * 0.0914 * 1000 = 15657.3\ kN$

$\Phi_c P_n = 15657.3\ kN \geq P_u = 6456.3\ kN$ no buckling.

<u>Local Buckling:</u>

Since section is compact, local buckling control is not required.

<u>Combined Flexure and Axial Force:</u>

$\frac{P_r}{P_c} \geq 0.20$ $\qquad$ $\frac{P_r}{P_c} + \frac{8}{9}(\frac{M_{rx}}{M_{cx}} + \frac{M_{ry}}{M_{cy}}) \leq 1.0$

$$\frac{P_r}{P_c} = \frac{6456.3}{15657.3} = 0.412$$

$\frac{P_r}{P_c} + \frac{8}{9}\left(\frac{M_{rx}}{M_{cx}} + \frac{M_{ry}}{M_{cy}}\right) = 0.12 + \frac{8}{9}\left(\frac{502.9}{6979.5} + \frac{74.8}{6979.5}\right) = 0.486 \leq 1.0$

Section is OK.

5.4.2 Capacity check for columns

Selected cross-section for columns: CHSS1400 x 50

Load Combination: 1.3D + 1.5L governs.

$L_c = 5.02$ m

$A_c = 0.2121\ m^2$

$I_x = I_y = 0.0484\ m^4$

$Z_x = Z_y = 0.0912\ m^3$

r = 0.4776 m

$P_u = 20019.9$ kN (compression)

$M_{ux} = 9453.7$ kNm

$M_{uy} = 0$ kNm

$\Phi_b M_n = \Phi_b M_p = \Phi_b F_y Z = 0.9 * 275 * 10^3 * 0.0912 = 22572$ kNm

Slenderness:

$\frac{D}{t} \leq 0.11 \frac{E}{F_y} = 0.11 \frac{200000}{275} = 80$

$\frac{D}{t} = \frac{1400}{50} = 28 \leq 80$ section is non-slender.

Compactness:

$\frac{D}{t} \leq 0.07 \frac{E}{F_y} = 0.07 \frac{200000}{275} = 50.91$

$\frac{D}{t} = 28 \leq 50.91$ section is compact.

Buckling Check:

$\frac{KL}{r} \leq^{?} 4.71\sqrt{\frac{E}{F_y}} = 4.71\sqrt{\frac{200000}{275}} = 127.02$

$\frac{KL}{r} = \frac{1*5.02}{0.4776} = 10.51 \leq 127.02$

$F_e = \frac{\pi^2 E}{(\frac{KL}{r})^2} = \frac{\pi^2 * 200 * 10^3}{10.51^2} = 17870\ MPa$

$F_{cr} = \left[0.658^{\frac{Fy}{Fe}}\right] * F_y = 0.658^{\frac{275}{17870}} * 275 = 273.2\ MPa$

$\Phi_c P_n = \Phi_c A_{gc} F_{cr} = 0.9 * 0.2121 * 273.2 * 1000 = 52151\ kN$

$\Phi_c P_n = 52151\ kN \geq\ P_u = 20019.9\ kN$ no buckling.

Local Buckling:

Since section is compact, local buckling control is not required.

Combined Flexure and Axial Force:

$\frac{P_r}{P_c} \geq 0.20$ $\qquad$ $\frac{P_r}{P_c} + \frac{8}{9}(\frac{M_{rx}}{M_{cx}} + \frac{M_{ry}}{M_{cy}}) \leq 1.0$

$$\frac{P_r}{P_c} = \frac{20019.9}{52151} = 0.384$$

$$\frac{P_r}{P_c} + \frac{8}{9}\left(\frac{M_{rx}}{M_{cx}} + \frac{M_{ry}}{M_{cy}}\right) = 0.384 + \frac{8}{9}\left(\frac{9453}{22572} + \frac{0}{22572}\right) = 0.756 \leq 1.0$$

Section is OK.

5.4.3 Capacity check for beams

Selected cross-section for beams: CHSS1200 x 30

Load Combination: 1.1D 1.1L + E_e^0 governs.

L_b = 20.67 m

A_b = 0.1103 m^2

$I_x = I_y$ = 0.0189 m^4

$Z_x = Z_y$ = 0.0411 m^3

r = 0.4138 m

P_u = 808 kN (compression)

$V_{u,1}$ = 698.2 kN

$V_{u,2}$ = 88.7 kN

M_{ux} = 4363.4 kNm

M_{uy} = 626.8 kNm

$$\Phi_b M_n = \Phi_b M_p = \Phi_b F_y Z = 0.9 * 275 * 10^3 * 0.0411 = 10172.25 \text{ kNm}$$

Slenderness:

$$\frac{D}{t} \leq 0.11\frac{E}{F_y} = 0.11\frac{200000}{275} = 80$$

$\frac{D}{t} = \frac{1200}{30} = 40 \leq 80$ section is non-slender.

Compactness:

$$\frac{D}{t} \leq 0.07\frac{E}{F_y} = 0.07\frac{200000}{275} = 50.91$$

$\frac{D}{t} = 40 \leq 50.91$ section is compact.

Local Buckling:

Since section is compact, local buckling control is not required.

Buckling Check:

$$\frac{KL}{r} \leq^{?} 4.71\sqrt{\frac{E}{F_y}} = 4.71\sqrt{\frac{200000}{275}} = 127.02$$

$$\frac{KL}{r} = \frac{0.7*20.67}{0.4138} = 34.97 \leq 127.02$$

$F_e = \frac{\pi^2 E}{(\frac{KL}{r})^2} = \frac{\pi^2 * 200 * 10^3}{34.97^2} = 1614\ MPa$

$F_{cr} = \left[0.658^{\frac{Fy}{Fe}}\right] * F_y = 0.658^{\frac{275}{1614}} * 275 = 256\ MPa$

$\Phi_c P_n = \Phi_c A_{gc} F_{cr} = 0.9 * 0.1103 * 256 * 1000 = 25420\ kN$

$\Phi_c P_n = 25420\ kN \geq\ P_u = 808\ kN$ no buckling.

Shear Check

$\Phi_v V_n =\ F_{cr} A_g / 2$

$F_{cr} = \max\left(\frac{1.60E}{\sqrt{\frac{L_v}{D}}\left(\frac{D}{t}\right)^{\frac{5}{4}}}; \frac{0.78E}{\left(\frac{D}{t}\right)^{\frac{3}{2}}}\right) \leq 0.6F_y = 165\ MPa$

$\Phi_v V_n = \frac{F_{cr} A_g}{2} = \frac{0.9 * 165 * 0.1103 * 1000}{2} = 8189\ kN$

$\Phi_v V_n = 8189\ kN > V_{u,1} = 698.2$ kN

Combined Flexure and Axial Force:

$\frac{P_r}{P_c} = \frac{808}{25420} = 0.032 < 0.20$

$\frac{P_r}{2P_c} + \left(\frac{M_{rx}}{M_{cx}} + \frac{M_{ry}}{M_{cy}}\right) = 0.032 + \frac{4363.4}{10172.25} + \frac{626.8}{10172.25} = 0.522 \leq 1.0$

Section is OK.

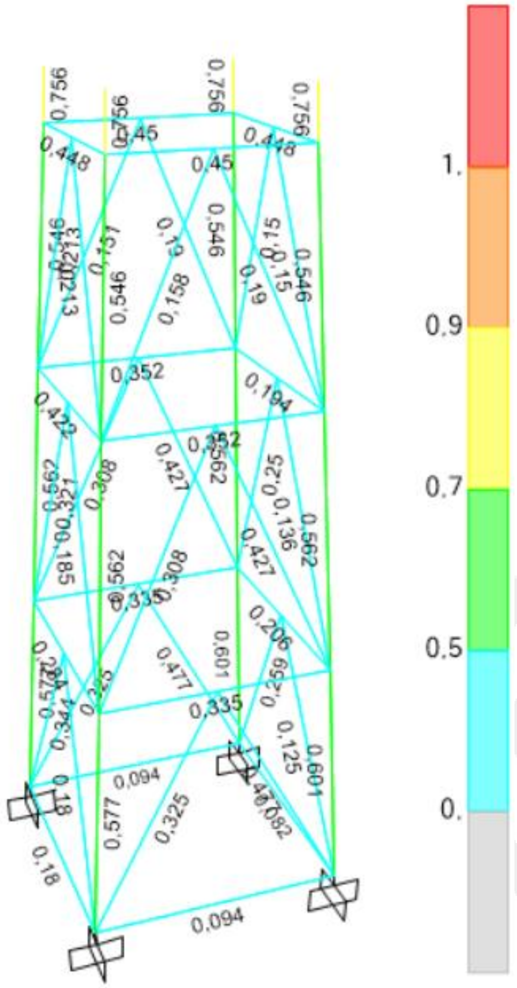

Figure 5.8 : Capacity ratio of structural members for inverted v-bracing system.

Figure 5.8 shows the capacity ratios of the members for inverted v-bracing system.

5.5 Linear Analysis for K-Bracing System

Table 5.5 : Base reactions for k-bracing system.

Load Case	F_x (kN)	F_y (kN)	F_z (kN)	M_x (kNm)	M_y (kNm)	M_z (kNm)
E_e^0	-14026.09	0.00	-20223.69	-323579.04	-1237854.54	224417.47
E_e^{45}	-9668.83	-6395.75	-20518.53	391877.32	-749295.02	64545.57
E_e^{90}	-2372.73	-8252.62	-20183.67	626126.05	52845.77	-80061.98
D	0	0	66290.94	1060654.95	-1060654.95	0
L	0	0	10000	160000	-160000	0

Table 5.5 shows the base reactions for the platform with k-bracing.

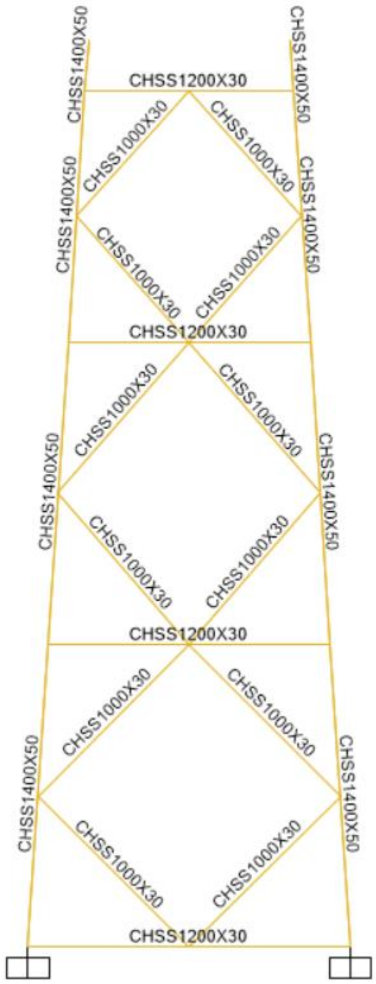

Figure 5.9 : Selected cross sections for k-bracing system.

Figure 5.9 shows the selected cross sections for k-bracing system. According to Figure 5.9,

Selected cross-section for columns: CHSS1400 x 50

Selected cross-section for beams: CHSS1200 x 30

Selected cross-section for braces: CHSS1000 x 30

5.5.1 Capacity check for braces

Selected cross-section for braces: CHSS1000 x 30

Load Combination: 1.1D + 1.1L + E_e^0 governs.

L_{br} = 19.875 m

A_{br} = 0.0914 m^2

$I_x = I_y$ = 0.0108 m^4

$Z_x = Z_y$ = 0.0282 m^3

r = 0.343 m

P_u = 4230 kN (compression)

M_{ux} = 295.3 kNm

M_{uy} = 532.3 kNm

$\Phi_b M_n = \Phi_b M_p = \Phi_b F_y Z = 0.9 * 275 * 10^3 * 0.0282 = 6979.5$ kNm

Slenderness:

$\frac{D}{t} \leq 0.11 \frac{E}{F_y} = 0.11 \frac{200000}{275} = 80$

$\frac{D}{t} = 33.33 \leq 80$ section is non-slender.

Compactness:

$\frac{D}{t} \leq 0.07 \frac{E}{F_y} = 0.07 \frac{200000}{275} = 50.91$

$\frac{D}{t} = 33.33 \leq 50.91$ section is compact.

Global Buckling Check:

$\frac{KL}{r} \leq^{?} 4.71\sqrt{\frac{E}{F_y}} = 4.71\sqrt{\frac{200000}{275}} = 127.02$

$\frac{KL}{r} = \frac{0.8*19.875}{0.343} = 46.36 \leq 127.02$

$F_e = \frac{\pi^2 E}{(\frac{KL}{r})^2} = 918.6\ MPa$

$F_{cr} = \left[0.658^{\frac{Fy}{Fe}}\right] * F_y = 0.658^{\frac{275}{918.6}} * 275 = 242.6\ MPa$

$\Phi_c P_n = \Phi_c A_{gbr} F_{cr} = 0.9 * 242.6 * 0.0914 * 1000 = 19957.4\ kN$

$\Phi_c P_n = 19957.4\ kN \geq\ P_u = 4230\ kN$ no buckling.

Local Buckling:

Since section is compact, local buckling control is not required.

Combined Flexure and Axial Force:

$\frac{P_r}{P_c} \geq 0.20$ $\qquad$ $\frac{P_r}{P_c} + \frac{8}{9}(\frac{M_{rx}}{M_{cx}} + \frac{M_{ry}}{M_{cy}}) \leq 1.0$

$$\frac{P_r}{P_c} = \frac{4230}{19957.4} = 0.212$$

$\frac{P_r}{P_c} + \frac{8}{9}\left(\frac{M_{rx}}{M_{cx}} + \frac{M_{ry}}{M_{cy}}\right) = 0.212 + \frac{8}{9}\left(\frac{295.3}{6979.5} + \frac{532.3}{6979.5}\right) = 0.317 \leq 1.0$

Section is OK.

5.5.2 Capacity check for columns

Selected cross-section for columns: CHSS1400 x 50

Load Combination: 1.3D + 1.5L governs.

L_c = 5.02 m

A_c = 0.2121 m^2

$I_x = I_y$ = 0.0484 m^4

$Z_x = Z_y$ = 0.0912 m^3

r = 0.4776 m

P_u = 20019.9 kN (compression)

M_{ux} = 9453.7 kNm

M_{uy} = 0 kNm

$\Phi_b M_n = \Phi_b M_p = \Phi_b F_y Z = 0.9 * 275 * 10^3 * 0.0912 = 22572$ kNm

<u>Slenderness:</u>

$\frac{D}{t} \leq 0.11 \frac{E}{F_y} = 0.11 \frac{200000}{275} = 80$

$\frac{D}{t} = \frac{1400}{50} = 28 \leq 80$ section is non-slender.

<u>Compactness:</u>

$\frac{D}{t} \leq 0.07 \frac{E}{F_y} = 0.07 \frac{200000}{275} = 50.91$

$\frac{D}{t} = 28 \leq 50.91$ section is compact.

<u>Buckling Check:</u>

$\frac{KL}{r} \leq^{?} 4.71 \sqrt{\frac{E}{F_y}} = 4.71 \sqrt{\frac{200000}{275}} = 127.02$

$\frac{KL}{r} = \frac{1*5.02}{0.4776} = 10.51 \leq 127.02$

$F_e = \frac{\pi^2 E}{(\frac{KL}{r})^2} = \frac{\pi^2 * 200 * 10^3}{10.51^2} = 17870\ MPa$

$F_{cr} = \left[0.658^{\frac{Fy}{Fe}}\right] * F_y = 0.658^{\frac{275}{17870}} * 275 = 273.2\ MPa$

$\Phi_c P_n = \Phi_c A_{gc} F_{cr} = 0.9 * 0.2121 * 273.2 * 1000 = 52151\ kN$

$\Phi_c P_n = 52151\ kN \geq\ P_u = 20019.9\ kN$ no buckling.

<u>Local Buckling:</u>

Since section is compact, local buckling control is not required.

<u>Combined Flexure and Axial Force:</u>

$\frac{P_r}{P_c} \geq 0.20$ $\qquad$ $\frac{P_r}{P_c} + \frac{8}{9}(\frac{M_{rx}}{M_{cx}} + \frac{M_{ry}}{M_{cy}}) \leq 1.0$

$$\frac{P_r}{P_c} = \frac{20019.9}{52151} = 0.384$$

$\frac{P_r}{P_c} + \frac{8}{9}\left(\frac{M_{rx}}{M_{cx}} + \frac{M_{ry}}{M_{cy}}\right) = 0.384 + \frac{8}{9}\left(\frac{9453}{22572} + \frac{0}{22572}\right) = 0.756 \leq 1.0$

Section is OK.

5.5.3 Capacity check for beams

Selected cross-section for beams: CHSS1200 x 30

Load Combination: 1.3D + 1.5L governs.

L_b = 20.67 m

A_b = 0.1103 m^2

$I_x = I_y$ = 0.0189 m^4

$Z_x = Z_y$ = 0.0411 m^3

r = 0.4138 m

P_u = 1538.6 kN (compression)

$V_{u,1}$ = 347.8 kN

$V_{u,2}$ = 28 kN

M_{ux} = 2929 kNm

M_{uy} = 145 kNm

$\Phi_b M_n = \Phi_b M_p = \Phi_b F_y Z = 0.9 * 275 * 10^3 * 0.0411 = 10172.25$ kNm

<u>Slenderness:</u>

$\frac{D}{t} \leq 0.11 \frac{E}{F_y} = 0.11 \frac{200000}{275} = 80$

$\frac{D}{t} = \frac{1200}{30} = 40 \leq 80$ section is non-slender.

<u>Compactness:</u>

$\frac{D}{t} \leq 0.07 \frac{E}{F_y} = 0.07 \frac{200000}{275} = 50.91$

$\frac{D}{t} = 40 \leq 50.91$ section is compact.

<u>Local Buckling:</u>

Since section is compact, local buckling control is not required.

<u>Buckling Check:</u>

$\frac{KL}{r} \leq^? 4.71\sqrt{\frac{E}{F_y}} = 4.71\sqrt{\frac{200000}{275}} = 127.02$

$\frac{KL}{r} = \frac{0.7*20.67}{0.4138} = 34.97 \leq 127.02$

$F_e = \frac{\pi^2 E}{(\frac{KL}{r})^2} = \frac{\pi^2 * 200 * 10^3}{34.97^2} = 1614\ MPa$

$F_{cr} = \left[0.658^{\frac{Fy}{Fe}}\right] * F_y = 0.658^{\frac{275}{1614}} * 275 = 256\ MPa$

$\Phi_c P_n = \Phi_c A_{gc} F_{cr} = 0.9 * 0.1103 * 256 * 1000 = 25420\ kN$

$\Phi_c P_n = 25420\ kN \geq\ P_u = 1538.6\ kN$ no buckling.

<u>Shear Check</u>

$\Phi_v V_n =\ F_{cr} A_g/2$

$$F_{cr} = \max\left(\frac{1.60E}{\sqrt{\frac{Lv}{D}}\left(\frac{D}{t}\right)^{\frac{5}{4}}};\frac{0.78E}{\left(\frac{D}{t}\right)^{\frac{3}{2}}}\right) \leq 0.6F_y = 165\ MPa$$

$$\Phi_v V_n = \frac{F_{cr} A_g}{2} = \frac{0.9 * 165 * 0.1103 * 1000}{2} = 8189\ kN$$

$\Phi_v V_n = 8189\ kN > V_{u,1} = 347.8$ kN

<u>Combined Flexure and Axial Force:</u>

$$\frac{P_r}{P_c} = \frac{1538.6}{25420} = 0.061 < 0.20$$

$$\frac{P_r}{2P_c} + \left(\frac{M_{rx}}{M_{cx}} + \frac{M_{ry}}{M_{cy}}\right) = 0.03 + \frac{2929}{10172.25} + \frac{145}{10172.25} = 0.332 \leq 1.0$$

Section is OK.

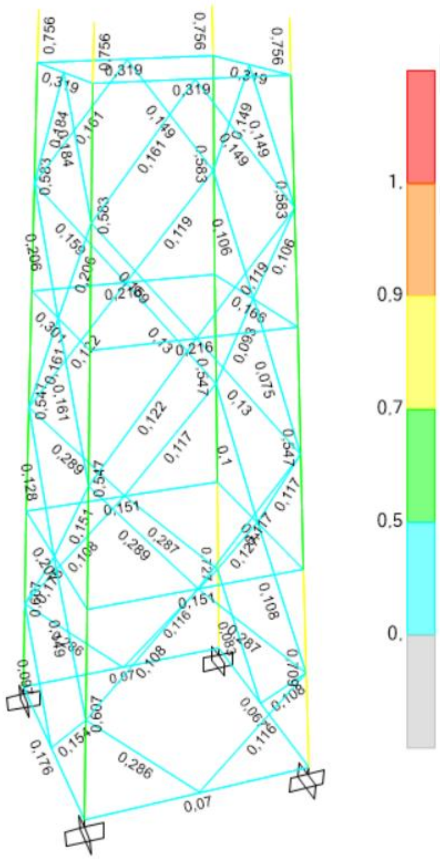

Figure 5.10 : Capacity ratio of structural members for k-bracing system.

Figure 5.10 shows the capacity ratios of the members for k-bracing system.

5.6 Linear Analysis Results

Linear analysis was completed for all configurations to determine sections of structural members of the platform and they were selected as CHSS1400x50, CHSS1200x30, and CHSS1000x30 for column, beams and braces, respectively. In nonlinear metocean pushover analysis chapter, these sections will be used in order to compare different bracing systems.

Table 5.6 : Base shears at storm conditions for different bracing systems.

Bracing Configuration	Wave Direction	Base Shear for X Direction (kN)	Base Shear for Y Direction (kN)	Resultant Base Shear (kN)
Diagonal	0^0	11855	301	11859
	45^0	8280	4940	9642
	90^0	2301	6412	6812
X-Bracing	0^0	13968	0	13968
	45^0	9642	6369	11556
	90^0	2369	8187	8523
V-Bracing	0^0	13804	0	13804
	45^0	9460	6277	11353
	90^0	2405	7953	8309
Inverted V-Bracing	0^0	14098	0	14098
	45^0	9637	6425	11582
	90^0	2440	8211	8566
K-Bracing	0^0	14026	0	14026
	45^0	9669	6396	11593
	90^0	2373	8253	8587

Table 5.6 shows base shears at storm condition for different bracing systems and different wave directions. These base shears will be used to determine reserve strength ratios of the platform.

6. METOCEAN PUSHOVER ANALYSIS

In previous sections, sections of structural members are determined. All members are circular hollow structural sections. In FEMA-356 [16] and ASCE41-17 [19] documents there is no specified moment-rotation relationship data for circular hollow sections. Only axial force-axial deformation data is available for circular hollow sections. For this reason, in this study, in order to represent nonlinearity, only axial force-axial deformation relationships are used according to ASCE41-17 [19]. Table 6.1, Figure 6.1 and Figure 6.2 show the force-deformation relationship for the sections CHSS1400x50, CHSS1200x30 and CHSS1000x30.

Table 6.1 : Force deformation relationship for members.

L =1.0 m		CHSS1400X50		CHSS1200X30		CHSS1000X30	
Force	Deformation	Pp (kN)	Δp (m)	Pp (kN)	Δp (m)	Pp (kN)	Δp (m)
P/Pp	Δ/Δp	64160.3	0.0015	33365.8	0.0015	27648.5	0.0015
-0.3	-9	-19248.1	-0.0136	-10009.7	-0.0136	-8294.6	-0.0136
-0.3	-0.5	-19248.1	-0.0008	-10009.7	-0.0008	-8294.6	-0.0008
-1.015	-0.5	-65122.7	-0.0008	-33866.2	-0.0008	-28063.2	-0.0008
-1	0	-64160.3	0.0000	-33365.8	0.0000	-27648.5	0.0000
0	0	0.0	0.0000	0.0	0.0000	0.0	0.0000
1	0	64160.3	0.0000	33365.8	0.0000	27648.5	0.0000
1.24	8	79558.7	0.0121	41373.5	0.0121	34284.1	0.0121
0.6	8	38496.2	0.0121	20019.5	0.0121	16589.1	0.0121
0.6	9	38496.2	0.0136	20019.5	0.0136	16589.1	0.0136

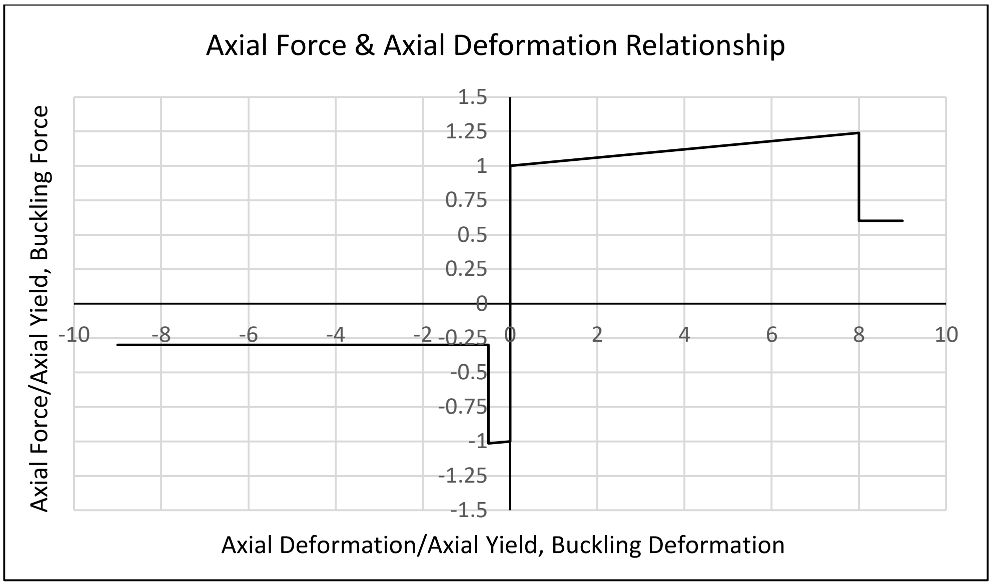

Figure 6.1 : Force deformation relationship for circular hollow structural sections.

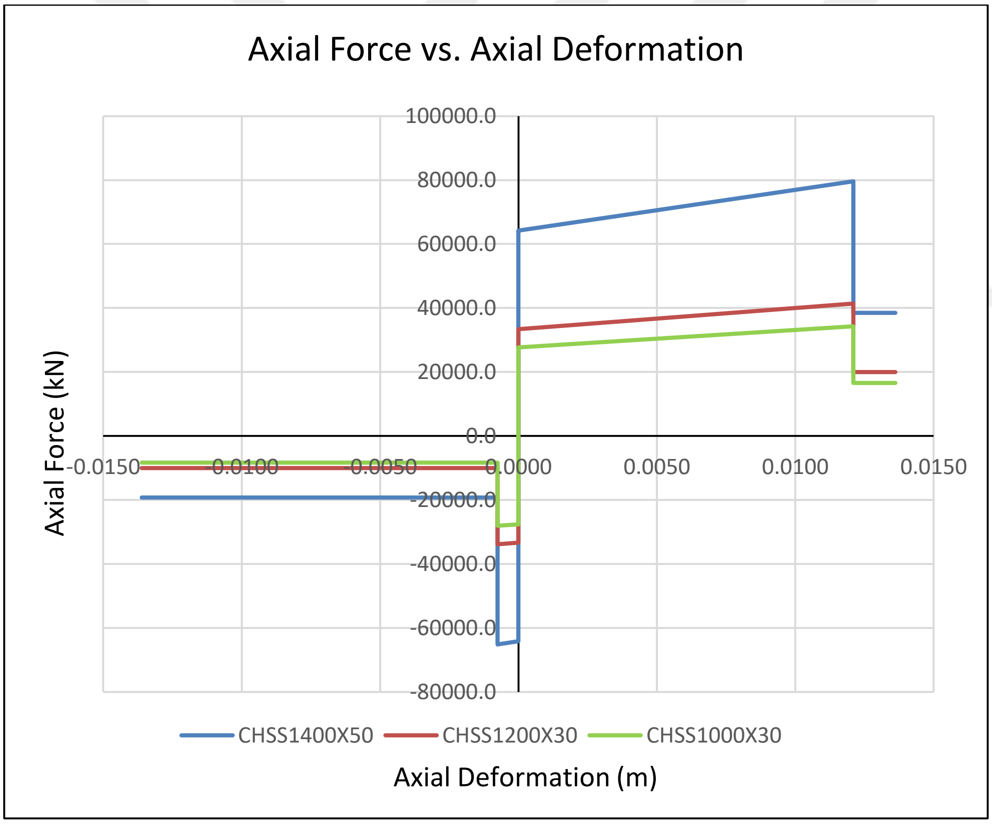

Figure 6.2 : Axial force vs. axial deformation for circular hollow structural sections.

For each bracing system, 3 different nonlinear pushover load cases are created by using finite element software SAP2000 [12] because of 3 different storm cases. They are shown in Figure 6.3, Figure 6.4 and Figure 6.5.

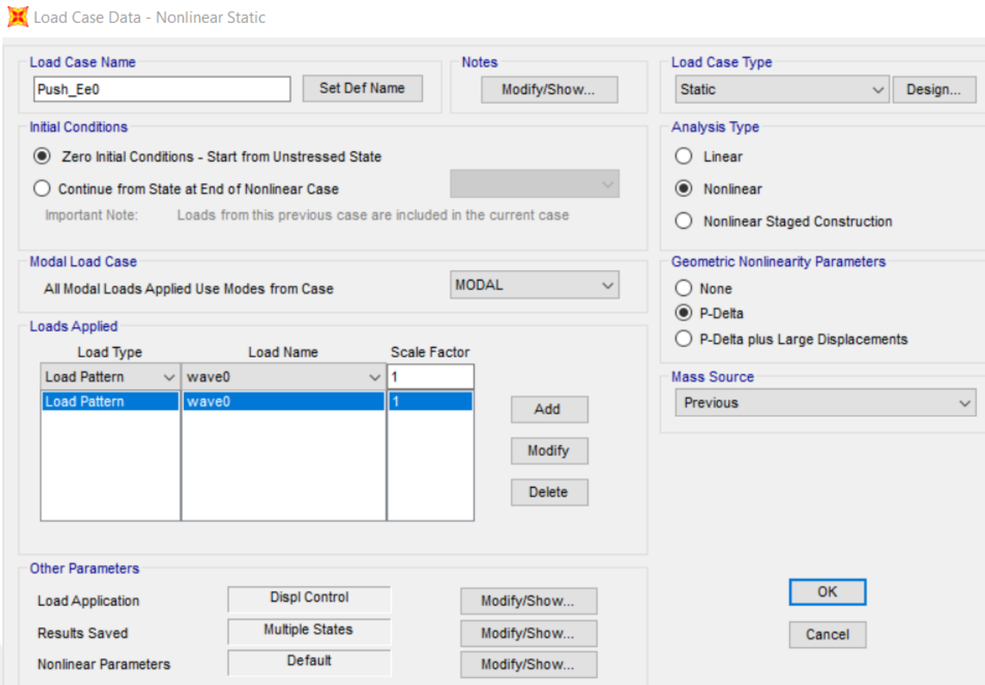

Figure 6.3 : Generating nonlinear load case for 0^0 wave direction.

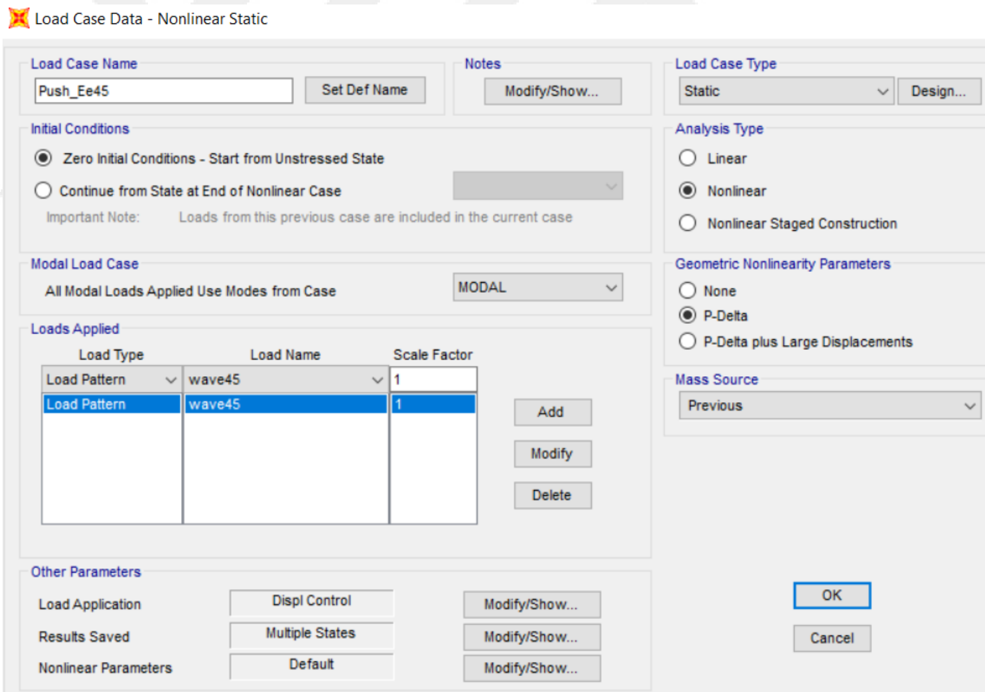

Figure 6.4 : Generating nonlinear load case for 45^0 wave direction.

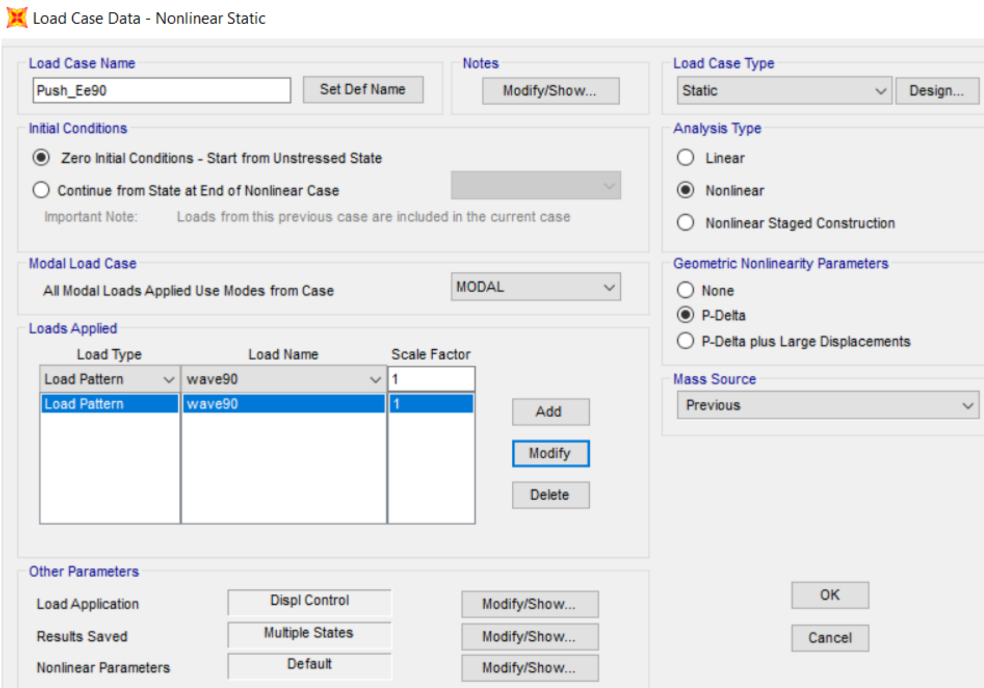

Figure 6.5 : Generating nonlinear load case for 90^0 wave direction.

Nonlinear pushover load cases are created and these load cases are the application of metocean loading applied to the structure which is incremented in steps in any specific direction until whole collapse. Eventually, base shear versus top displacement curves for each bracing system and storm case are plotted and reserve strength ratios are obtained.

6.1 Metocean Pushover Analysis Results for Diagonal Bracing System

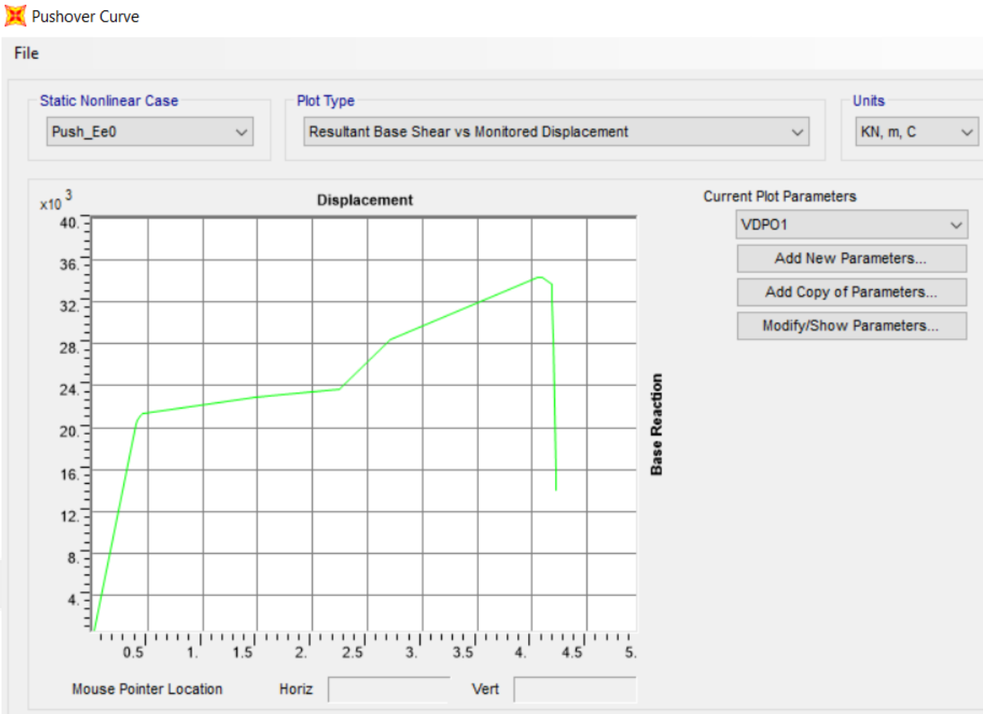

Figure 6.6 : Base shear vs. top displacement curve for diagonal bracing system E_e^0.

According to Figure 6.6, $BS_{Ee0,storm}$ = 11859 kN

$BS_{Ee0,ultimate}$ = 34384 kN

$$RSR_{Ee0} = \frac{\mathrm{BS}_{Ee0,ultimate}}{\mathrm{BS}_{Ee0,storm}} = \frac{34384}{11859} = 2.90$$

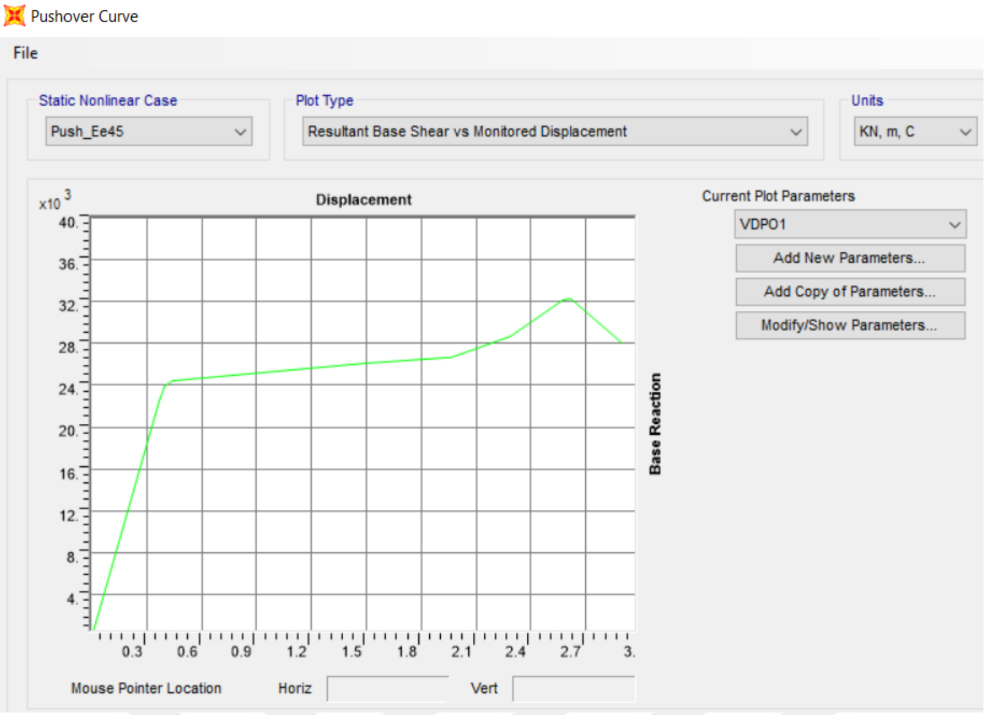

Figure 6.7 : Base shear vs. top displacement curve for diagonal bracing system E_e^{45}.

According to Figure 6.7, $BS_{Ee45,storm}$ = 9642 kN

$BS_{Ee45,ultimate}$ = 32316 kN

$$RSR_{Ee45} = \frac{BS_{Ee45,ultimate}}{BS_{Ee45,storm}} = \frac{32316}{9642} = 3.35$$

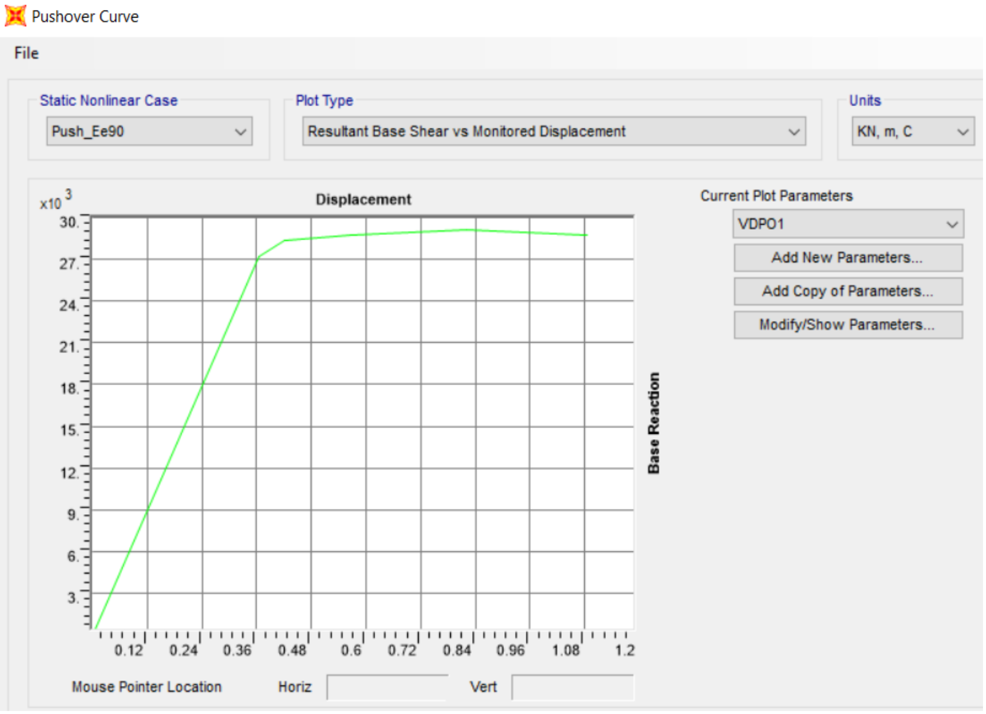

Figure 6.8 : Base shear vs. top displacement curve for diagonal bracing system E_e^{90}.

According to Figure 6.8, $BS_{Ee90,storm}$ = 6812 kN

$BS_{Ee90,ultimate}$ = 29108 kN

$$RSR_{Ee90} = \frac{BS_{Ee90,ultimate}}{BS_{Ee90,storm}} = \frac{29108}{6812} = 4.27$$

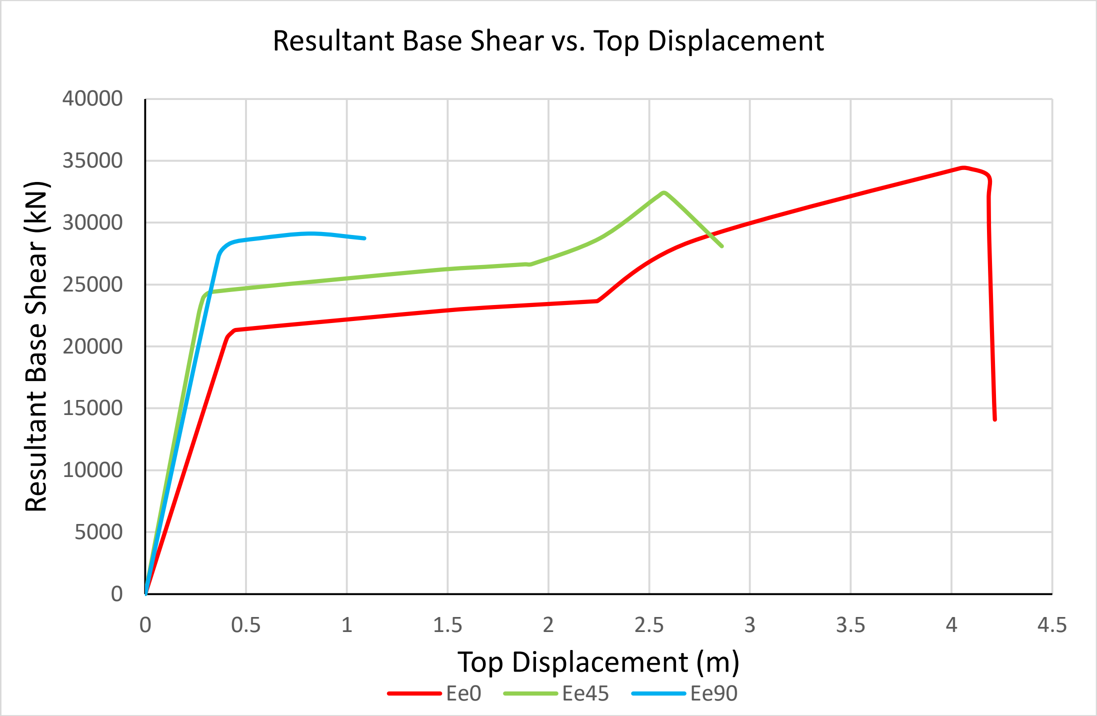

Figure 6.9 : Base shear vs. top displacement curve for diagonal bracing system.

Figure 6.9 shows the base shear and top displacement curve for diagonal bracing systems.

6.2 Metocean Pushover Analysis Results for X-Bracing System

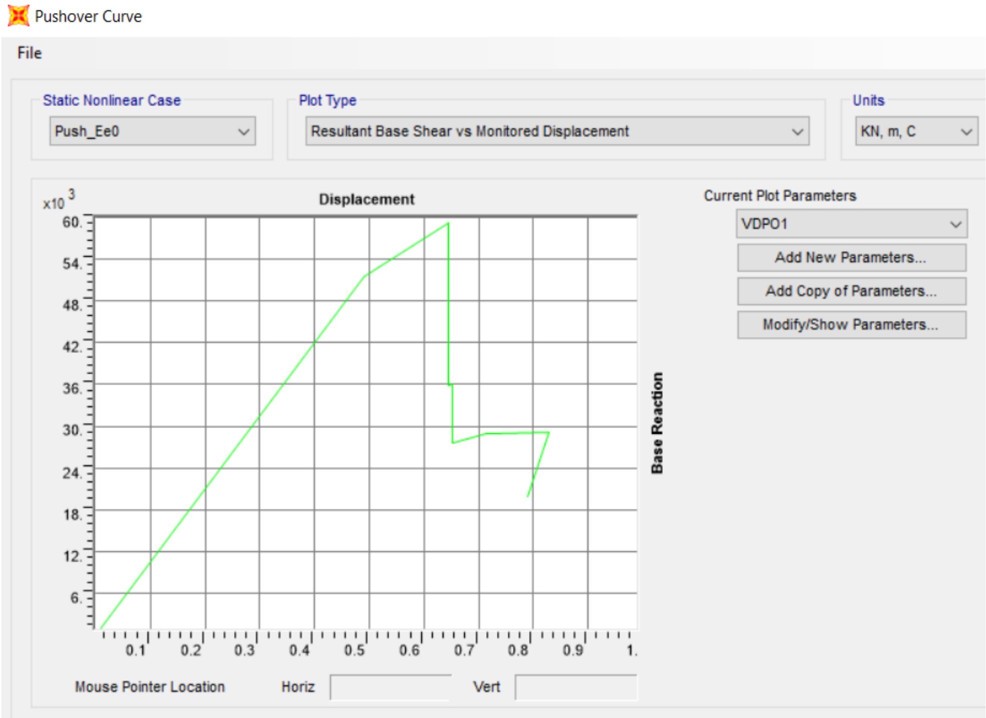

Figure 6.10 : Base shear vs. top displacement curve for x-bracing system E_e^0.

According to Figure 6.10, $BS_{Ee0,storm}$ = 13968 kN

$BS_{Ee0,ultimate}$ = 59198 kN

$$RSR_{Ee0} = \frac{\mathrm{BS}_{Ee0,ultimate}}{\mathrm{BS}_{Ee0,storm}} = \frac{59198}{13968} = 4.24$$

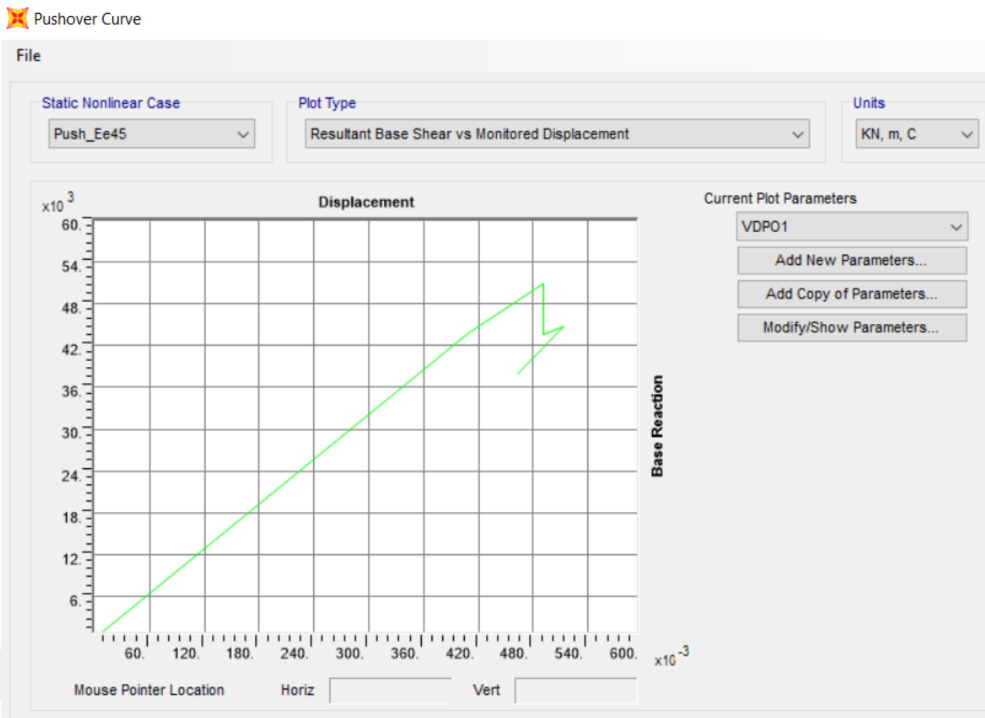

Figure 6.11 : Base shear vs. top displacement curve for x-bracing system E_e^{45}.

According to Figure 6.11, $BS_{Ee45,storm}$ = 11556 kN

$BS_{Ee45,ultimate}$ = 50845 kN

$$RSR_{Ee45} = \frac{BS_{Ee45,ultimate}}{BS_{Ee45,storm}} = \frac{50845}{11556} = 4.40$$

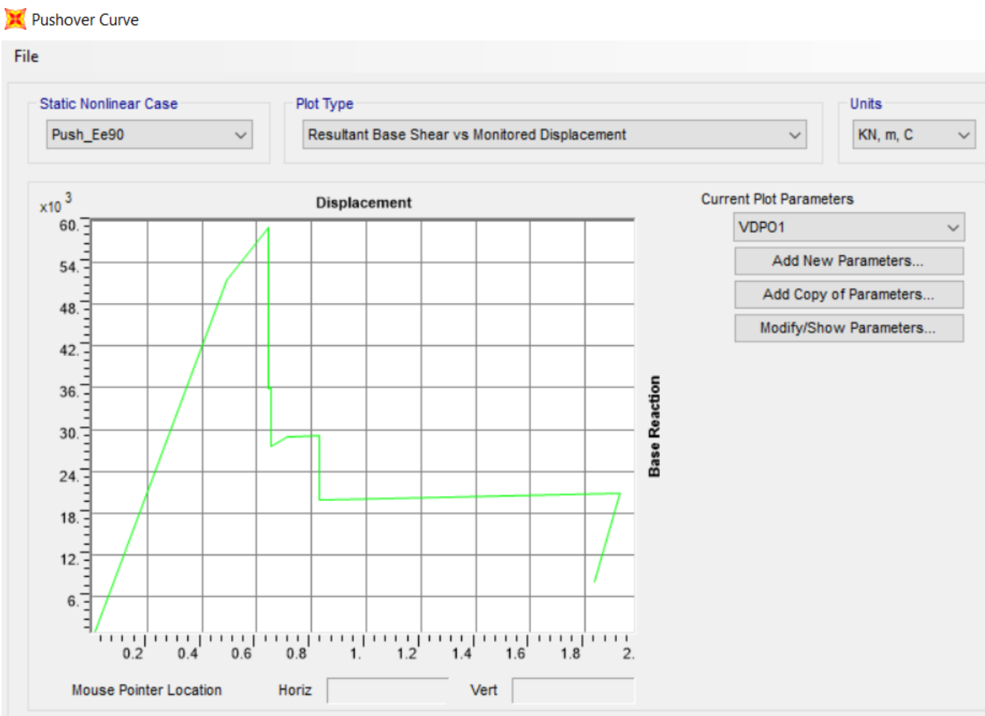

Figure 6.12 : Base shear vs. top displacement curve for x-bracing system E_e^{90}.

According to Figure 6.12, $BS_{Ee90,storm}$ = 8523 kN

$BS_{Ee90,ultimate}$ = 59073 kN

$$RSR_{Ee90} = \frac{BS_{Ee90,ultimate}}{BS_{Ee90,storm}} = \frac{59073}{8523} = 6.93$$

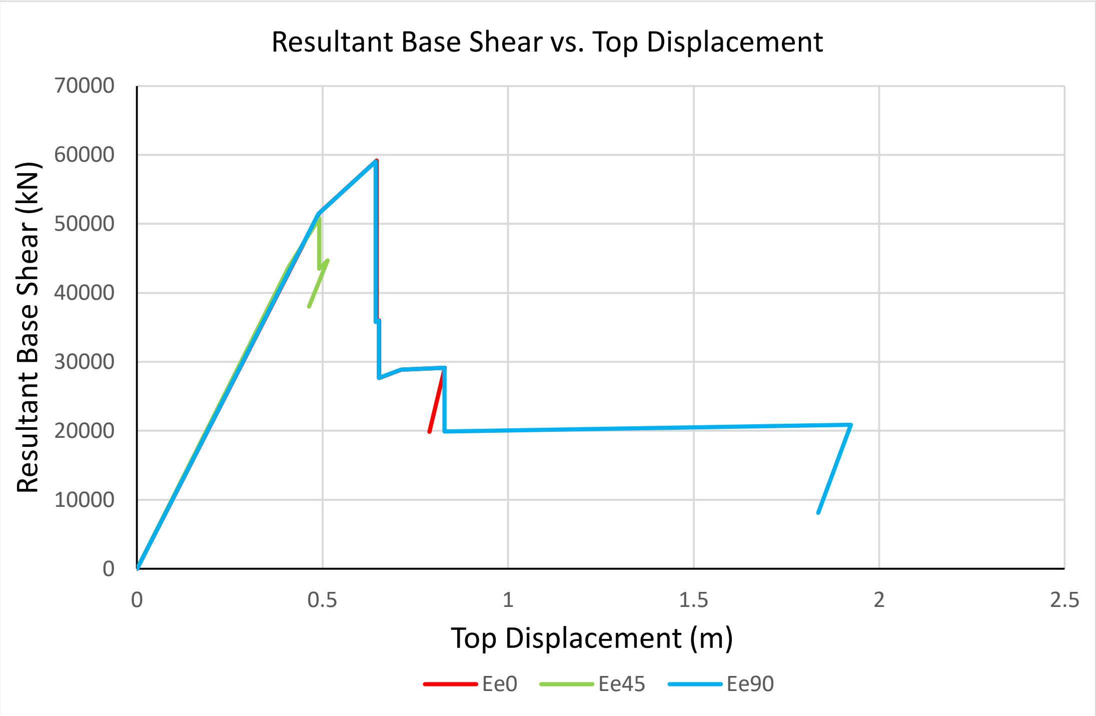

Figure 6.13 : Base shear vs. top displacement curve for x-bracing system.

Figure 6.13 shows the base shear and top displacement curve for x-bracing systems.

6.3 Metocean Pushover Analysis Results for V-Bracing System

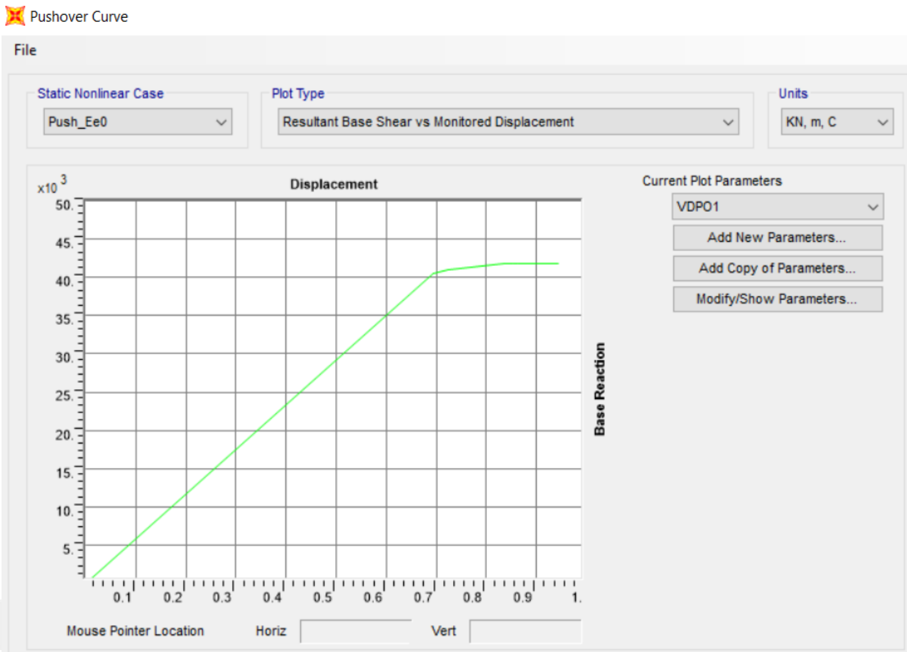

Figure 6.14 : Base shear vs. top displacement curve for v-bracing system E_e^0.

According to Figure 6.14, $BS_{Ee0,storm}$ = 13804 kN

$BS_{Ee0,ultimate}$ = 41835 kN

$$RSR_{Ee0} = \frac{BS_{Ee0,ultimate}}{BS_{Ee0,storm}} = \frac{41835}{13804} = 3.03$$

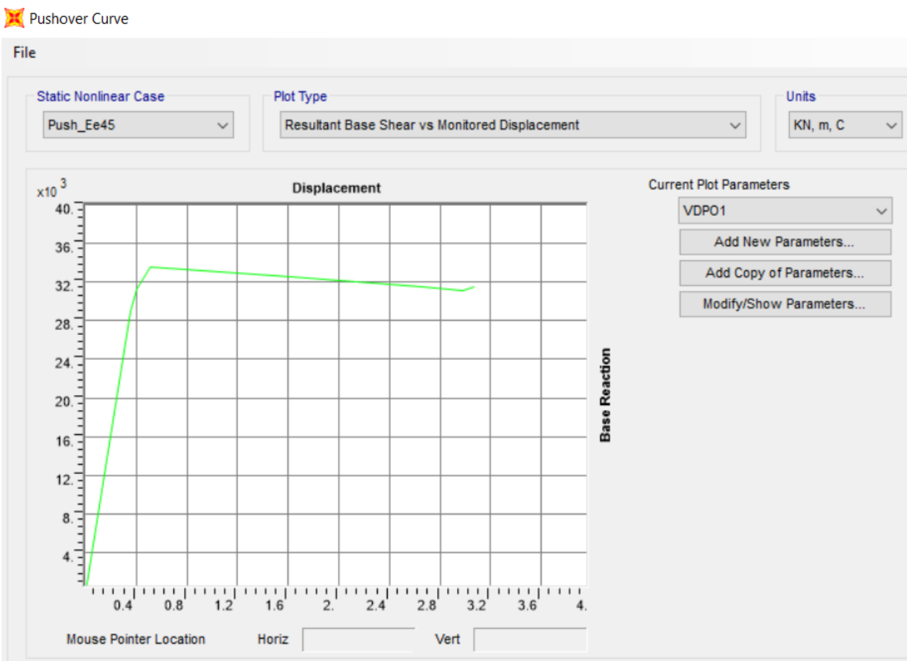

Figure 6.15 : Base shear vs. top displacement curve for v-bracing system E_e^{45}.

According to Figure 6.15, $BS_{Ee45,storm}$ = 11353 kN

$BS_{Ee45,ultimate}$ = 33614 kN

$$RSR_{Ee45} = \frac{\mathrm{BS}_{Ee45,ultimate}}{\mathrm{BS}_{Ee45,storm}} = \frac{33614}{11353} = 2.96$$

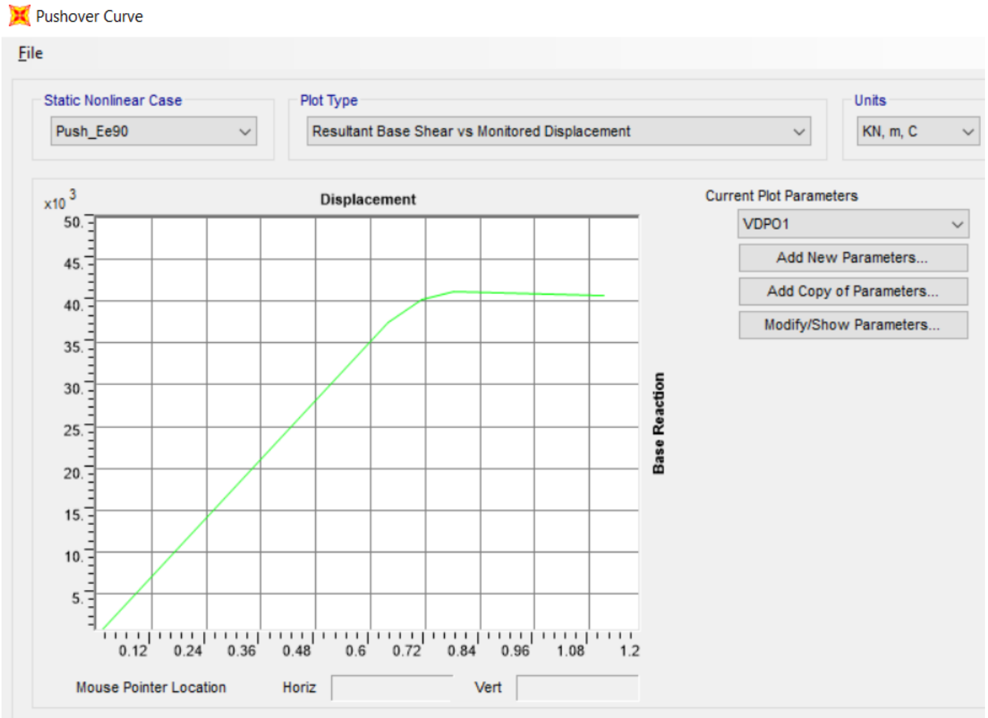

Figure 6.16 : Base shear vs. top displacement curve for v-bracing system E_e^{90}.

According to Figure 6.16, $BS_{Ee90,storm}$ = 8309 kN

$BS_{Ee90,ultimate}$ = 41145 kN

$$RSR_{Ee90} = \frac{\mathrm{BS}_{Ee90,ultimate}}{\mathrm{BS}_{Ee90,storm}} = \frac{41145}{8309} = 4.95$$

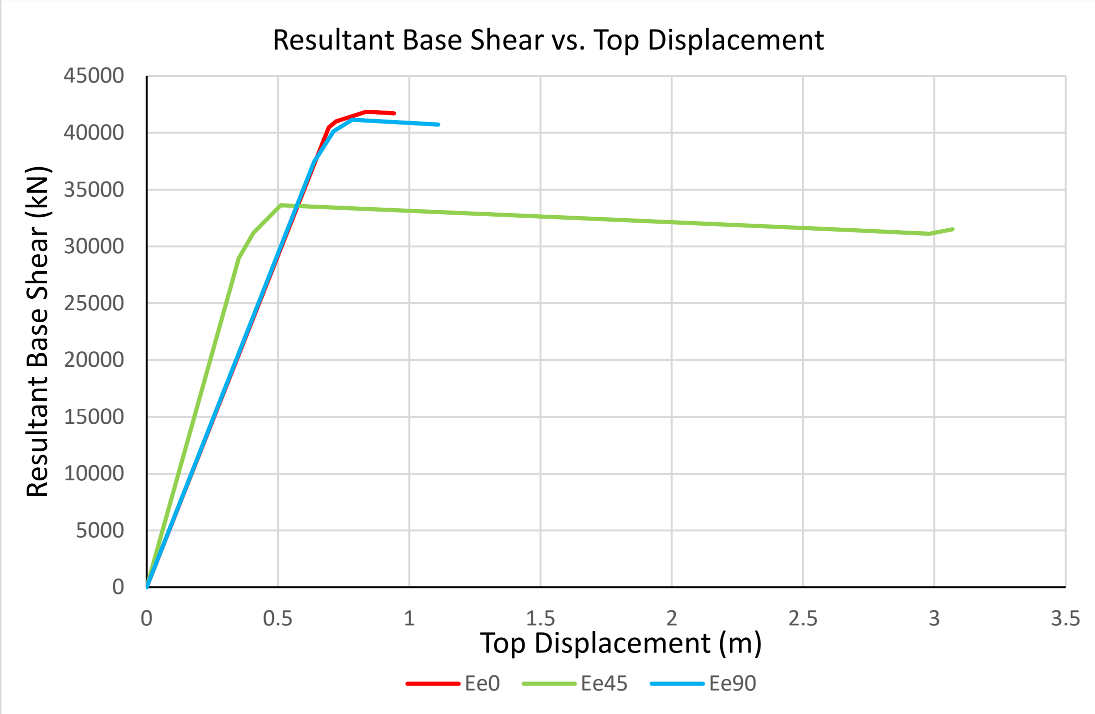

Figure 6.17 : Base shear vs. top displacement curve for v-bracing system.

Figure 6.17 shows the base shear and top displacement curve for v-bracing systems.

6.4 Metocean Pushover Analysis Results for Inverted V-Bracing System

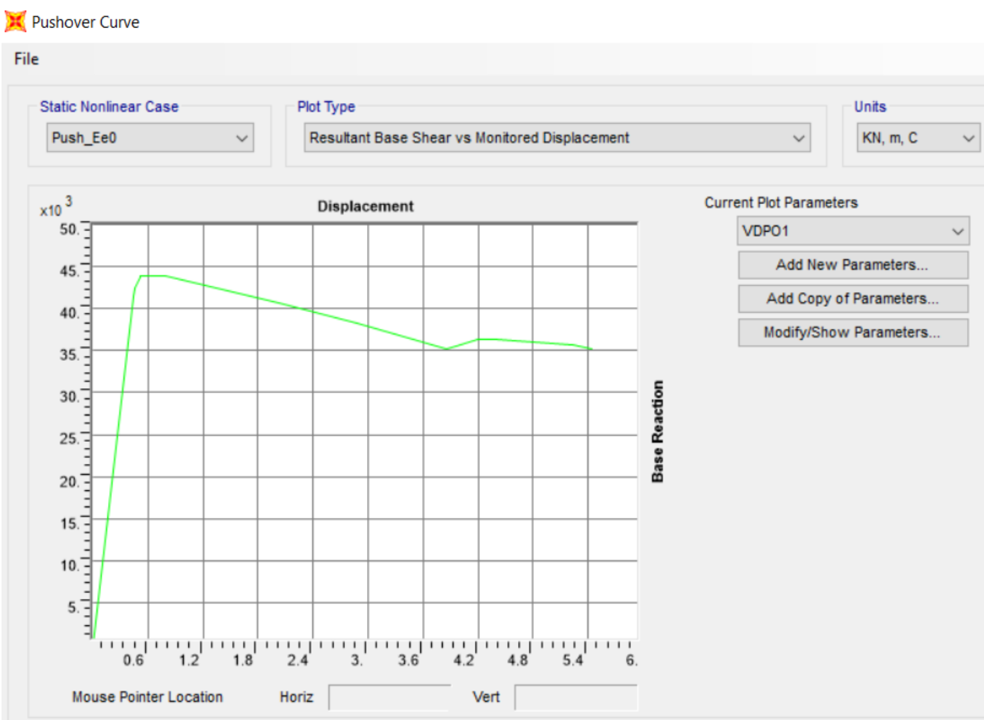

Figure 6.18 : Base shear vs. top displacement curve for inverted v-bracing system E_e^0.

According to Figure 6.18, $BS_{Ee0,storm}$ = 14098 kN

$BS_{Ee0,ultimate}$ = 43932 kN

$$RSR_{Ee0} = \frac{BS_{Ee0,ultimate}}{BS_{Ee0,storm}} = \frac{43932}{14098} = 3.11$$

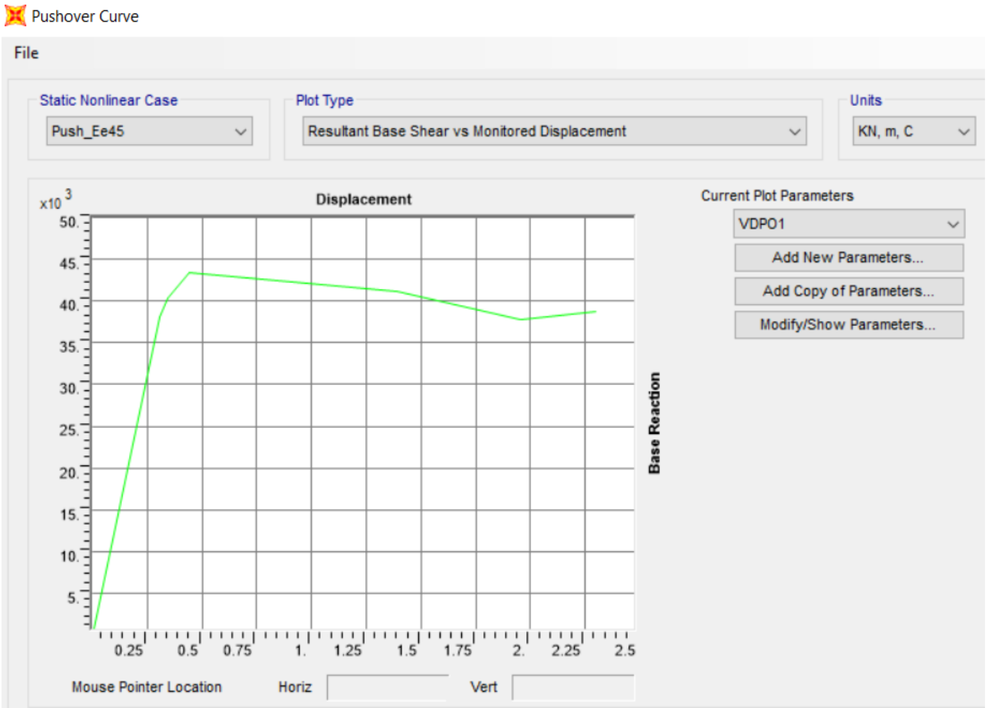

Figure 6.19 : Base shear vs. top displacement curve for inverted v-bracing system E_e^{45}.

According to Figure 6.19, $BS_{Ee45,storm}$ = 11582 kN

$BS_{Ee45,ultimate}$ = 43457 kN

$$RSR_{Ee45} = \frac{BS_{Ee45,ultimate}}{BS_{Ee45,storm}} = \frac{43457}{11582} = 3.75$$

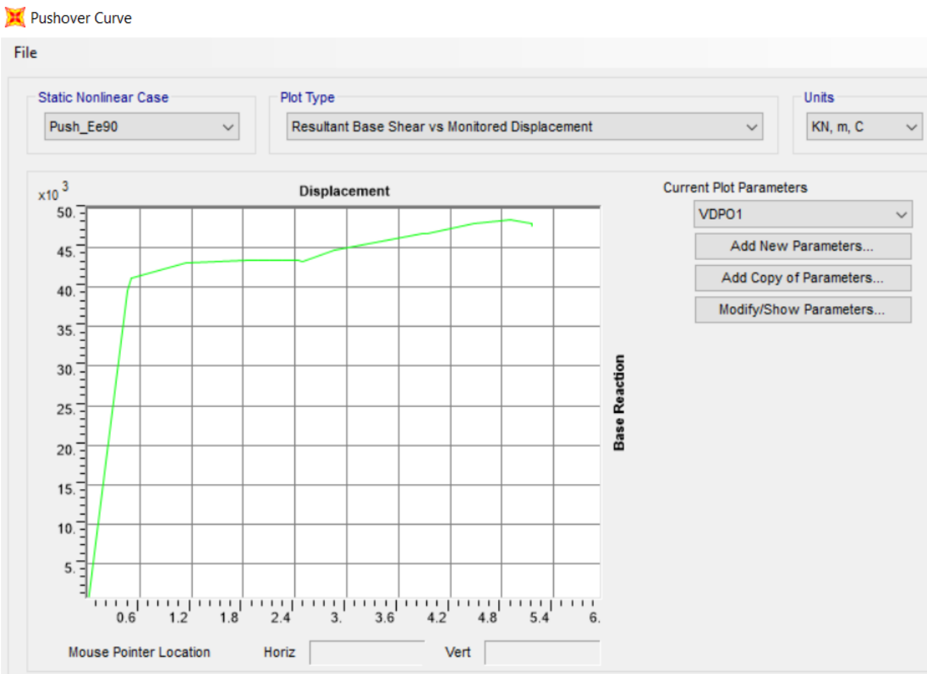

Figure 6.20 : Base shear vs. top displacement curve for inverted v-bracing system E_e^{90}.

According to Figure 6.20, $BS_{Ee90,storm}$ = 8566 kN

$BS_{Ee90,ultimate}$ = 48506 kN

$$RSR_{Ee90} = \frac{BS_{Ee90,ultimate}}{BS_{Ee90,storm}} = \frac{48506}{8566} = 5.66$$

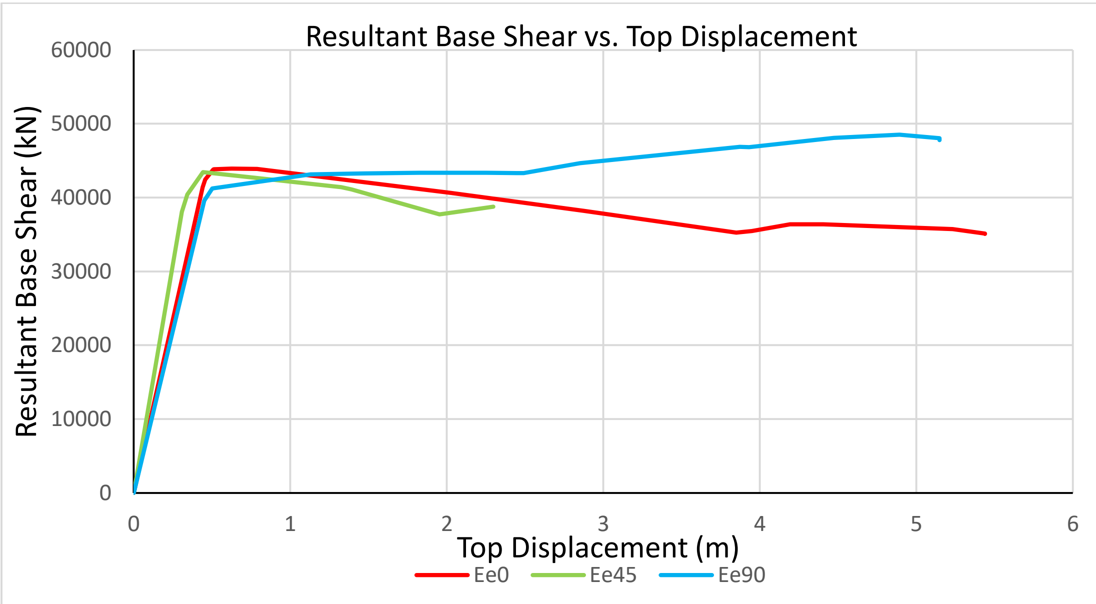

Figure 6.21 : Base shear vs. top displacement curve for inverted v-bracing system.

Figure 6.21 shows the base shear and top displacement curve for inverted v-bracing systems.

6.5 Metocean Pushover Analysis Results for K-Bracing System

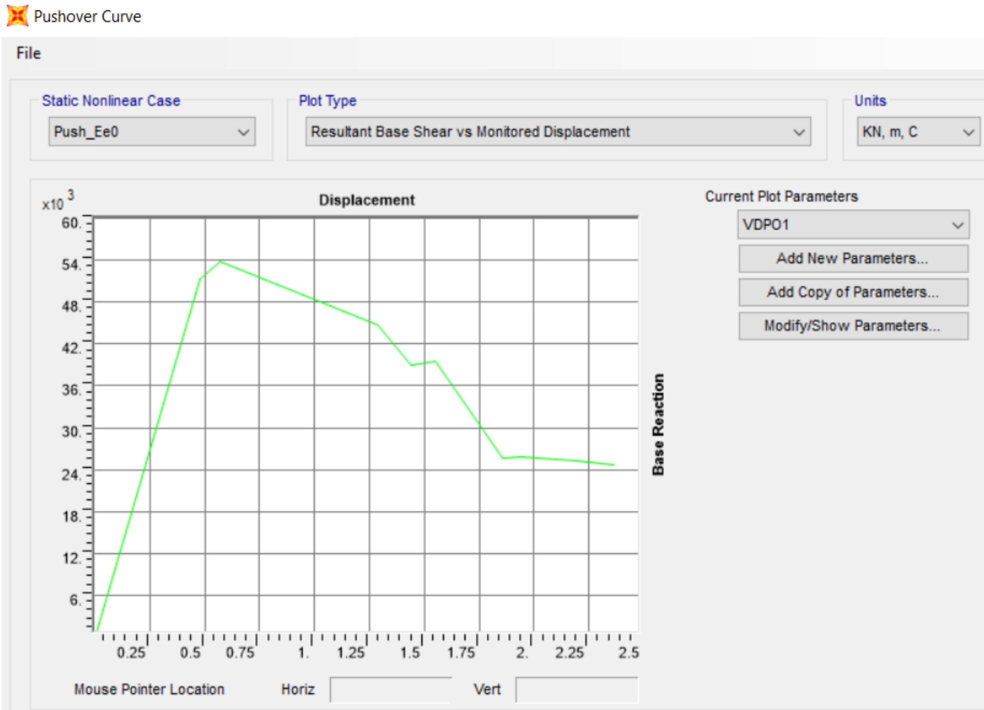

Figure 6.22 : Base shear vs. top displacement curve for k-bracing system E_e^0.

According to Figure 6.22, $BS_{Ee0,storm}$ = 14026 kN

$BS_{Ee0,ultimate}$ = 53765 kN

$$RSR_{Ee0} = \frac{BS_{Ee0,ultimate}}{BS_{Ee0,storm}} = \frac{53765}{14026} = 3.83$$

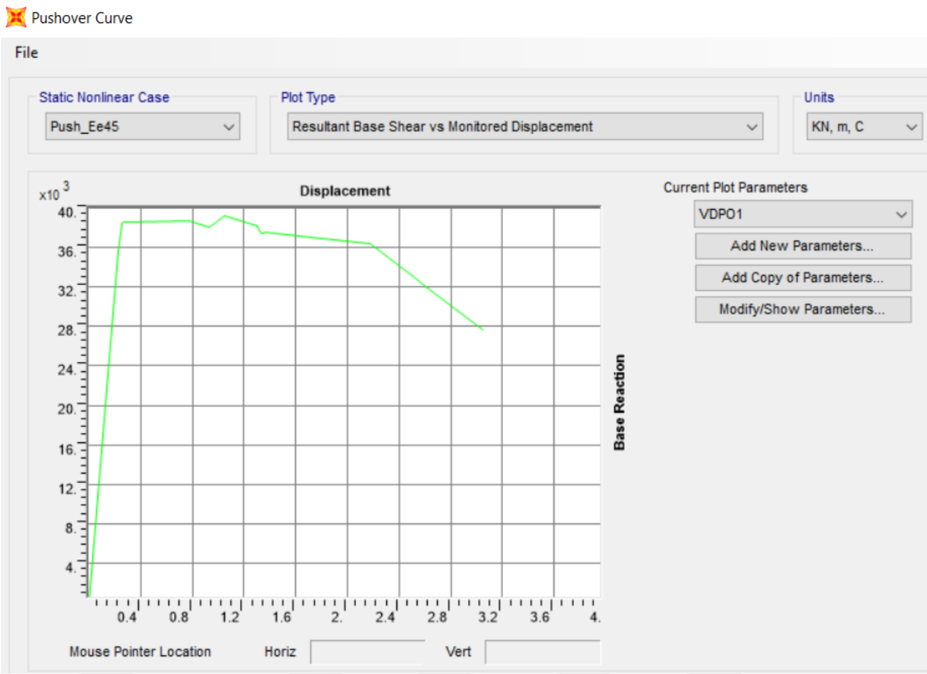

Figure 6.23 : Base shear vs. top displacement curve for k-bracing system E_e^{45}.

According to Figure 6.23, $BS_{Ee45,storm}$ = 11582 kN $BS_{Ee45,ultimate}$ = 39274 kN

$$RSR_{Ee45} = \frac{BS_{Ee45,ultimate}}{BS_{Ee45,storm}} = \frac{39274}{11593} = 3.39$$

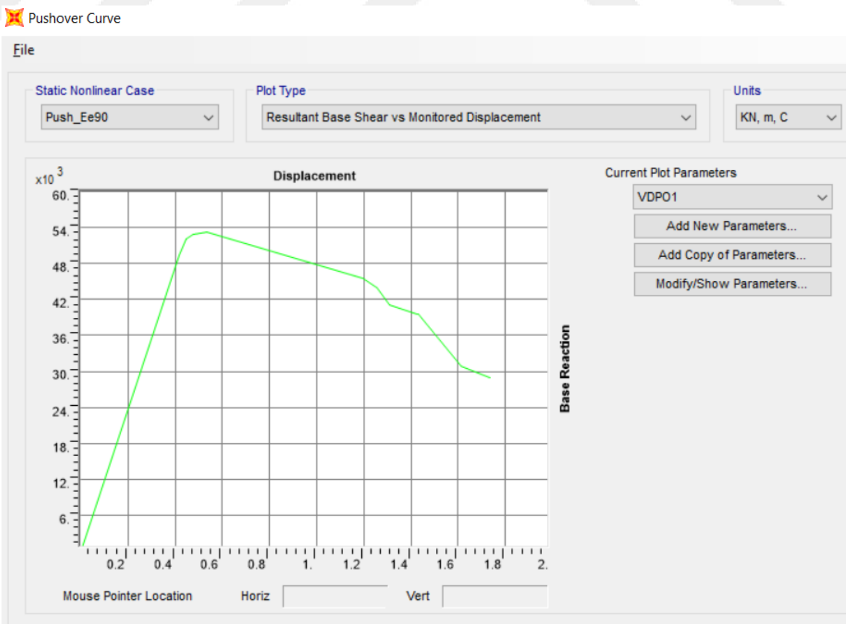

Figure 6.24 : Base shear vs. top displacement curve for k-bracing system E_e^{90}.

According to Figure 6.24, $BS_{Ee90,storm}$ = 8309 kN $BS_{Ee90,ultimate}$ = 53260 kN

$$RSR_{Ee90} = \frac{BS_{Ee90,ultimate}}{BS_{Ee90,storm}} = \frac{53260}{8587} = 6.41$$

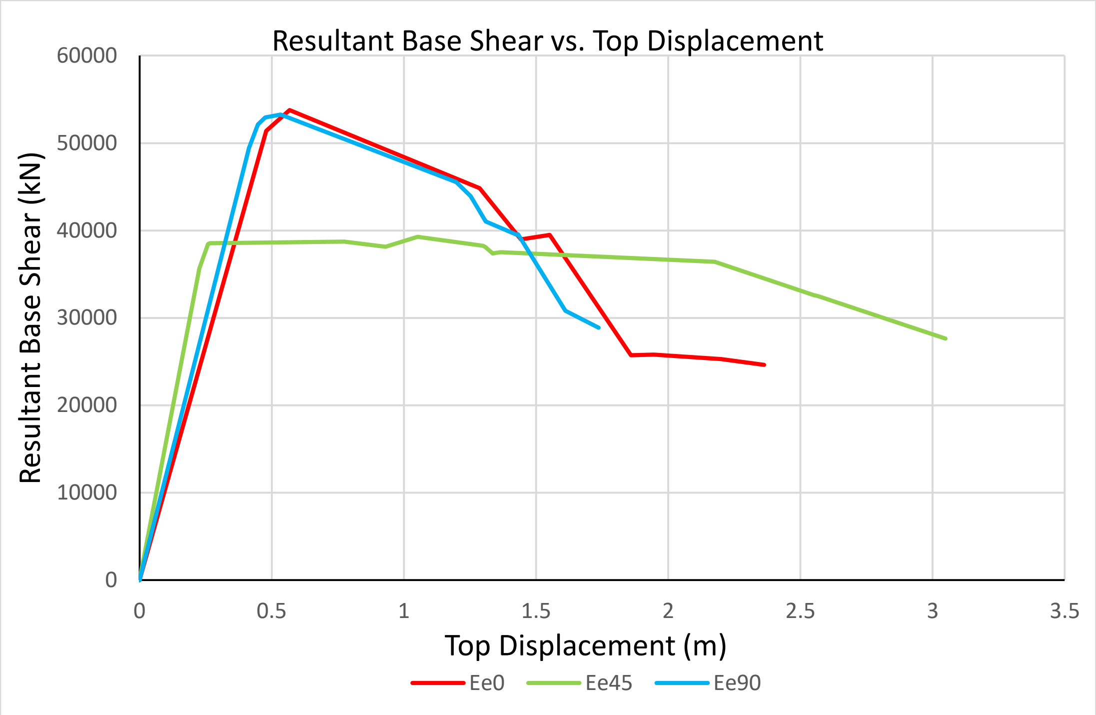

Figure 6.25 : Base shear vs. top displacement curve for k-bracing system.

Figure 6.25 shows the base shear and top displacement curve for k-bracing systems.

7. CONCLUSION

In this study, metocean nonlinear pushover analysis is performed to a jacket type offshore platform with 5 different bracing systems for 3 wave directions in order to determine RSR and compare 5 different bracing systems.

First of all, 100-year extreme metocean conditions are determined. Then, dynamic wave plus current forces are transformed to static forces with using Morrison's Equation and Airy Wave Theory with taking into account important considerations such as marine growth, tides and non-structural elements for all storm directions.

After calculating wave plus current forces, linear analysis is performed by using wave plus current forces with dead and live loads with appropriate combinations in order to determine cross sections of members. All structural sections are selected as circular hollow structural section because of having same strength in all directions and minimizing storm forces. The dimensions of structural members in all model are chosen the same in order to compare properly.

Then, nonlinear metocean pushover analysis is done for each storm direction.

Finally, reserve strength ratios of a jacket type offshore platform with 5 different bracing systems are determined for 3 wave directions.

Nonlinear metocean pushover analysis results are summarized for all bracing systems and storm directions in Figure 7.1, Table 7.1 and Table 7.2. Figure 7.1 shows storm resultant base shear and top dislacement curves for all storm directions and all bracing systems. Table 7.1 shows storms resultant base shears, ultimate resultant base shears, reserve strength ratios of all platforms for each storm direction and overall reserve strength ratios which are the lowest one for all directions considered.

Also, Table 7.2 shows reserve strength ratios and top displacements corresponding to wave directions for all bracing systems of the platform.

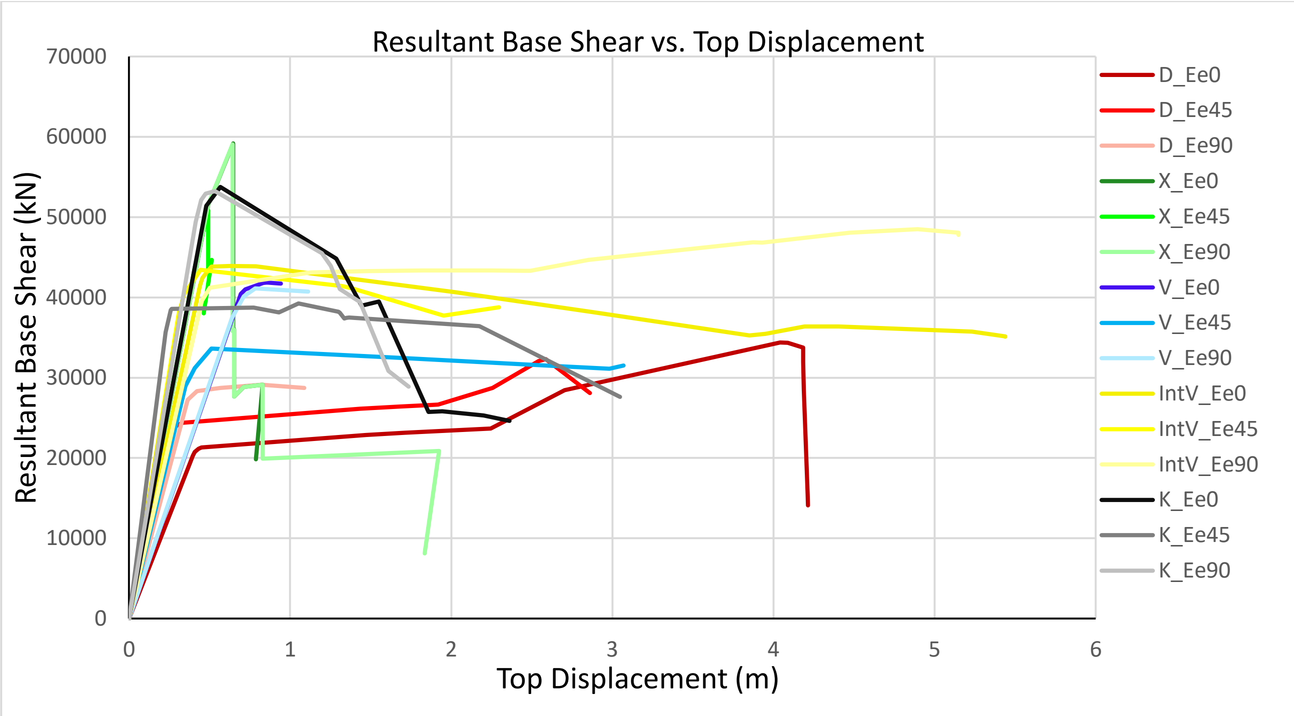

Figure 7.1 : Base shear vs. top displacement curve for all bracing systems.

Table 7.1 : Base shears and RSR values of all bracing systems.

Bracing Configuration	Wave Direction	Storm Resultant Base Shear (kN)	Ultimate Resultant Base Shear (kN)	Reserve Strength Ratio (RSR)	Overall RSR
Diagonal	0^0	11859	34384	2.90	2.90
	45^0	9642	32316	3.35	
	90^0	6812	29108	4.27	
X-Bracing	0^0	13968	59198	4.24	4.24
	45^0	11556	50845	4.40	
	90^0	8523	59073	6.93	
V-Bracing	0^0	13804	41835	3.03	2.96
	45^0	11353	33614	2.96	
	90^0	8309	41145	4.95	
Inverted V-Bracing	0^0	14098	43932	3.11	3.11
	45^0	11582	43457	3.75	
	90^0	8566	48506	5.66	
K-Bracing	0^0	14026	53765	3.83	3.39
	45^0	11593	39274	3.39	
	90^0	8587	53260	6.41	

Table 7.2 : Base shears and RSR values of all bracing systems.

Bracing Configuration	Wave Direction	Reserve Strength Ratio (RSR)	Maximum Top Displacement in Wave Direction (m)
Diagonal	0^0	2.90	4.22
	45^0	3.35	2.89
	90^0	4.27	1.08
X-Bracing	0^0	4.24	0.83
	45^0	4.40	0.55
	90^0	6.93	1.92
V-Bracing	0^0	3.03	0.94
	45^0	2.96	4.34
	90^0	4.95	1.12
Inverted V-Bracing	0^0	3.11	5.46
	45^0	3.75	3.24
	90^0	5.66	5.15
K-Bracing	0^0	3.83	2.36
	45^0	3.39	4.67
	90^0	6.41	1.98

Analyzes show that the effects of bracing systems designed to resist the effects of horizontal load (storm loadings) on the structural system create significant differences. The highest reserve strength ratios are achieved in X-bracing system for all storm direction and also the highest overall reserve strength ratio is achieved in X-bracing system.

Furthermore, the lowest reserve strength ratio is determined in diagonal bracing system. Although in X-bracing system the total projected area of members and the total storm forces are close to the other bracing systems except diagonal bracing system, X-bracing system has high strength.

Therefore, it can be easily said that X-bracing system is the most efficient bracing configuration for this jacket type offshore platform.

REFERENCES

[1] **Sadeghi, K., and Dilek, H**. (2019). An Introduction to the Design of Offshore Structures. *Academic Research International, 10* (1), (pp.19-27).

[2] **El-Reedy, M.A.** (2012). Offshore Structures Design, Construction and Maintenance, (pp.1-3), London.

[3] **Haritos, N.** (2007). Introduction to the Analysis and Design of Offshore Structures-An Overview. *EJSE Special Issue: Loading on Structures.*

[4] **Nallayarasu, S.** (2010). Offshore Structures, Analysis and Design. Retrieved from http://www.gcsolutions.ir/fa/images/pdf/OFFSHORE_STRUCTURES.pdf

[5] **Bea, R. G.** (1996). Nonlinear Performance of Offshore Platforms in Extreme Storm Waves. *Journal of Waterway, Port, Coastal, and Ocean Engineering*, *122*(2), 68–74. doi: 10.1061/(ASCE)0733-950x(1996)122:2(68).

[6] **Raheem, S.E.A.** (2013). Nonlinear Response of Fixed Jacket Offshore Platform Under Structural and Wave Loads. *Coupled Systems Mechanics, 10* (1), 111–126. doi: 10.12989/csm.2013.2.1.111

[7] **Ishwarya, S., Arockiasamy, M., and Senthil, R.** (2016). Inelastic Nonlinear Pushover Analysis of Fixed Jacket-Type Offshore Platform with Different Bracing Systems Considering Soil-Structure Interaction. *Journal of Shipping and Ocean Engineering*, 241-254. doi: 10.17265/2159-5879/2016.04.006

[8] **Mahar, J.A., and Adnan, M.I.** (2018). Analysis of Offshore Jacket Structure in the Syrian Coast by Using Computer Modeling. *American Journal of Innovative Research and Applied Sciences, 7* (2), 91–96.

[9] **Tabandeh, M., Biria, H., and Karimi, M.** (2018). Structural Integrity Assessment of Fixed Offshore Platforms Based on Pushover Analysis, *1st Conference on Asset Integrity Management in Oil and Gas 25-26 June 2018,* Iran.

[10] **Das, B., and Janardhan, P.** (2017). Model Development and Load Analysşs of Offshore Jacket Structure Using SAP2000. *International Journal for Research in Applied Science and Engineering Technology*, *5*(4), 1482–1493. doi: 10.22214/ijraset.2017.4263

[11] **Nguyen, D., and Sinsabvarodom, C.** (2015). Nonlinear Behavior of a Typical Oil and Gas Fixed-Jacket Offshore Platform with Different Bracing Systems Subjected to Seismic Loading. *The 20th National Convention on Civil Engineering 8-10 July 2015,* Chonburi, Thailand.

[12] **CSI.** (2017). Computer and Structures Inc., SAP200 Integrated Software for Structural Analysis and Design v20.0, Berkeley, California.

[13] **API RP2A.** (2010). Recommended Practice for Planning, Designing and Constructing Fixed Offshore Platforms - Working Stress Design. Offshore

Technology Conference, American Petroleum Institute, API RP2A 21st Edition.

[14] **ISO 19902.** (2007). ISO 19902:2007, Petroleum and natural gas industries — Fixed steel offshore structures.

[15] **DNV.** (2010). Environmental Conditions and Environmental Loads, Recommended Practice DNV-RP-C205, Det Norske Veritas.

[16] **FEMA 356.** (2000). Prestandard and Commentary for the Seismic Rehabilitation of Buildings, Federal Emergency Management Agency, Washington, DC.

[17] **AISC 360-10.** (2010). Specification for Structural Steel Buildings (AISC 360-10) and Commentary, American Institute of Steel Construction, Chicago, IL.

[18] **AISC360-16.** (2016). Specification for Structural Steel Buildings (AISC 360-16) and Commentary, American Institute of Steel Construction, Chicago, IL.

[19] **ASCE 41-17.** (2017). Seismic Evaluation and Retrofit of Existing Buildings, American Society of Civil Engineers, Virginia.

CURRICULUM VITAE

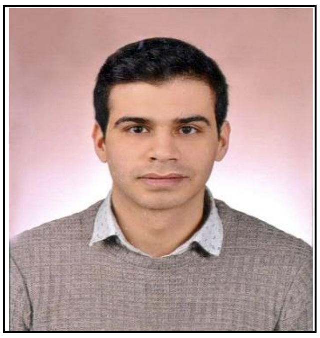

Name Surname : **Erdem EREZ**

Place and Date of Birth : **Antalya 1993**

E-Mail : **erez17@itu.edu.tr**

EDUCATION :

- **B.Sc.** : 2017, Middle East Technical University, Faculty of Engineering, Department of Civil Engineering